Master Thesis

submitted within the UNIGIS MSc. programme
at the Department of Geoinformatics - Z_GIS
University of Salzburg, Austria
under the provisions of UNIGIS India framework

Comparison of Land Use Land Cover Classification Obtained from Three Methods

A Case Study of Hetauda Sub-Metropolitan City, Nepal - 2020

By

Menaka Hamal
105252

A thesis submitted in partial fulfillment of the requirements of
the degree of
Master of Science (Geographical Information Science & Systems) – MSc (GISc)

Advisor (s):

Dr Shahnawaz

University of Salzburg, Austria

Kathmandu, 19. 06. 2021

Science Pledge

By my signature below, I certify that my thesis report is entirely the result of my own work. I have cited all sources of information and data I have used in my Thesis and indicated their origin.

Kathmandu, 19 June 2021

Place and Date	Signature

Acknowledgments:

I would like to gratefully acknowledge my thesis supervisor Dr. Shahanawaz of the University of Salzburg, Austria for his helpful comments, communication, and advice in thesis proposal development and report preparation. I gratefully thank my kids for understanding my academic situation and having me as a part of their study colleagues after everyday school. I would like to thanks my beloved husband for his continuous support for the entire study period.

I am especially indebted to Dr. Him Lal Shresth, the Associate Professor and Coordinator of UNIGIS Programme of Kathmandu Forestry College for his valuable advice and follow-up of thesis work progress. I also would like to acknowledge the professors and colleagues of KAFCOL for their direct and indirect support during the thesis period.

I would like to express my special thanks to the colleagues of the Forest Division Office, District Coordination Committee, Hetauda Sub-Metropolitan Office of Makwanpur district for their cooperation and for providing valuable information. I would like to thank my friend Achyut Lamichhane for giving prompt response and providing spatial information of the Hetauda Metropolitan City during the study period.

It would like to acknowledge International Centre for Integrated Mountain Development where I used work station effectively almost every weekend to complete my academic tasks and colleagues of Geospatial Theme who always prompted to support and answer the queries regarding research matter.

Abstract:

The Land Use Land Cover (LULC) classification using satellite imagery has been widely practiced at a local to a global scale. The data and classified maps have become the most used remotely sensed data in various domains such as socio-economic, natural resources conservation and management, environment, urban planning. Considering the applicability of the data and suitability of the classification methods to extract LULC thematic classes of Hetauda Sub-metropolitan City of Nepal, the three methods – the supervised classification in ERDAS Imagine, Segment Mean Shift in ArcGIS, and the Object-Based Image Analysis (OBIA) in eCognition, were used with the Sentinel-2B satellite imagery. The atmospherically and radiometrically corrected imagery was used to extract the six LULC classes – forest, agriculture, built-up area, bare area, grassland, and waterbody. The training samples were selected through visual interpretation based on the knowledge of the area to train the Maximum Likelihood Classifier (MLC) in supervised classification and segment mean shift classification, and to train the nearest neighbor classifier in OBIA. The samples were drawn directly from the enhanced imagery in supervised classification however those collected among rasterized superpixels in segment mean shift classification and vectorize polygons in OBIA.

The overall accuracy of the classified image using segment mean shift was found to be highest by 90%, OBIA was found to be second-highest 89% and supervised classification secured 85%. Similarly, kappa statistics showed a strong level of agreement of highest 0.88 in segment mean shift, 0.86 in object-based image analysis, and 0.81 in supervised classification. The average individual class accuracy varies among classes, the forest was found to be 98% reliable whereas the waterbody was found to be 71%. The segment mean shift method was found to be more accurate and appropriate than the pixel-based direct supervised classification for the LULC classification of the Hetauda Sub-metropolitan city of Nepal.

Table of Contents

List of Tables

List of Figures

List of Maps

Chapter-1: Introduction

1.1. Background

The LULC classification using satellite imagery has been widely practiced at a local to a global scale. The worldwide advancements in sensor technology, access to free satellite imageries to the public, availability of user-friendly spatial data analysis tools and techniques might be a reason for user interest in the extraction of LULC information. The LULC data and classified maps have become the most used remotely sensed data in various domains such as socio-economic, natural resources conservation and management, environment, urban planning, and so on (Li et al., 2014).

The various types of image classification methods have been used in LULC classification. The unsupervised classification technique in which the pixels that have common characteristics are grouped by the computer solely (Enderle & WeihJr, 2005). The computer determines the pixels that have similar spectral pattern and classify them without any supervision. The user's involvement is to specify the algorithm during the classification process to get the desired classes (Duda & Canty, 2002). However, the knowledge of the area is required to relate the classified features to the actual features of the ground (Al-Fares, 2013). Similarly, in the supervised classification technique, the user selects the sample pixels based on the knowledge of the area. The representative training pixels are chosen to identify the similar other pixels in the imagery (Enderle & WeihJr, 2005). The sufficient selected pixels have been trained to the algorithms to classify the required coverage (Lillsand et al., 2015).

In object-based image analysis, both spectral and spatial information of the imagery have been used in the classification process (Blaschke, 2010). This method involves the categorization of pixels first based on the spectral characteristics, texture, shape, and

spatial homogeneity with the surrounding pixels. Based on the homogeneity criteria, the image is segmented into discrete objects or features (Ma et al., 2017); those objects are selected based on the field knowledge as sample data and train the classifier to classify the image as our requirements. Similarly, the segment means shift classification in ArcGIS is also an emerging image classification method. In this method, the pixels are grouped based on the similar characteristics of the adjacent pixels and formed superpixels or segments. Those superpixels are classified using supervised and unsupervised classification depending on the purpose of the study (ESRI, 2020). This study follows the supervised classification in three methods – supervised classification in ERDAS, Segment Mean Shift Classification in ArcGIS, and OBIA in eCognition.

The range of satellite imageries for the land measurement purposes have been available through different sources. The Landsat, MODIS and ASTER, VIIRS, IKONOS-2, OrbView-3 and so on data can be acquired from the USGS earth explorer and other web services, GEOS-R and NOAA-20 data from NOAA web portal, Sentinel-2A, Sentinel-2B and so on data from the ESA open access portal. However, free access data are in low resolution, some are commercial use, some are not available on their revisit time. The Sentinel 2 dataset are currently available and widely used.

Sentinel 2B is one of the European optical imaging satellites launched by the European Space Agency's Copernicus Program on 7 March 2017 to monitor the variability in land surface conditions. It provides high-resolution data in comparison to the other open-source satellite imagery. It uses a sun-synchronous orbit at a mean altitude of 786km and carries a high-resolution multispectral imager that has a 290 km swath width. The imager passively collects new data every 5 days to revisit a particular location in a push broom concept. It samples 13 spectral bands with different spatial resolutions - four bands at 10 m, six bands at 20 m, and three bands at 60 m. It has a 12-bit radiometric resolution that gives a potential range of brightness level from 0 - 4095.

The different types of remote sensing software are available and popular depending on the type of application and requirement of the study such aa ERDAS Imagine, ArcGIS, eCognition and so on. The ERDAS is one of the raster-based software that has been widely used to extract information from images and capable of resolving multiple geospatial tasks (Intergraph, 2018) and this software becomes popular for pixel-based classification (Basayigit, 2015). Similarly, eCognition is advanced geo-analysis software used to improve, accelerate, and automate the interpretation of a variety of geospatial data. It enables users in feature extraction and provides a platform to transform geo-data into to geo-information. The inbuilt rule set within this software used for the variety of desired spatial analysis and popular for object-based image analysis (Trimble, 2021). Likewise, ArcGIS allows handling and analyzing diverse geographic information by visualizing geographical statistics through layer-building maps. It works on vector as well as raster data with a range of applications in different domains and geography (ESRI, 2021).

The comparison of the classified image of an area using different methods has been practices in various studies (Lu, 2007). (Estoque et al., 2018) assessed and compared the eight remotely sensed maps of Philippine forest cover in the year 2010. Likewise, a similar study was conducted for Loess Plateau in China and compared the LULC classification. (Yang et al., 2017) has taken eight forest products in the year 2010 with a medium resolution (30–50 m) and compared their accuracies. Similarly, (Bai et al., 2014) have taken five global land cover data sets which were produced using different moderate resolution satellite images to looked into the consistencies and discrepancies among those data sets in China. Every land cover data set was produced using different classification methods however those are compared to find the most accurate classification methods and maps for the particular area.

Assessing the reliability of remotely sensed maps before the intended application is a crucial part of image classification (Congalton, 2001). During the assessing process, the

classified thematic categories of the image are verified to the same categories of the reference image (Ahlqvist et al., 2015). The reference data has been generated by applying the appropriate sampling technique or points/pixels are manually generated in the reference image or collect ground truth points visiting the study area to verify with the classified points/pixels. Then, the reference data have been verified with the position of the object of the classified image or vice versa (UoT, 2021). The verified data run through the statistical accuracy measures – the most common measure for LULC classification are the confusion matrix for finding out the performance of a classification model, and the Kappa statistics to measure the level of agreement (Foody, 2010). This study follows the point sampling method where sample points are generated using a stratified random sampling technique. Each LULC class is taken as a stratum in which the points are allocated randomly. The allocated points are verified with the original image to compute the confusion matrix and kappa statistics for finding out the reliability of the classified map.

The major natural resources of Nepal such as forest, grassland, agricultural land, urban areas, and snow cover has been changing for decades. The previous study and trend show that the area of agricultural land has increased while the forest land has increased, the grassland has decreased, the urban land has increased, shrinkage of snow cover and predicted that it will further be reduced in future. The past references show that the LULC study becomes challenging due to disasters, anthropogenic activities, and knowledge gaps regarding temporal and spatial data availability (Paudel et al., 2016). Considering challenges and necessities, Poudel et al., 2016 recommended that the LULC research is essential for integrating spatial data at a different level of the administrative boundary, using various methods to test the result, correlate and analyze the LULC dataset from global to the local level for research and development. The land and land resources have been changing over the years mostly due to anthropogenic activities in Nepal (FAO, 2020) and the population is increasing rapidly especially in the urban areas.

Hetauda Sub-Metropolitan City is one of the populated cities of Nepal. People have been

migrating to the city from Terai, Mountain, Hill, and rural villages nearby for searching for work, better education, and infrastructures. Because of the high population and the demand for land resources, the evident show that an agricultural land has been converted to the built-up area, the natural water has been diverted into ponds for fishery and other agriculture use, the forest and grassland have been exploiting due to excessive use and building infrastructures over it. The riverbanks are widening due to the shrinkage of river water flow and flood occurrence in monsoon. The LULC assessment of the city has also not been conducted for a decade due to unviability of high resolution satellite imagery and the lack of affordable capacity of organizations to purchase high cost of the satellite image, the insufficient technical human resources, as well as other technical difficulties (GoN, 2020). Considering those circumstances, this study is expected to be a fundamental input to know the existing condition of LULC and suggest for the better land use development of the city and government and non-government organizations working in policy formulation and decision-making and could be a reference knowledge for the expected researchers on the relevant areas.

1.2. Aims and Objectives

The general aim of the study is the LULC of the Hetauda Sub-Metropolitan City of Nepal.

The specific objectives are:

- To access the accuracy of the LULC classification performed through three methods - Supervised Classification, Segment Mean Shift Classification, and Object-Based Image Analysis.
- To develop LULC classified maps.

The objectives of the study will be fulfilled after data acquisition, required image processing, and classification techniques, and reviewing the literature.

1.3. Study Area

The Hetauda Sub-metropolitan City is located at the south of Makwanpur district of Nepal with the latitude 27°32′ 31” to 27°19’27” north and the longitude 85°53′27” to 85°11′24” east, the altitude ranges approximately from 300 to 1800 meter above sea level. It occupies 261.58 square kilometers. It was established in 1969 as a Municipality. However, after the new constitution was imposed in Nepal, the area has widened and was declared as Sub-metropolitan in 2017. The Sub-metropolitan is surrounded by Bakaiya rural municipality in the east, Manahari and Raksirang rural municipality in the west, Bhimphedi, Makwanpurgadi, and Kailesh rural municipality in the North, and Bara and Parsa district in the South.

The city has been administratively divided into 19 wards as the lowest developmental unit. All wards are divided into three areas mainly based on the density of population and road access - urban, semi-urban, and rural by the metropolitan city office. The urban ward number includes 2, 4, 5, and 10, the semi-urban area ward number includes 1, 3, 6, 7, 8, 9, 11, and the remaining 8 wards fall under the rural category. The urban wards occupy 12.48 km^2 that covers 5% area of the sub-metropolitan city, the semi-urban covers 62.09 km^2 which covers 24% and the rural wards inhibit 187.01 km^2 which is 71% of the total area of the sub-metropolitan city (MOFAGA, 2019).

The temperature and land structure of the city is suitable for agricultural production and good for human life (DoA, 2018). The city is known as inner Terai where the tropical climate is dominant; when the elevation raises, the sub-tropical climate is characterized; and the lower temperate climate existed with the rising elevation at the highest (MOFAGA, 2019). The temperature is varied throughout the city depending on the different seasons. It ranges from 7^0 in winter and 35^0 in summer and humidity is lowest in winter and highest during monsoon.

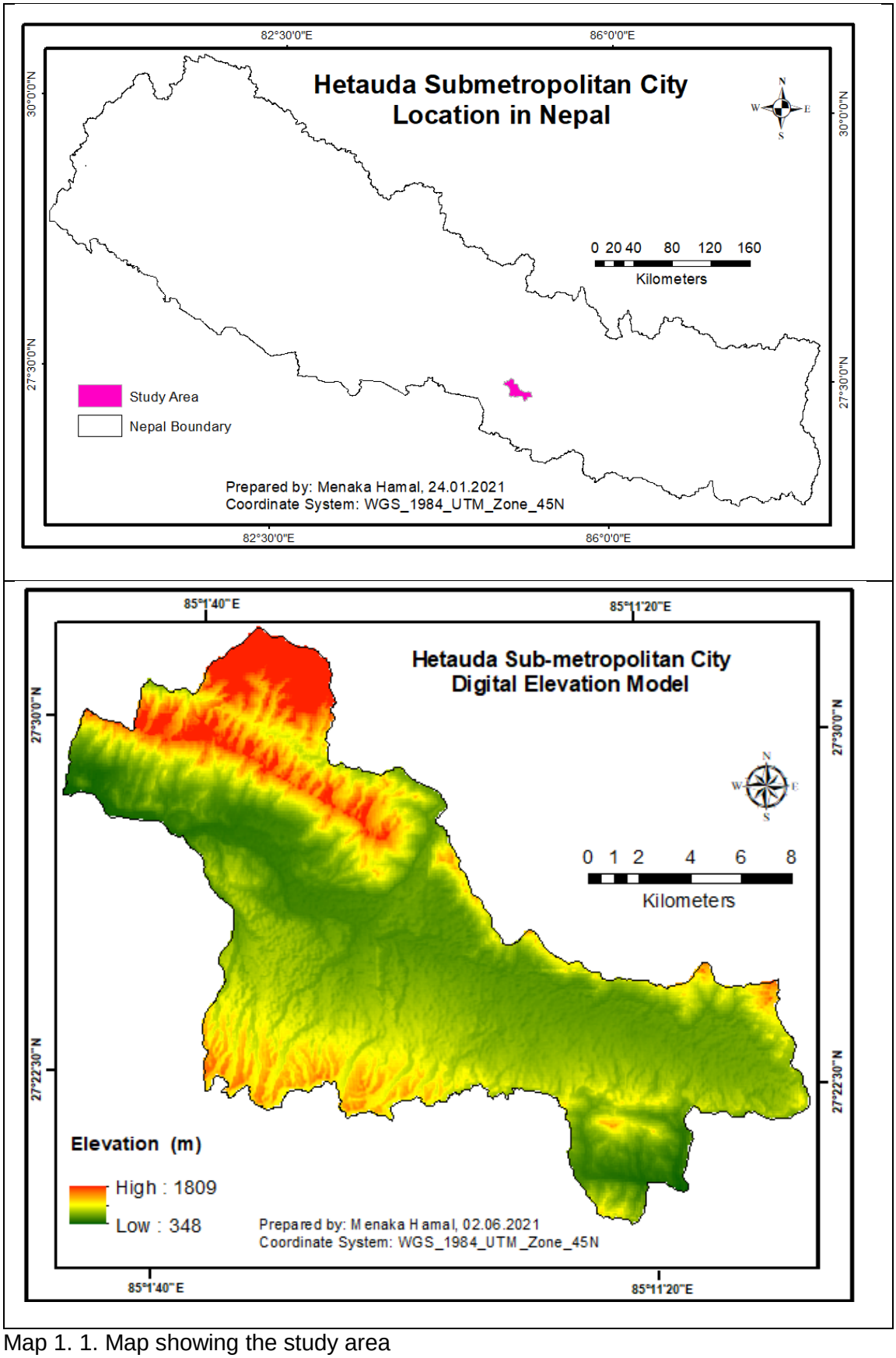

Map 1. 1. Map showing the study area

The above map of Map 1.1. shows the location of the sub-metropolitan city in the south of Nepal. The below map is showing the digital elevation model - the 90-meter DEM of Shuttle Radar Topography Mission. It depicts the range of elevation starts from 345 meters to 1809 meters of the city in different color codes. The red shows the highest elevation lowering height with the lighter color and the dark green shows the lowest point rising elevation with the lighter color and yellow shades in between.

According to the national census 2011, the total number of inhabitants who resided in the sub-metropolitan city was 152,875, among them the gender constitutes 74964 males and 77911 females. The average population density of the city was 548 per square kilometer and the total number of households was 34270. However, according to the city profile 2017, the population has increased to 152,875 which constitute 47964 males and 77911 females due to the addition of new wards in the expansion of the administrative units at a local level, and the population density also increased from 548 km^2 in 2011 to 584 per km^2 in 2017 (GoN, 2017).

Hetauda sub-metropolitan city becomes a high migrant's influx hub where people from Terai, Mountain, and rural Hilly part of the same and adjacent districts reside there. The productive land of the city turned into a built-up area and the natural resources are being highly demanded in private and commercial use. According to the city profile 2017, 41.46 % of the city covers by forest, and agricultural land occupies 41% of the total land. The rest of the areas such as barren land, built-up, bush, grass, orchard, pond, sand, and water are part of the city coverage.

This chapter opens with the background of the study that gives an overview of the remote sensing data and sources, image classification tools, and techniques and software used for LULC classification. In addition, it gives the significance of the study for the particular area and beyond. This is followed by the research aims and objectives and the study area that gives the location, elevation, temperature, population, and existing land coverage of the city.

Chapter-2: Methodology

This section gives an overview of the data, steps of data acquisition, image preprocessing, and the three methods of image classification followed by the accuracy assessment.

2.1. Methodological Flow Chart

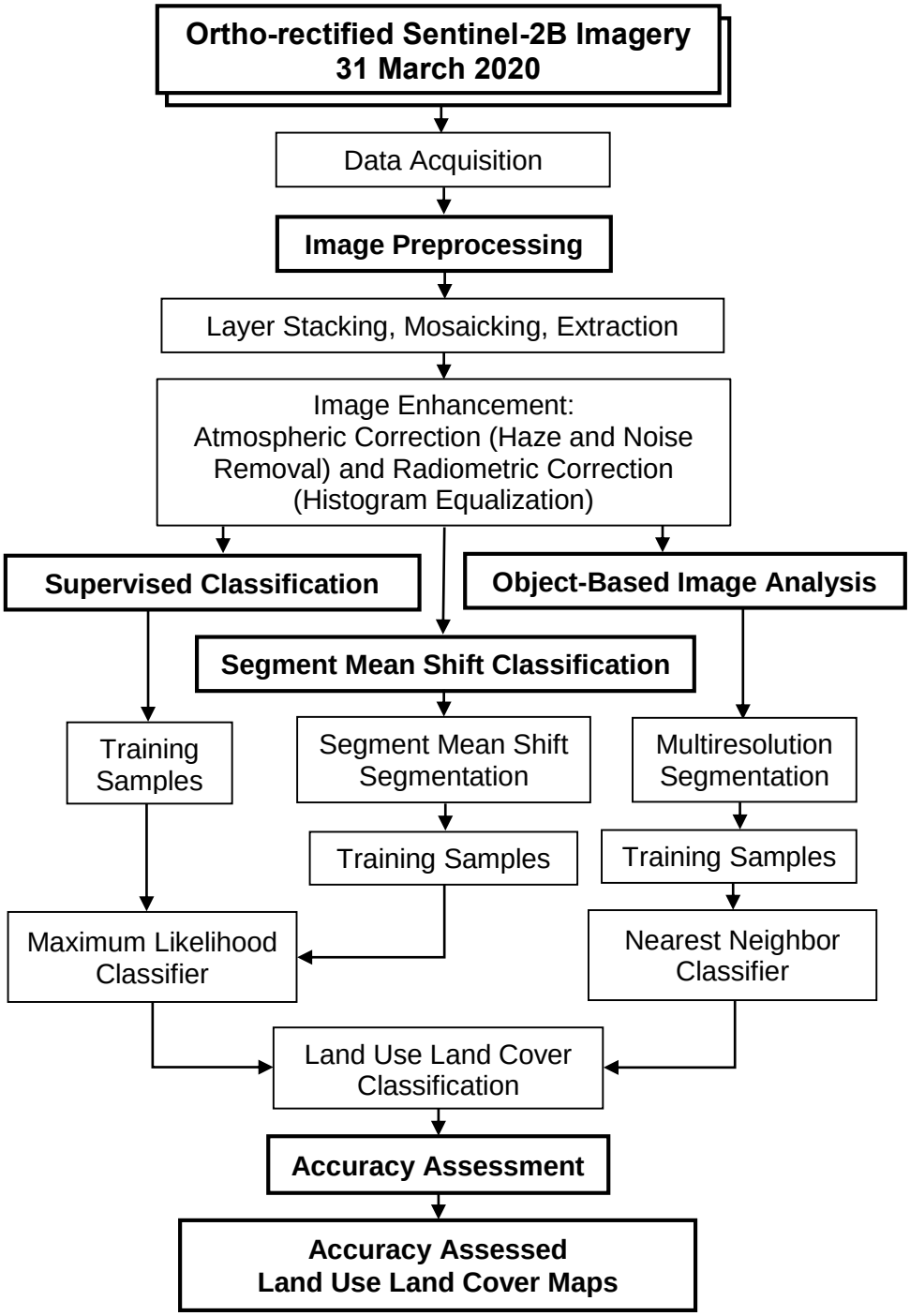

Figure 2.1. The process flow chart

Figure 2.1 shows the steps of LULC classification with three classification methods – supervised classification, Segment Mean Shift classification, and Object-Based Image Analysis, from the data description, data acquisition to the accuracy assessed LULC classification.

2.2. Data Acquisition

The study is based on the two multispectral imageries of Sentinel-2B acquired on 31 March 2020. The city is covered by a certain portion of those two imageries. One image covers the western half and the other covers the eastern half of the sub-metropolitan city. The data tiles that have 100-meter x 100-meter coverage, located at UTM grid codes - 45RTL and 45RUL, were accessed from the Copernicus Open Access Hub (ESA, 2020). The minimum cloud cover of Imagery 1 was found by 0.0 % and the Imagery 2 was found by 0.025 %. The datasets were geo-referenced and orthorectified with UTM/WGS84 projection (Table 2.1).

Table 2. 1. Detail of image used in the study area

Imagery	Satellite	Date	UTM Grid Code	Ground coverage
1	Sentinel-2B	31-Mar-20	45RTL	The western half of Hetauda Sub-metropolitan city
2	Sentinel-2B	31-Mar-20	45RUL	The eastern half of Hetauda Sub-metropolitan city

The separate data tiles have 13 spectral bands extend from the Visible and Near Infra-Red (VNIR) to the Short Wave Infra-Red (SWIR). Four bands were at 10m spatial resolution - blue (490nm), green (560nm), red (665nm), and near-infrared (842nm). Six bands were at 20m spatial resolution - four narrow bands were for vegetation characterization (705nm, 740nm, 783nm, and 865nm) and two larger SWIR bands were (1610nm and 2190nm) for applications such as snow/ice/cloud detection or vegetation moisture stress assessment. Three bands were at 60m spatial resolution mainly for cloud screening and atmospheric corrections (443nm for aerosols, 945 for water vapor, and

1375nm for cirrus detection) (ESA, 2021).

Table 2. 2. Sentinal-2 bands for LULC classification

Sentinel-2 Bands	Wavelength (μm)	Resolution (m.)
Blue (B2)	456 - 532	10
Green (B3)	536 - 582	10
Red (B4)	646 - 685	10
Near-infrared (B8)	774 - 907	10

Out of 13 bands, 4 bands at 10 m spatial resolution: blue (456 – 532 nm), green (536 - 582nm), red (646 – 685 nm), and near-infrared (774 – 907 nm) were used for the study. In Table 2.2, B2, B3, and B4 are the natural color bands used to display imagery the same way our eye see such as vegetation looks green, urban features see white and grey, water see from dark to light blue depending on its cleanness. The B8 is good at reflecting chlorophyll so that it helps to distinguish the vegetation layer easily, and urban features look white.

2.3. Image Preprocessing

Image preprocessing has been performed to suppress unwilling distortions and enhance the image features for further processing (Sonka et al., 2014). The preprocessing operations steps have been followed to improve the data quality and interpretability of the satellite imagery (Milan et al, 2020). The image quality improvement followed in this study includes combining multiple images of different bands into single imagery, assembling overlapping images to maintain a global frame, extraction of data from the larger set, atmospheric and radiometric correction to enhance image features for further processing. The imagery was corrected to create a more meaningful representation of the objects on the scene and improve the image utility later (Lillesand et al., 2015). The multiple bands were composited to make single imagery for both datasets and were mosaicked to maintain

a global frame. Then the cells were extracted with the city boundary and enhanced by atmospheric and radiometric correction.

2.3.1. Layer Stacking

Layer stacking is often used when individual spectral bands are provided in separate files (ERDAS, 2016). This process combines multiple separate bands or layers in a single image (Lillesand et al., 2015). The Sentinel-2B georeferenced imageries had separate bands or layers. Among those bands, some of the bands can be used for land measurement purposes (Copernicus, 2020). Among the land measurement purpose bands - band 2, band 3, band 4, and band 8, were found to be fit for the land use land data extraction. All single-band data had an equal number of rows and columns of 10980

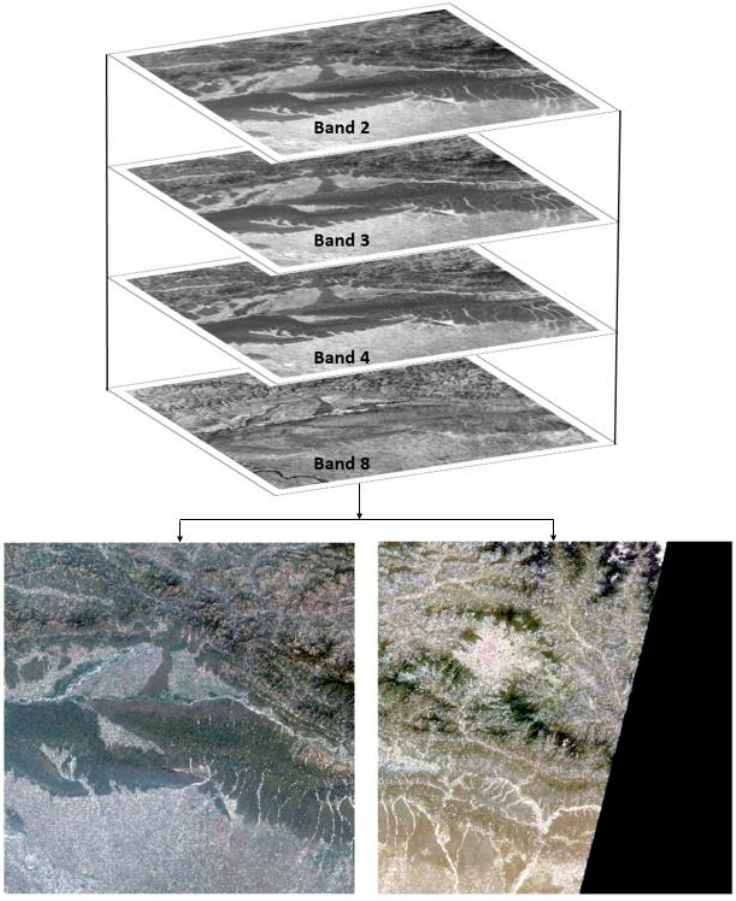

Figure 2.2.Multiband Stacked Imageries

and have 10-meter spatial resolution and each was a greyscale image. The greyscale images need to layer stack to get the color image with the NIR band to get the desired output (Towards, 2020). The four required bands were layered stacked.

Figure 2.2 shows that the four bands were stacked based on the similar cell size to form multiband single imagery for two datasets using the layer stack tool in ERDAS. Both datasets had distinct colors and could not use separately. Therefore both datasets were run for mosaicking.

2.3.2. Image Mosaicing

Image mosaicing is used to assemble and stitch overlapping portions of the images to constitute the global frame (Ait-Aoudia et al, 2012). The two multispectral composite imageries were mosaicked to combine two imageries that cover a spatial extent of the city boundary. For mosaicking, the imagery, the two Sentinel-2B layer stacked tiles - One is UTM grid cod 45RUL that covers the eastern half of the city and the other is 45RTL that covers the western half of the city, were taken. The size of the data tiles were 100 km*100 km. Those were found to be overlapped by 10 km. The overlap part of the imageries had to join the edges and consider the pixel values of a raster of the overlap area to produce a single raster dataset.

The overlapping cell values of the first raster were extracted using the LAST mosaic operator that determines the pixel value from the last raster dataset which is overlapping (ESRI,2021). Using this operator in ArcGIS, the pixel values of the second raster for the overlap area of the combined raster were set. Similarly, the color map from the second raster was considered as the color of the whole mosaic raster. Figure 2.3 illustrates the result of a mosaic where the last option is selected. The Imagery covering the western half of the city and the Imagery covering the eastern half of the city. The resultant combined raster resembles the color of Imagery 2 after using the LAST operator.

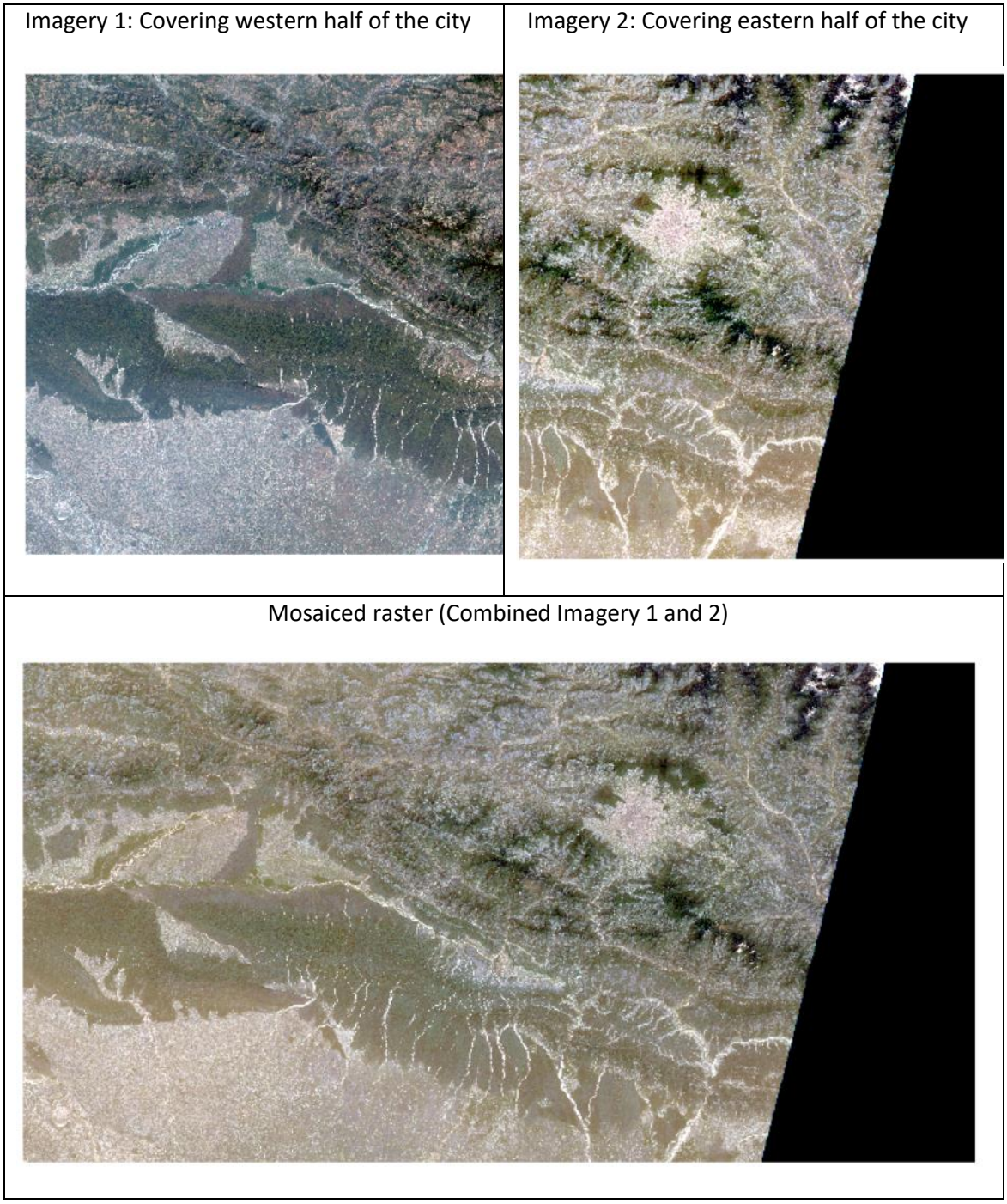

Figure 2.3. Dataset mosaicking

After performing the mosaicking process, the combined raster becomes visually similar to Raster 2 (Figure 2.3), and the cell values across the imagery also resemble. Then the mosaiced raster got ready for extraction by the city boundary.

2.3.3. Data Extraction

The data extraction of an area of interest for a specific purpose is a key step of utilizing satellite data for further analysis and in a diverse application (Serpico et al., 2012). The satellite data extraction is usually done when the image covers more area than required and so the imageries (Knorn et al., 2009). The mosaicked imagery for this study got spread further than the coverage of the administrative boundary. Therefore, the required cells were extracted (Lillesand et al., 2015) from the mosaic scene with the area of the Sub-metropolitan City boundary (Map 2.1).

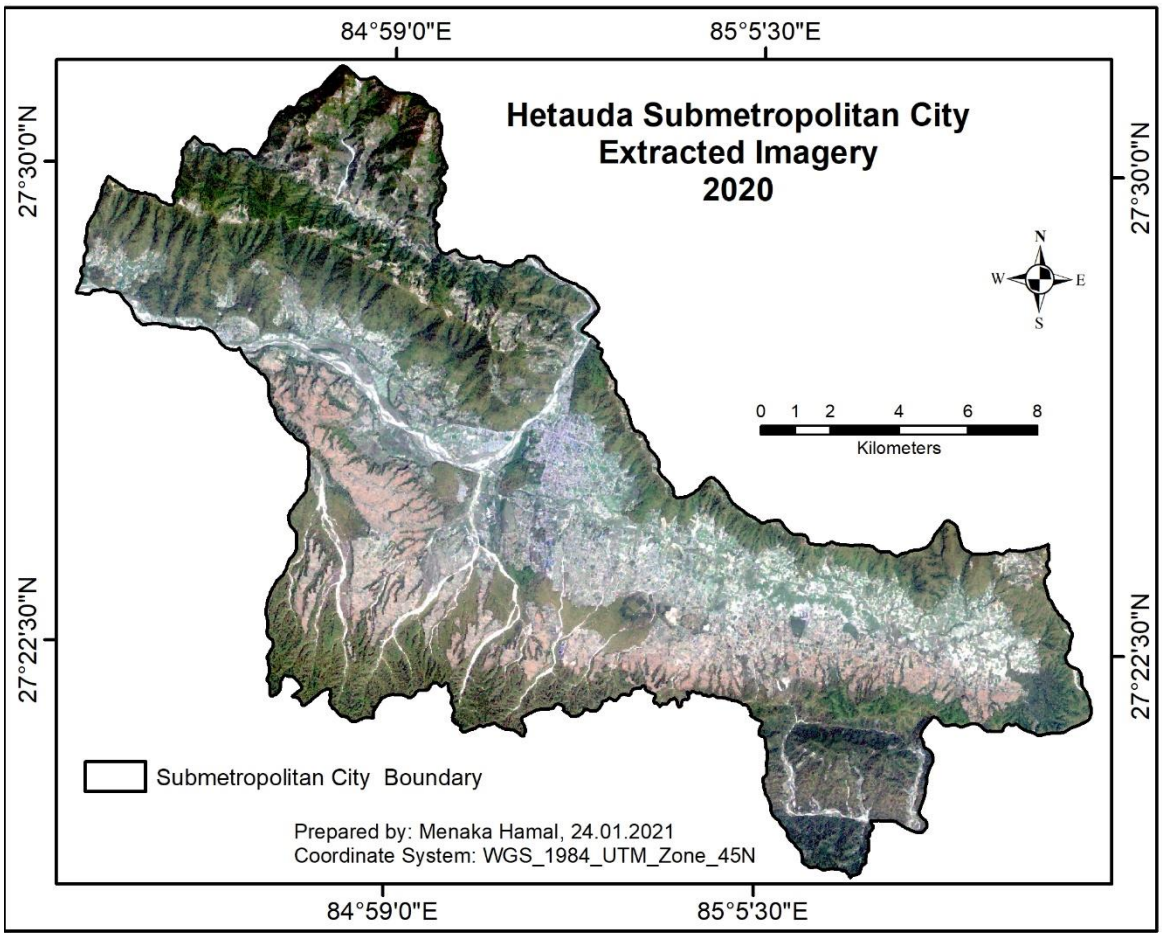

Map 2. 1. Extracted imagery by Heatauda Sub-metropolitan City boundary

Map 2.1 shows the extracted dataset from the Sentinel 2B mosaicked imagery with the city boundary.

2.4. Image Enhancement

Image enhancement has been done in digital image processing to improve the image quality and information content in it before further analysis (Lillesand et al., 2015). The widespread practice is contrast enhancement that improves the contrast in an image by stretching the range of intensity values to span the desired range values, spatial filtering that improve the naturally occurring fault, shear zone, and lines on the image. The multispectral imagery has more than RGB bands to display imagery with a false-color composite that used to identify objects more clear such as vegetation looks red because the vegetation is very reflective in NIR and the color applied is red, the deep water body looks dark due to NIR bands, in true color composite water body reflect light to dark blue as it reflected in the green wavelength and the color applied is blue. False-color composite is mostly used in remote sensing that helps to identify image objects clearly by band combination choosing bands manually as our desired requirement (Haldar, 2018).

The satellite imageries are not free from atmospheric and radiometric distortion due to cloud and the atmospheric aerosols that obscure objects on the image and affect the radiometric reflectance value that can mislead the output (Hadjimitsis & Themistocleous, 2008). To reduce those distortions, the subsetted imagery was corrected atmospherically and radiometrically to improve the image quality and information content.

2.4.1. Atmospheric Correction

The atmospheric correction is considered the most important part of the pre-processing of the satellite imagery and avoidance of it can produce erroneous results later (Hadjimitsis & Themistocleous, 2008). Therefore, imagery needs geometrically and radio-metrically corrected before being used for analysis (Lillesand et al., 2015). The data used here were already orthorectified using DEM to correct ground geometric distortions and pixel radiometric measurements were provided in Top-Of-Atmosphere (TOA) reflectance

(coded in 12 bits) with all parameters to transform them into radiances (SUHET, 2015). Though the satellite imageries look clear, these are not free from atmospheric distortion so data need to be atmospherically corrected (Tilton et al., 2015).

The correction of atmospheric effect on the image is crucial because the visible bands of shorter wavelengths are highly affected by atmospheric scatterings such as suspended gases, water vapor, and aerosols (Mustak, 2013). To remove the haze from the image, the point spread method in the haze reduction function in ERDAS was used to sharpen the imagery. This function removed the atmospheric aerosols and molecules that scatter and absorb in the atmosphere so that the visibility and readability of the image have increased.

2.4.2. Radiometric Correction

The imagery objects and background may have a uniform electronic response and different materials often reflect similar amounts of radiant flux throughout the bands so that the scene has a low contrast ratio (Lillesand et al., 2015). Similarly, the insufficient sensitivity of the sensors to detect and record the contrast of the terrain and scattering of electromagnetic energy by the atmosphere can reduce the contrast of the scene. The data distortions also occur due to the illumination of the objects so that the brightness of the objects gets affected. The majority of reflectance values were found to be below. Therefore, to normalize those values and get approximately the true values of the objects of interest, the histogram equalization was performed in ERDAS. Histogram equalization maintains the contrast of the data by applying a nonlinear contrast stretch that redistributes pixel values so that there is approximately the same number of points with each value within a range. Similarly, the noise correction was done in ERDAS using the noise reduction function. The edge-preserving smoothing technique was applied to reduce the noise so that the visibility of the obscure information increases.

Segment Mean Shift Method also works with accepted bits of raster which is free of distortion. The contrast stretching, haze correction, noise correction, histogram modification, and pseudo-coloring were done based on the nonlinear point operation method in ERDAS because this method effectively preserves edges and details of images (Haldar, 2018). The image that was enhanced using a nonlinear method in supervised classification was used for this method.

The atmospherically and radiometrically corrected imagery was used for OBIA. The rule of thumb that if the objects are not visible, the OBIA may mislead the visual interpretation of the image (Veljanovski et al., 2011). Therefore, the image that has been enhanced using a nonlinear method in supervised classification was used in OBIA.

2.5. Supervised Classification

The supervised classification techniques have been followed to extract information classes from the preprocessed extracted satellite imagery for the thematic map creation (Vaiopoulos, 1999). The simple supervised classification was performed in ERDAS Imagine to get the accuracy assessed LULC classification and the maps.

2.5.1. LULC Classification Scheme

The classification scheme covers both land use and land cover of a certain area (LaGro J. A.,2005). Following the classification system, the LULC classes have been categorized depending on the desired objectives, available features on the image, and applicability of the required ground coverage (Ai et al., (2020). The range of classes has been chosen for land use land cover classification for a specific area (FAO, 2021). This study partially followed the predefined land use land cover classes that have been used in the previous land cover study. The major LULC classification scheme developed by the Hetauda Sub-metropolitan city office has a total of ten classes, According to City profile 2017 of the city, such as barren land, built up, bush, cultivation, forest, grass, orchard, pond, and sand and

water body (GoN, 2017). Based on those classes, in this study, the pond and water body category were named a single water body class, sand and barren land was named as barren land only, bush and grassland were merged to a name grassland. The cultivation was renamed into class agriculture. Hence, there are six classes of LULc in total - Agriculture, Bare Area, Builtup Area, Forest, Grassland, and Waterbody.

Table 2. 3. Image classification scheme

SN	LULC Type	Class Description	LULC Classes for the Study
1	Cultivation	Farmland	Agriculture
2	Orchard	Fruit plantation area	
3	Barren Land	Unused degraded land	Bare Area
4	Sand	Constitutes of riverbank either from the dry or wet river	
5	Built-up	Settlements, industrial, commercial, and facilities	Builtup Area
6	Forest	Area covered by vegetation	Forest
7	Bush	Natural shrubs	Grassland
8	Grass	Pasture/herbaceous plant area	
9	Pond	Natural and artificial water-filled area	Waterbody
10	Waterbody	Area covered by flowing water	

Table 2.3 shows that the LULC types set by the Hetauda sub-metropolitan city office, a brief description of the land type, and the. Among the 10 classes in the above table, the farmland and fruit plantation area categories into an agriculture class, unused degraded land and constitutes of dry or wet riverbank are considered as the barren land, natural shrubs and pasture area given the grassland class, the natural and artificial water-filled area and flowing water come under the waterbody class. The forest that is covered by the vegetation becomes in a forest class, and built-up such as settlements, industrial, commercial, and human-built facilities fall under the built-up area category. Altogether, the six LULC classes have been used for the study.

2.5.2. Training Samples

The training samples for LULC have been a prerequisite for supervised classification (Lillesand et al., 2015). Training data has been collected based on the prior knowledge of the study area and the purpose of the study, to classify LULC into assigned classes. Training samples for the supervised classification must be both representative and complete (Lillsand et al., 2015). The role of the analyst becomes prime in taking sufficient samples in a specific geographical area.

In supervised classification, the rule of thumb that the more samples that can be used in training, the better the statistical representation of each spectral class. In theory, the number of signatures should be a minimum of the number of spectral bands plus 1 (n + 1) (Lillesand et al., 2015). Following this rule, a minimum of 4 +1 = 5 samples has been collected from each land cover based on the visual interpretation. In this study, more than five samples were collected based on how large the area coverage by the respective information classes. The number of samples has also been taken more than a hundred to adequately represent the spectral variability in an image (Talukdar et al., 2020). The number always depends upon the nature of information classes sought and the complexity of the geographic area (Lillesand et al., 2015). Looking at the coverage of the geographical area, some classes have taken more samples and some selected less but not lesser than 5 each class.

The signatures were collected from the pre-processed subset imagery following the rule of thumb that the more training samples, the better the statistical representation of each spectral class. Therefore, based on the coverage of area through visual interpretation, the required samples were drawn (Table 2.4) from the imagery for each class using polygon tool in ERDAS across the scene taking into account the samples are normally distributed for the respective land coverage in the city. Then a signature file was created to train the MLC in the supervised classification.

Table 2. 4. Number of training samples for supervised classification

SN	LULC classes	Number of Samples
1	Agriculture	47
2	Bare Area	35
3	Built-up Area	47
4	Forest	47
5	Grassland	21
6	Waterbody	35

Map 2.2 shows the number of samples – 47 polygons for each, collected from the forest, agriculture, and built-up area as compare to other classes because of the high coverage in a city. Similarly in the bare area and water body relatively less than is 35 polygons have been collected and the fewest in grassland that is 21 polygons were collected due to less coverage.

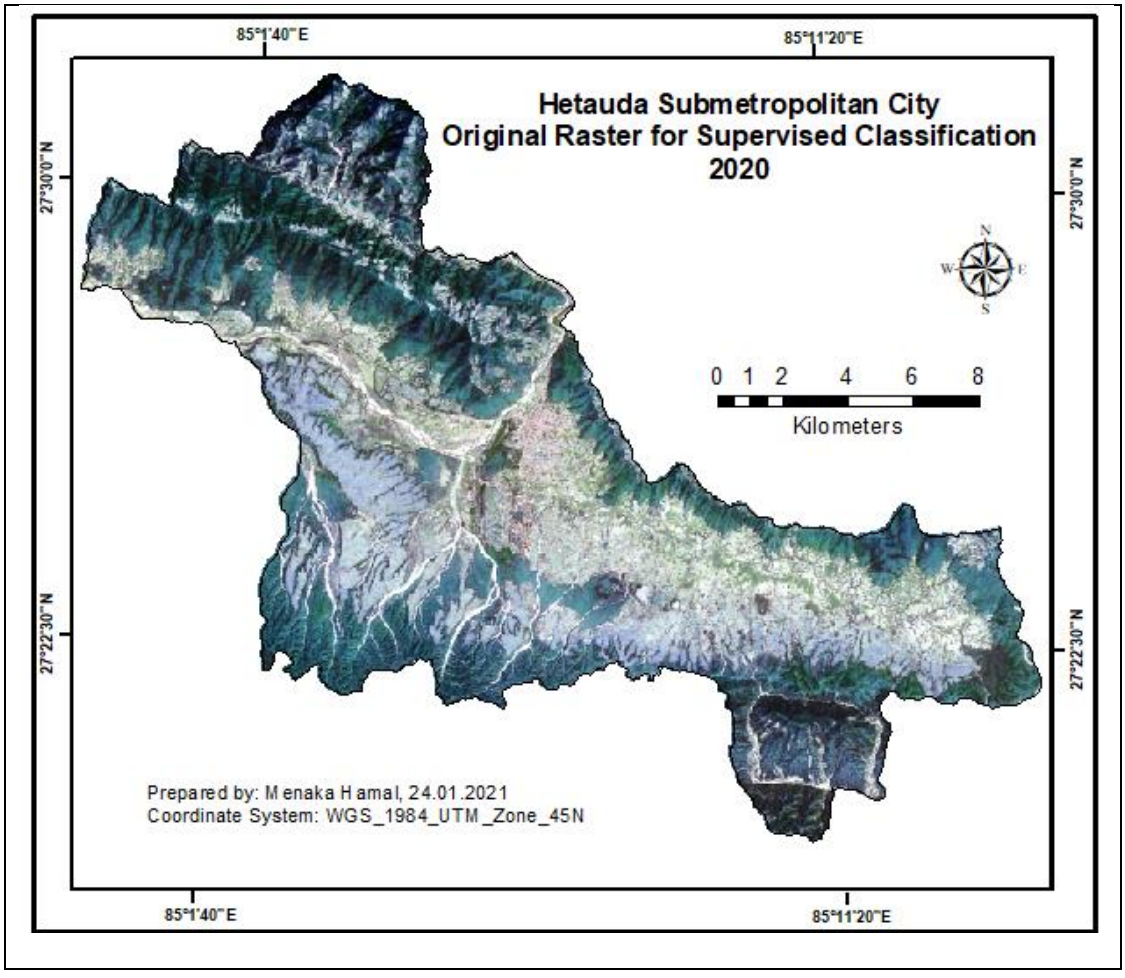

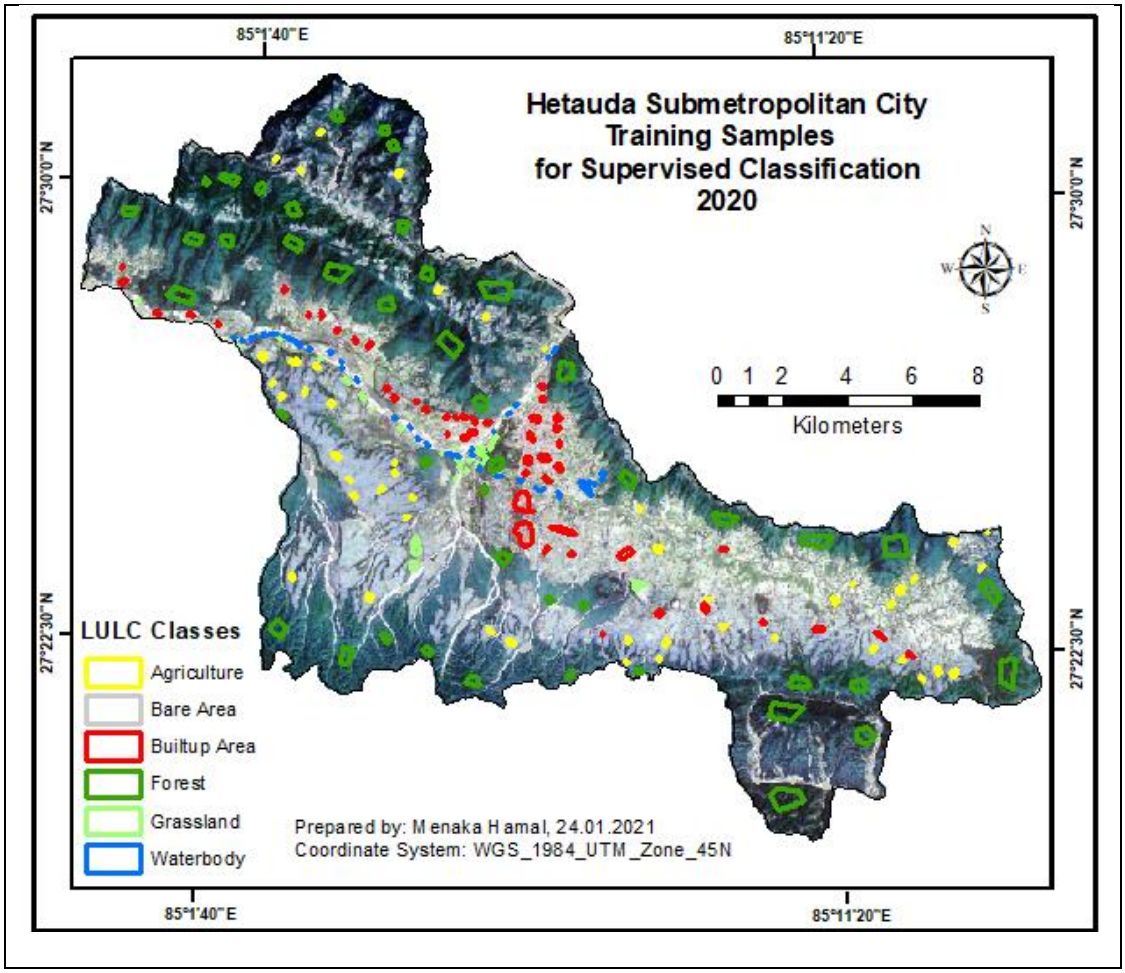

Map 2. 2. Original raster and training samples for supervised classification

Therefore, training samples were evaluated in histogram distribution (Annex 1) of individual categories whether those are normally distributed and the number of samples has been increased as much as possible depending on the coverage. The NIR histogram was repeatedly tried to be normally distributed for forest, agriculture, and grassland however the bare land and built-up area has left-skewed due to bright pixels and the water has twin pixels. The mean, standard deviation, and covariance (Annex 2) were evaluated for each category to check the relativeness of the training data. The minimum deviations were maintained for each of the classes. Similarly, the covariance value less than 1500 indicates spectrally similar (Lillesand, 2015) for the forest, agriculture, and grassland, built-up and bare land; however, the water has more than 2164 which indicates the pixels are matching with the other class (Annex 2).

2.5.3. LULC Classification

The classification stage becomes the heart of the supervised classification process where the computer-based evaluation of the spectral patterns is made using predefined decision rules to determine the identity of each pixel (Lillesand et al., 2015). To evaluate the spectral pattern based on the training samples as in interpretation keys, there are many classifiers such as minimum distance classifier, MLC, neural network, Mahalanobis distance, support vector machine etcetera. However, in this study, the MLC approach has been adopted. This algorithm has been chosen as it is known to be optimal in the sense of minimizing Bayesian error (Clark et al., 1974) and is implemented almost in all remote sensing and image processing software for pattern recognition.

Once the training samples of the required classes were collected using polygon tool in ERDAS based on the visual interpretation of the land coverage in the city, the inbuilt MLC was trained with the set of collected training samples from the same imagery to classify the unknown pixels of it.

2.5.4. Accuracy Assessment

After the classification, the accuracy assessment has become a crucial step of thematic mapping to estimate the percentage reliability of the products for further application (FAO, 2016). Further, "*A classification is not complete until its accuracy is assessed*" (Lillesand et al., 2015). The assessment in this study mainly covers the calculation of test points, allocation of those points to different classified strata, and their validation over the same location points of the original imagery to compute confusion matrix for finding out the reliability of classification.

2.5.4.1. Calculating Test Points

Finding out the required number of test points on a classified image is an initial step of accuracy assessment (Lillesand et al., 2015). The desired number of test points was

calculated based on the ratio of the area covered by each class following the rule of thumb is to have ten times the number of test points for each class (MGL, 2013). For calculating sample size, all the classes were given the rank as their area from lowest to highest. Each rank was divided by the total number of ranks and multiplied by the total number of pixels to assign the sample size for each class. Hence, the total number of pixels was 6*6*10 = 360 for the classified scene.

Table 2. 5. A sample size of test points for accuracy assessment

Class	**Ratio**	**Sample size**
Agriculture	5	5/21*360 = 86
Bare Area	4	4/21*360 = 69
Built-up Area	3	3/21*360 = 51
Forest	6	6/21*360 =103
Grass	2	2/21*360 = 34
Waterbody	1	1/21*360 = 17
Total	21	21/21*360 = 360

Table 2.5 shows that the classes that deserved the required number of test points. The ratio of the forest has the highest as it covers the large area of the city followed by agriculture, barren land, built-up area, grass, and water body. Accordingly, the calculated sample size is the highest of the forest where the lowest of the waterbody.

2.5.4.2. Allocation of the Test Points

After calculating the required sample points for each class, the stratified random procedure was implemented to allocates those points in each classified LULC using the Sampling Design Tool in ArcGIS. This tool takes all polygons with the same value of the respective class and is considered as part of the same strata (Buja & Menza, 2013). After selecting the sampling type and sampling design (Figure 2.3), the vectorized classified set of data was chosen as a sample frame in the input window. To enable sample frame, the classified raster was changed to the polygon features to meet the tool that makes classes into separate strata. After clicking the run button that enables the stratified input platform to

insert the calculated sample units in a separate column.

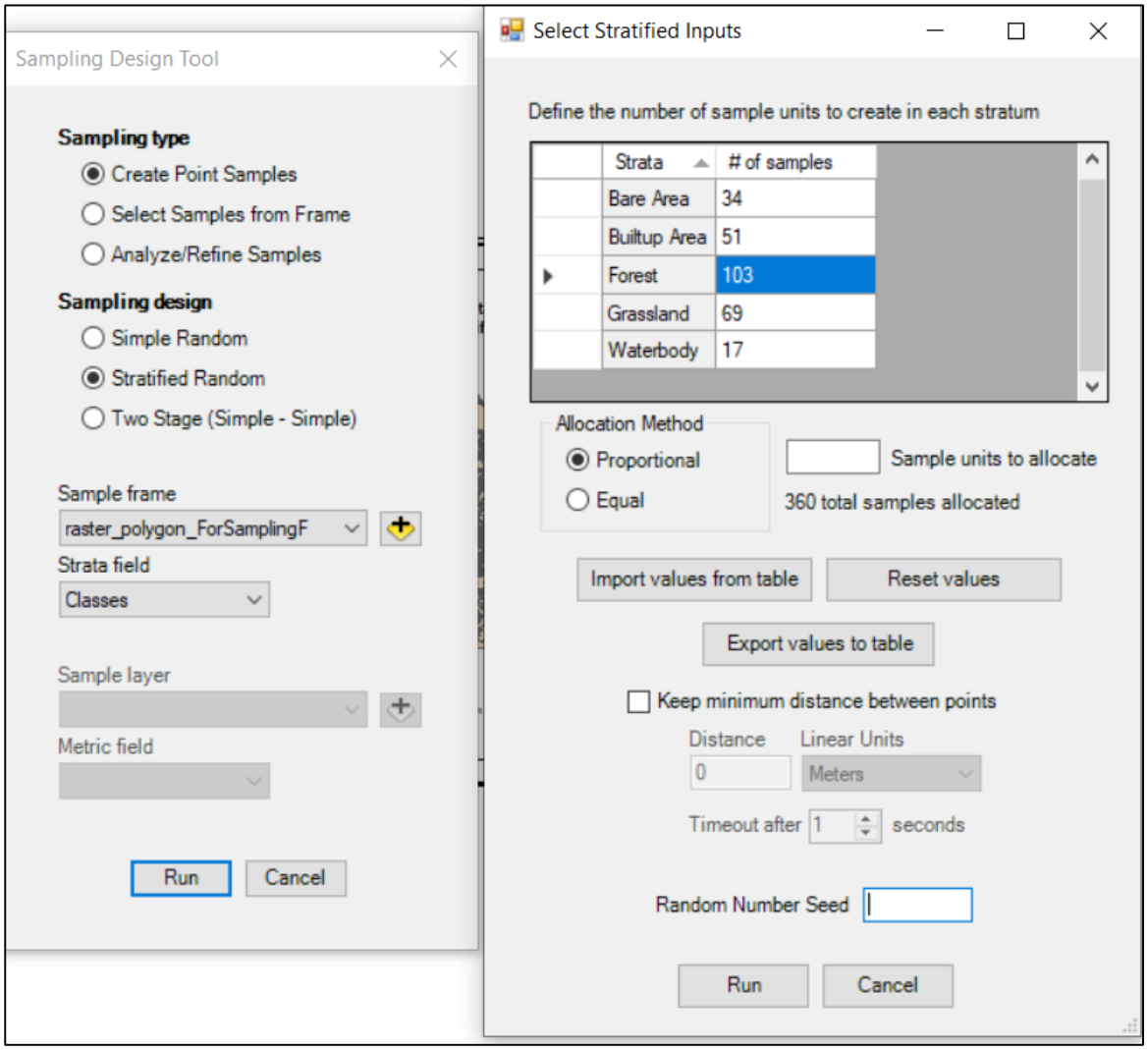

Figure 2.4. Point allocation for stratified random sampling

In Figure 2.4, the point sampling strategy was chosen to create points. The sample frame was the polygons and the strata were the polygon of each class in it. Each stratum was defined by inserting the calculated number of samples as specified in Table 2.8 considering the proportional distribution of the points across the strata. The proportionally distributed points for each stratum were considered validation points. Then the run button allowed all the allocated points to spread randomly across each stratum – forest, agriculture, grassland, bare area, built-up area, and waterbody.

2.5.4.3. Test Points Verification

The allocated points over the classified image were verified individually with the location of the original image to find out the number of correctly classified pixels (Ruppert et al., 2018). The classified maps and unclassified original imagery are loaded in ArcGIS along with the allocated points. Every point of each stratum was checked with the visual interpretation whether those are matched with the location of the original imagery. The reference points were recorded against the classified points in the attribute table to compute the confusion matrix (Map 2.3). The matrix provided the correctly classified and misclassified pixels, producer's accuracy, user accuracy, and Kappa statistics (Annand, 2017).

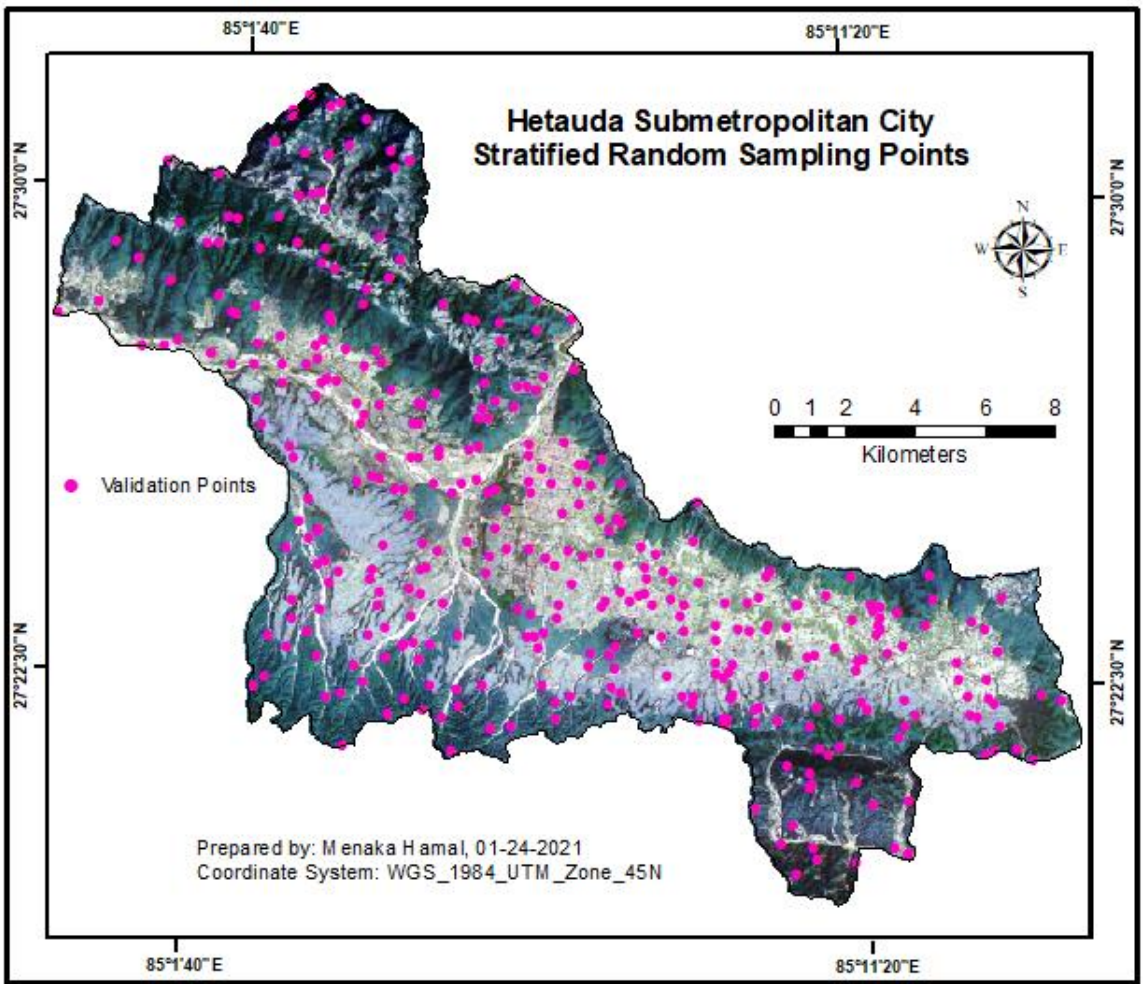

Map 2. 3. Stratified random points for accuracy assessment

The error of omission and commission was calculated based on those statistics. the whole classified map, as well as each LULC category, were compared by evaluating all the accuracy and errors.

2.5.4.4. Confusion Matrix

Following the verification of classified sample points to the reference points, the confusion matrix was computed using the ‘Compute Confusion Matrix’ tool of the spatial analyst in ArcGIS and got the total accuracy, producer accuracy, user accuracy, and Kappa statistics (Annand, 2017). The error of omission and the commission were calculated based on the user's and producer’s accuracy.

2.6. Segment Mean Shift Method

The segment mean shift method was implemented following the segment mean shift image segmentation cum supervised classification to extract the information classes from the same preprocessed imagery that was used in simple supervised classification. The entire mean shift image classification process was performed in ArcGIS.

2.6.1. Segment Mean Shift Segmentation

The image segmentation was performed based on the mean shift approach (ESRI, 2020c). The objects of the preprocessed imagery were grouped into segments as per the shapes, spectral and spatial characteristics using the Segment Mean Shift tool in ArcGIS. The tool created a segment or superpixels as per the pixel's proximity and similar spectral properties.

The segment mean shift segmentation tool demands the input of suitable parameter values that reflect the spectral and spatial characters of the objects on the imagery. The

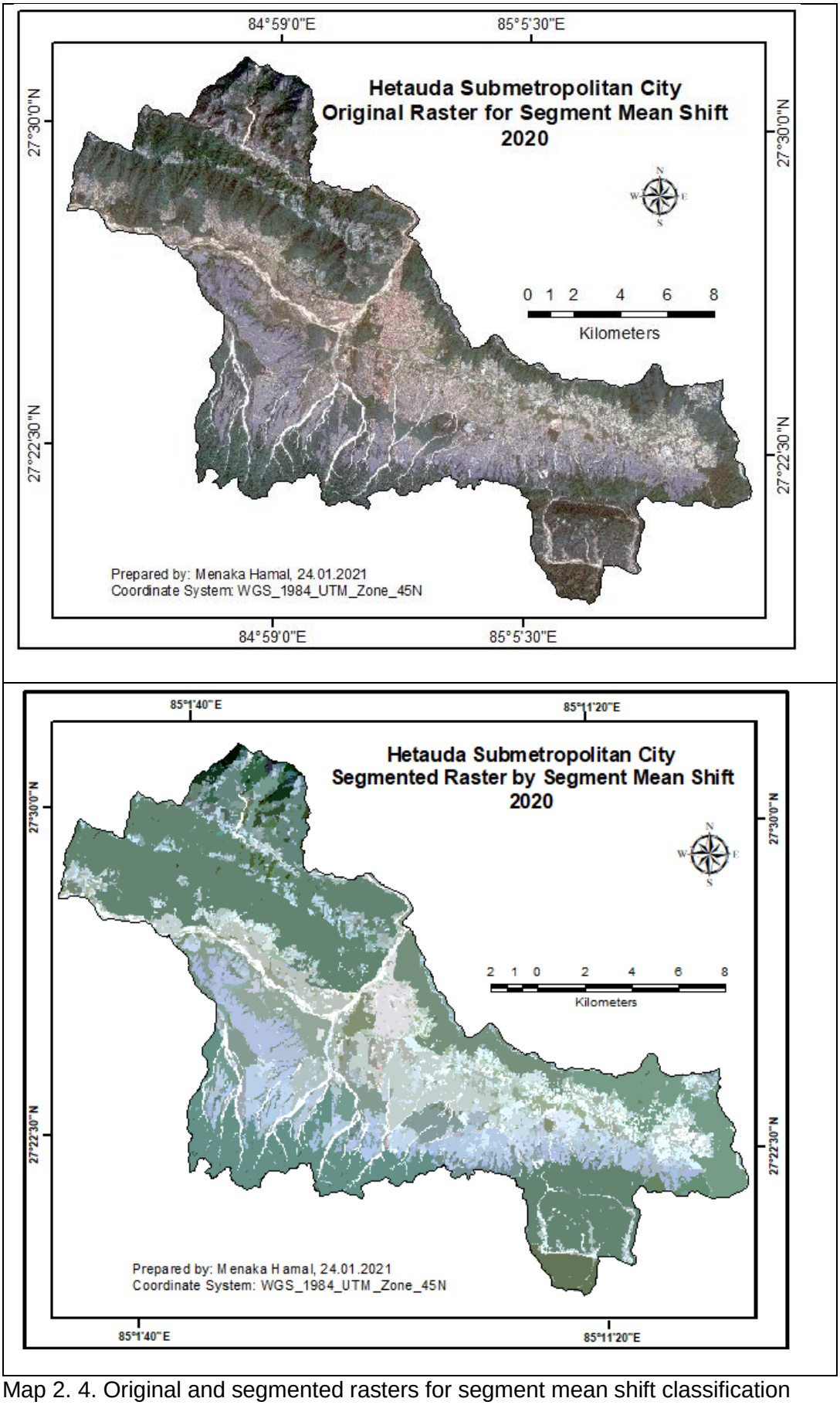

Map 2. 4. Original and segmented rasters for segment mean shift classification

user can repeatedly assign the values to determine the best fit size and shape of the segments until the size looks similar to the size of the object on the ground (ESRI, 2020b). The spectral values were iterated starting from 15.5 to 20 many times till the segments of the image are close to the real features of the scene. The lowest 15.5 has created spectrally smoother output and the highest 20 has created very small segments. The spectral value 18 was found to be relatively close to the shape of the object to meet the requirement.

Similarly, the spatial values were iterated to find out the best fit spatial value that covers the spatial objects of the scene as per our requirements. The spatial value 15 was found to be relatively the best fit for the objects of the imagery. Likewise, the segment size was iterated in complement with the spectral and spatial value that has the best fit. After the many iterations, the minimum segment size was set to 20 so that the superpixels smaller than this size merge with their best fitting neighbor segment. After finding the best fit spectral, spatial, and segment size value, the mean shift algorithm was run for creating superpixels throughout the imagery. The two maps in Map 2.4 - the above map presenting the objects before segmentation on the preprocessed original raster and the below has objects or superpixels after segmented imagery based on the best-fit input criteria.

2.6.2. Training Samples

The training sample has been collected in segment mean shift classification after completing segmentation with the segment mean shift algorithm. In a mean shift segmented raster, each superpixel was found to be represented by one average color value (Kurlin & Harvey, 2018). The pixel values were found to be similar in a segment whether the size is big or small or varies in color. Therefore, the sample was drawn from whole or partial segments depends on the size.

The samples were selected among the mean shift segmented superpixels using the polygon tool in ArcGIS. While collecting samples, the visual understanding of the color of

the superpixel that reflects the object and collect as a training dataset among many segments was quite challenging (Lillesand et al., 2015). However, the knowledge of the area made it quite easy in selecting samples (Stutz et al., 2018). As described in chapter-2 of ESRI's understanding of segmentation and classification chapter-2 (ESRI, 2020), the number of samples for a parametric classifier - the maximum likelihood classifier (MLC) needs a statistically significant number of samples to produce a meaningful probability density function and for that, need at least 20 samples with 100 pixels for each class to be statistically significant for MLC (ESRI, 2020).

Considering the minimum number of samples to be taken and following the rule of thumb that the more samples, the better the statistical representation of each spectral class, the maximum number of samples were collected based on the size of the coverage of each class (Table 2.6). The forest, agriculture, and built-up pixels were drawn relatively more considering the area covered by the class forest and similarly performed so for other classes as well (Figure 2.3). The forest features were found relatively high across the outskirts of the city except for the river outlet at the western side and some forest patches lie at the center of the city. Similarly, the distinct superpixels of the built-up area were concentrated at the center of the city presenting the dense settlements. The majority of the southern area of the city was surrounded by agricultural land and a few patches of it were located in the northern part. The grass segments were a few found adjacent to the forest area. The majority of bare land superpixels were located along river ridges and dry streams. The water segments were located along the river and the artificial water reservoirs such as fish farming and ponds for recreation.

Table 2. 6. Number of training samples for segment mean shift method

SN	LULC classes	Number of Samples
1	Agriculture	47
2	Bare Area	35
3	Builtup Area	47
4	Forest	47
5	Grassland	21
6	Waterbody	35

Table 2.6 shows the total number of samples taken for the segment mean shift classification. The number of samples was taken depending on the coverage of the geographical area. Following the supervised classification technique, the 47 polygon samples were taken for agriculture, forest, and built-up area considering the highest number with the large coverage; 35 for the bare area and water body which are slightly less than those segments; and 21 grasslands samples.

The first map in Map 2.5 presenting the segment mean shift segmented raster with visible clustered superpixels based on the reflectance of each feature on the imagery. This is prepared raster before drawing training samples. The second map below is showing the training samples of the different classes as per the assigned color code representing the respective LULC classes that are supposed to be trained for MLC.

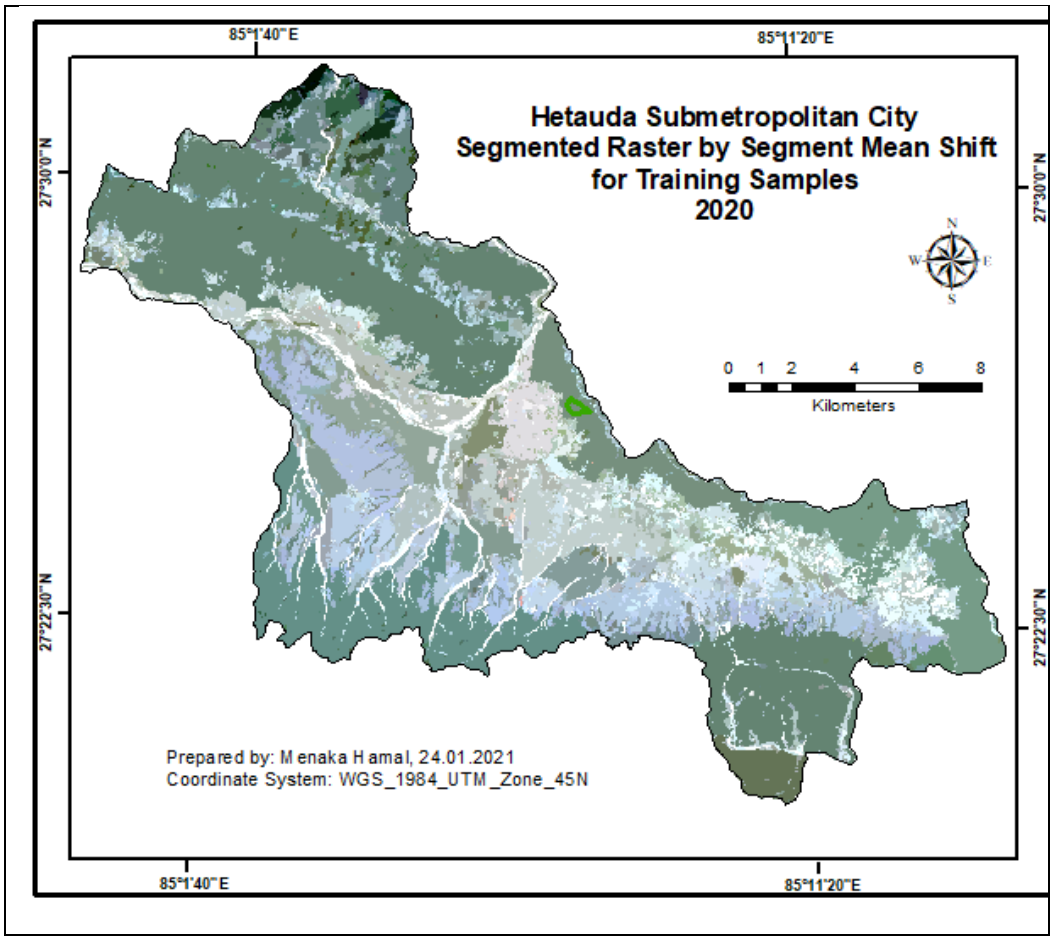

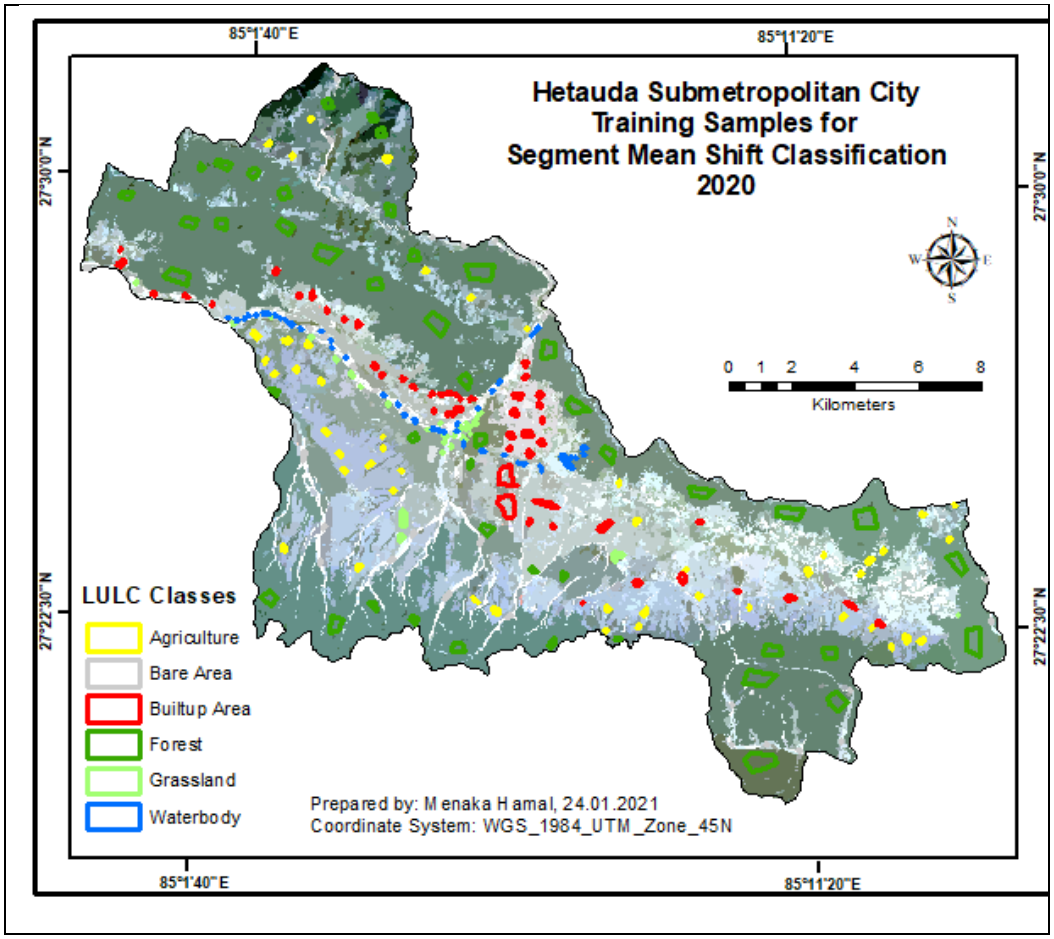

Map 2. 5. Training samples for segment mean shift

Sufficient samples and their Gaussian distribution be maintained for the maximum-likelihood classifier and the class sample mean vectors and covariance matrices must be calculated (Schowengerdt, 2007). Therefore, the training samples were evaluated looking at the distribution of the samples in the histogram for each category whether those are normally distributed. Likewise, the standard deviation and covariance statistics of each band were evaluated where those are sufficient to train the classifier

Annex 3 shows that the NIR histogram of the training data is normally distributed for the forest, built-up, and agriculture however the bare land, grassland, and water body histograms are right-skewed due to dark pixels. The standard deviation was relatively low and similar of all bands of training data across the forest, agriculture, and built-up area

whereas the water body and bare area have a few more at band three as compare to other bands.

The statistics table in Annex 3 shows that the covariance of forest training data has a low covariance value in three bands which indicates that the bands are providing independent information and better separation between the classes. Similarly in agriculture, and built-up training data has no overlap with other classes. However, the bare land that is not held by a person and any organization and few shrubs over there can make diversion of some pixels either to the grassland pixels or to the agriculture. Therefore the covariance values are high in Band 2 and 3 of bare area pixels. The covariance value of grassland training data pixels is also high in band 3. The waterbody training data has a high variance compared to the other training data due to the different colors of the river water and the fishery ponds. Fishery pond's training pixels would match with the agriculture training pixels.

2.6.3. LULC Classification

The LULC classification was performed after the training samples collected from the segment mean shift segmented raster using polygon tool in ArcGIS based on the visual interpretation of the land coverage in the city. The signature file was created containing the mean for each class, number of pixels, and variance and covariance matrix for the training class. This file was used to train the MLC to classify the pixels of the whole imagery based on the signatures (Clark et al., 1979).

2.6.4. Accuracy Assessment

After the classification of whole imagery through MLC in segment mean shift classification method, the accuracy assessment was performed to estimate the percentage reliability of the classified imagery for further application (FAO, 2016). The point sampling strategy for accuracy assessment was adopted.

2.6.4.1. Calculating Test Points

The calculated test points for simple supervised classification were used for the segment mean shift classification. The total 360 points - 103 for the forest, 34 for grass, 86 for agriculture, 51 for Built-up area, 69 for the bare area, 17 for the waterbody, were taken as the validation points (Table 2.5).

2.6.4.2. Allocation of the Test Points

The test points were allocated using the stratified random procedure to allocates calculated points in table 2.5 for each classified LULC using the Sampling Design Tool in ArcGIS. After selecting the sampling type and sampling design in Figure 2.3, the vectorized classified set of data was chosen as a sample frame. To enable sample frame, the classified raster was changed to the polygon features to meet the tool that makes classes into separate strata. After clicking the run button that enables the stratified input platform to insert calculated sample units in a separated column. Each stratum was defined by inserting the calculated number of samples as specified in Table 2.8 considering the proportional distribution of the points across the strata. Then the run button allowed all the allocated points to spread randomly across each stratum – forest, agriculture, grassland, bare area, built-up area, and waterbody.

2.6.4.3. Verification of Test Points

The test points verification was done individually with the location of the original image to find out the number of correctly classified pixels (Ruppert et al., 2018). The classified maps and unclassified original imagery are loaded in ArcGIS along with the allocated points. Every point of each stratum was checked with the visual interpretation whether those are matched with the location of the original imagery. The reference points were recorded against the classified points in the attribute table.

2.6.4.4. Confusion Matrix

After the verification of classified points with reference points in the attribute table, the confusion matrix was computed using the 'Compute Confusion Matrix' tool of the spatial analyst in ArcGIS. Based on the computed statistics in the matrix, got the total accuracy, producer accuracy, user accuracy, and Kappa statistics (Annand, 2017). The error of omission and the commission were calculated.

2.7. OBIA

The OBIA was performed following the multiresolution segmentation cum supervised classification in eCognition to extract the information classes from the same preprocessed imagery that was used in simple supervised classification.

2.7.1. Image Segmentation

The preprocessed imagery was used for the image segmentation (Hossain & Chen, 2019) in OBIA. The widely used algorithm – the Multiresolution Segmentation which is a bottom-up region merging technique that considers each pixel as a separate object and pairs those objects into bigger objects (Darwish et al., 2003), was applied to segment image objects.

Table 2. 7. Homogeneity criteria at a different level of segmentation for OBIA

Level	Scale Factor	Shape	Compactness
Level 1	40	0.1	0.5
Level 2	40	0.2	0.6
Level 3	40	0.3	0.7

The algorithm was executed at a different level (Table 2.7) to know the best fit scale factor and homogeneity criterion for that particular area image. For that, the iteration was executed at different levels of shapes and compactness values. The first level was created with scale factor 40, shape 0.1, and compactness 0.5. The majority of the intersected image objects were larger than the feature objects found based on visual checking.

Original Raster for Object-Based Image Analysis

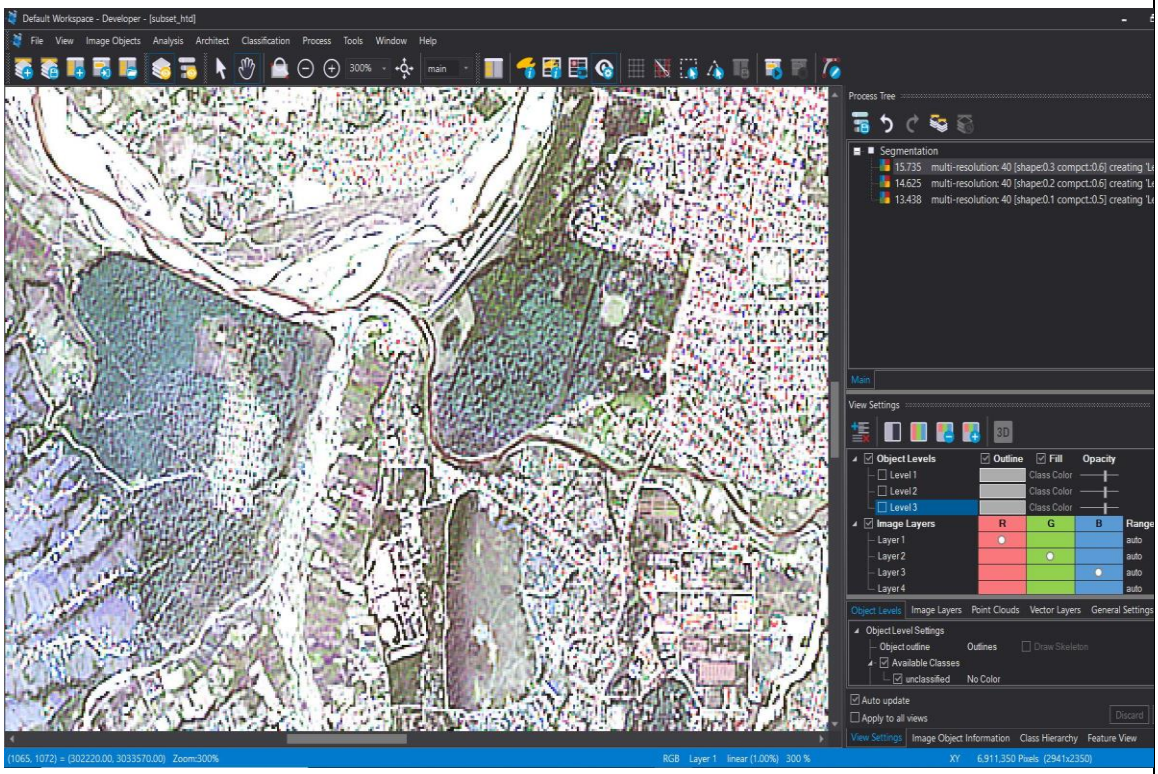

Segmented Raster for Object-Based Image Analysis

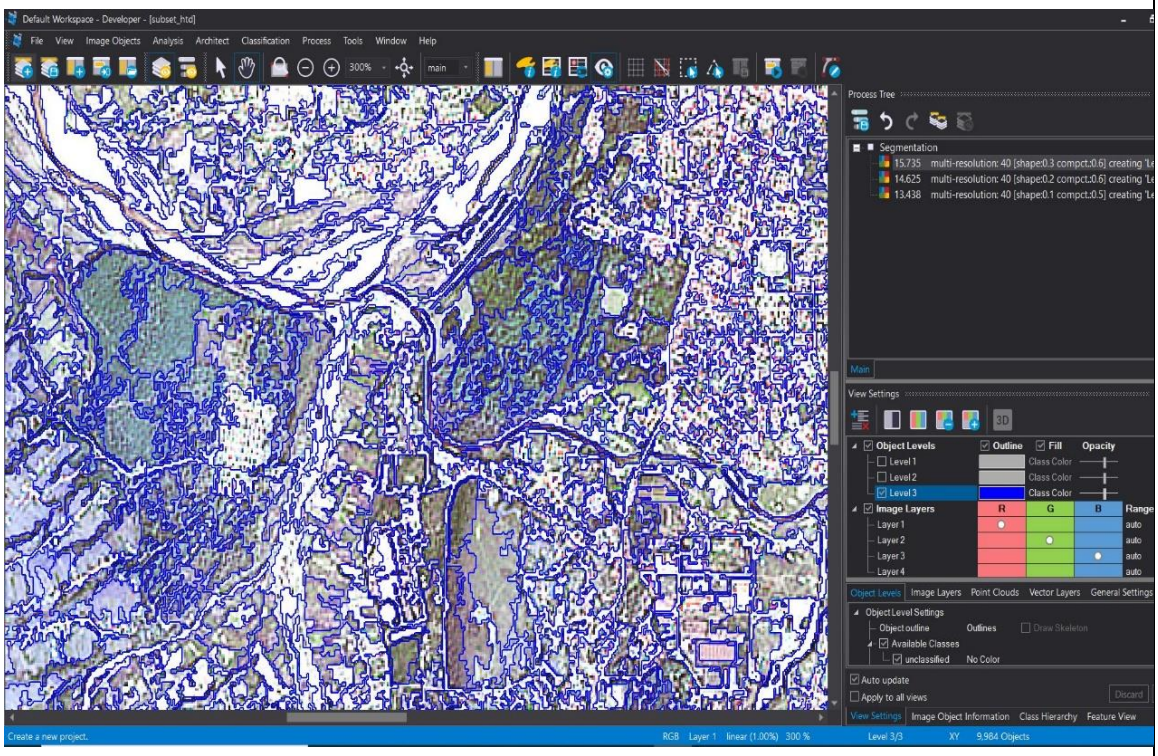

Figure 2.5. Original and segmented raster for OBIA

Therefore, the homogeneity criteria were altered in the second level. The shape was changed to 0.2 and the compactness changed to 0.6 to look at whether the segments are close to real objects by visual interpretation. The segmented objects were found to be relatively large in the second iteration after visual interpretation.

Therefore, the third iteration was executed; in this, the homogeneity criterion has been changed; the shape and compactness were increased. The shape increased to 0.3 and the compactness changed to 0.7, and again run for the multiresolution segmentation with the threshold of 40 remains unchanged. The segments produced by the third execution were a relatively better fit to the objects of the area. Therefore Level 3 homogeneity criterion of Table 2.7 is considered to be classified later.

Figure 2.5 depicts that the original raster clip in eCognition developer suite before segmentation showing the natural features on the ground. The below is the Level 3 segmented image or vectorized raster with the blue boundary lines showing a relatively close boundary to the features after three iterations with different homogeneity criteria – scale factor, shape, and compactness.

2.7.2. Training Samples for OBIA

Training sample collection based on the knowledge of the geographical area is a crucial step for every supervised classification (Lillesand et al., 2015). After the segmentation, the sample collection procedure was followed in OBIA. The training samples were drawn from the segmented raster that was vectorized by a multiresolution segmentation tool in eCognition for each class. Initially, the classes name were assigned by hierarchy for each category and select the standard color that was supposed to be displayed in the classified map later. Then, the standard nearest neighbor expression was generated to allow the algorithms for finding the specific feature that is closest to each other and the parent class has chosen to display (Figure 2.5). After generating classes, the algorithm, color, and

training sites were selected for each class based on visual interpretation of the objects in the imagery.

The rule of thumb that the more training samples for each class, the chance to get the result accurate (Anand, 2018). Therefore, the number of training samples from every class was drawn based on the number of segments available in the area coverage. Based on available vectorized polygons, the training datasets for each class were selected from the scene.

Table 2. 8. Training samples for OBIA

SN	LULC classes	Number of Samples
1	Agriculture	50
2	Bare Area	40
3	Builtup Area	40
4	Forest	50
5	Grassland	20
6	Waterbody	35

Table 2.8 shows that the LULC classes and the number of training samples drawn from the segmented raster to train the classifier. The number of segments varies depending on the area coverage by each class; the higher the features more the samples and vice versa. The more segments lied on forest and agricultural land, 50 for each class were selected. Similarly, 40 for built-up and so bare land. The 35 segments for a water body and 20 for grassland were drawn to train the classifier.

The above figure of Figure 2.6 depicts that the segmented raster in eCognition showing the segmented features on the ground. The visible features include forest patches, the river at the center, agricultural land, built-up, grasses, and the bare area adjacent to the riverbank, and so on. The below figure shows the segments of those objects with the blue boundary and the color-filled selected polygons taken from the vectorized raster for each class of imagery. The sample color-filled polygons showing the color of respective LULC classes that are supposed to be visualized after classification.

Segmented Raster for Object-Based Image Analysis

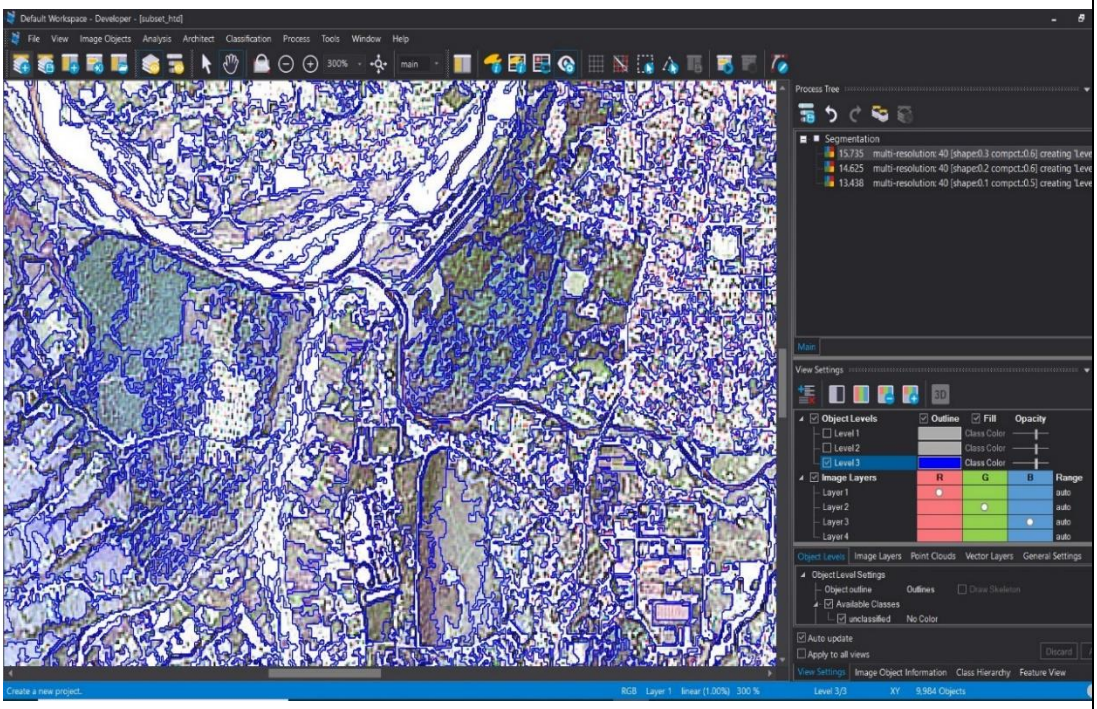

Training Samples for Object-Based Image Analysis

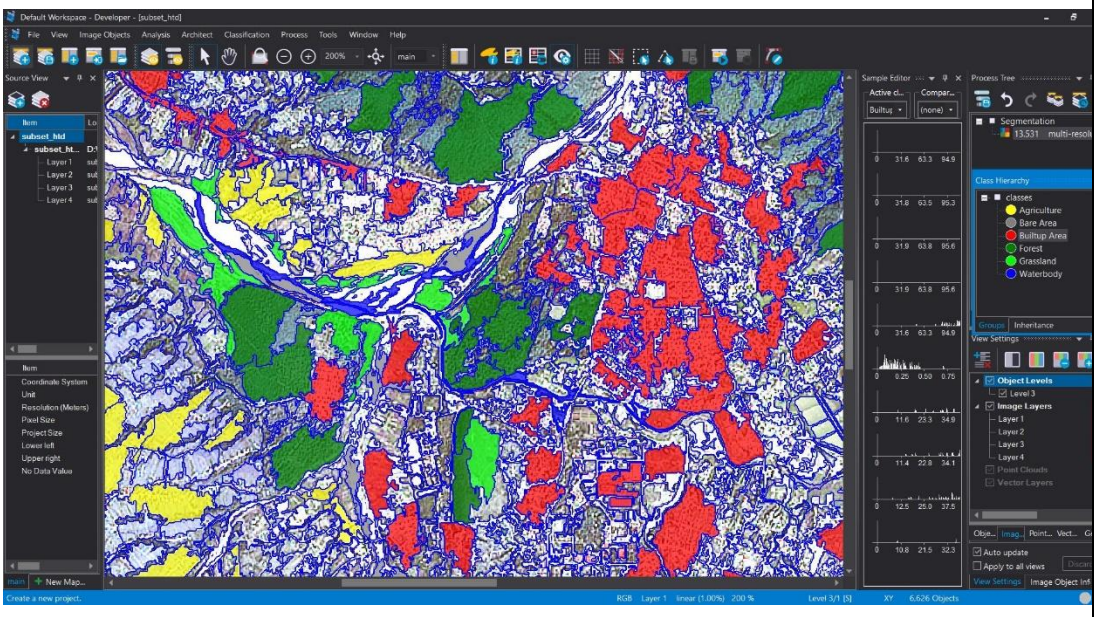

Figure 2.6. Original and training samples for OBIA

The distribution of training samples was evaluated through a histogram for individual categories (Annex 5). The effort was made to become the histogram normally distributed for each band (ESRI, 2020b) by recollecting and deleting the sample polygons. The mean

and standard deviation were evaluated whether samples are good enough to train the classifier (Lillesand et al., 2015). The agriculture, built-up, and forest training data were found to be normally distributed, and the histogram found near mean values. The standard deviation was also found low but in NIR band has a high standard deviation due to shadow pixels among the vegetation. The bare area histogram was left-skewed due to bright pixels but the standard deviation is low shows that nearly similar pixels existed in this class. In the case of grassland, after many collections based on the visual interpretation, the histogram showed that the data sparsely distributed from the mean value and standard deviation is comparatively high.

2.7.3. LULC Classification

After evaluating selected samples for each class, the classification step was carried out. For that. the Nearest Neighbor classifier was implemented to classify the whole imagery based on the training dataset as this classifier has been considered simple to implement and effective with the huge training dataset (eCognition, 2021). The algorithm has been executed in the class hierarchy window. Initially, the standard nearest neighbor expression was inserted into each assigned class and added object features layer values of mean and standard deviation to the standard nearest neighbor feature space (GISGeography, 2021). Then, the classification and hierarchical classification algorithm was executed in the process window to classify all objects in the entire image based on the selected samples.

2.7.4. Accuracy Assessment

The accuracy assessment was done for the classified imagery as a final step of classification was performed to estimate the percentage reliability of the classified image in OBIA as well. The point-based assessment was adopted with the same process as the simple supervised classifications.

2.7.4.1. Calculating Test Points

The number of test points calculated in simple supervised classification in Table 2.5 was used for the accuracy assessment in OBIA. Overall 360 points - 103 for the forest, 34 for grass, 86 for agriculture, 51 for the Built-up area, 69 for the bare area, and 17 for the waterbody were taken as LULC validation points.

2.7.4.2. Allocation of the Test Points

The test points were allocated using the stratified random sampling platform provided in Sampling Design Tool in Figure 2.4. All the calculated sample points of Table 2.5 were inserted and run for random distribution of points across each stratum. The procedure has been followed in OBIA as stated in simple supervised classifications.

2.6.4.3. Test Points Verification

The randomly distributed test points of the classified image were verified with the same location of the preprocessed imagery in ArcGIS following the procedure stated in the simple supervised classifications for the OBIA.

2.6.4.4. Computation of Confusion Matrix

The confusion matrix was computed after the verification of classified points with ground-truth points in the attribute table using Compute Confusion Matrix tool of Spatial Analyst. The matrix provided the total accuracy, producer accuracy, user accuracy, and Kappa statistics (Annand, 2017). The error of commission and error of omission was calculated based on the user's accuracy and producer's accuracy information of the matrix respectively.

The image classification and the accuracy assessment with three methods were performed.

Chapter-3: Result and Discussion

This chapter gives the accuracy assessed LULC maps prepared by using three classification methods with the area and percentage coverage of each thematic class.

3.1. LULC 2020 in the Supervised Classification Method

The metropolitan city is mostly covered by the forest in the northwest and the southeast region which is denoted by the leafy green color on Map 3.1. The forest patches are visible at the center of the city and surrounded by agricultural land that is denoted with yellow

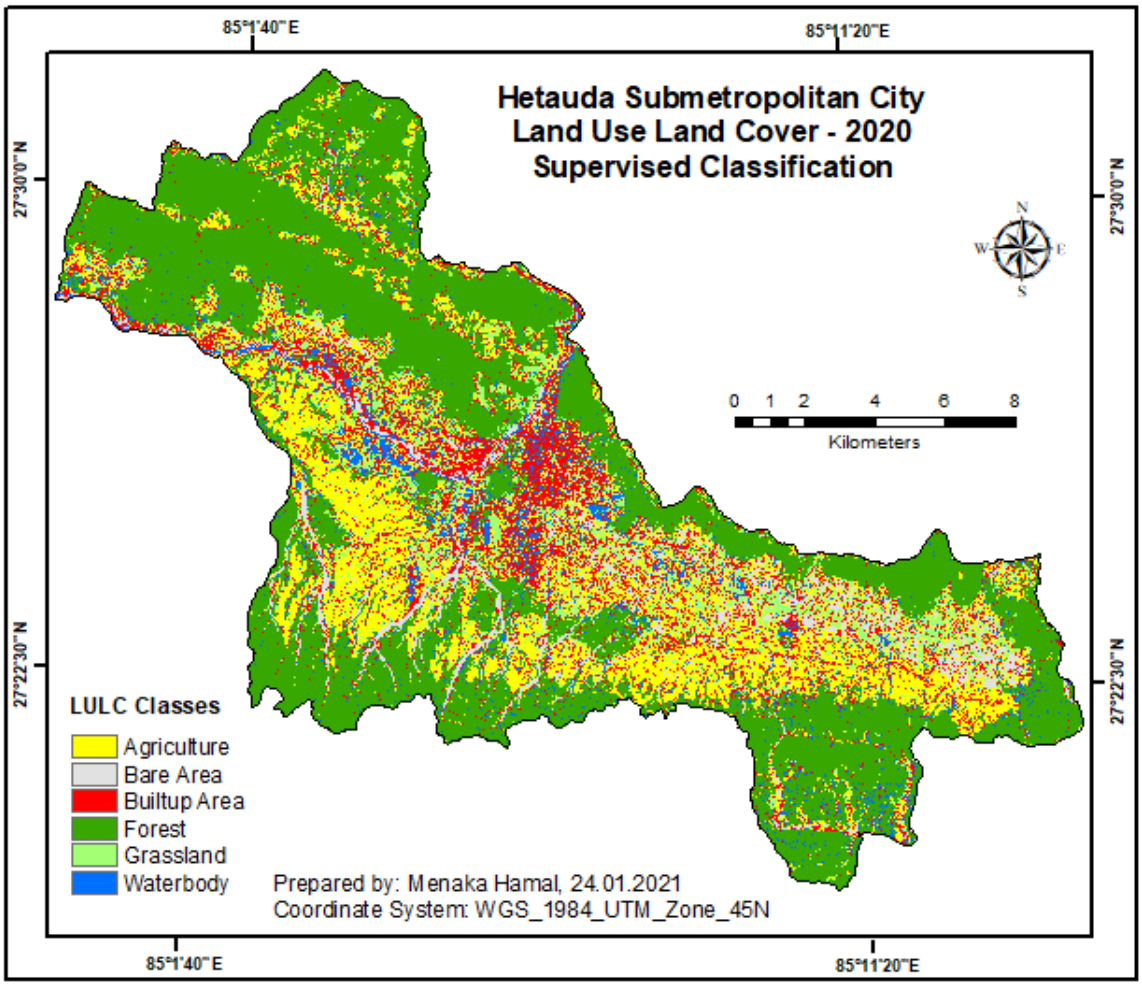

Map 3. 1. Land Use Land Cover 2020 in supervised classification

color. The forest area has more spacious and becomes dense due to the natural forest and the forest managed by the community and the department. Similarly, the forest protection

program has been implementing in a national forest as well as community forest for years hence the degraded land has converted to bushy land and this converted to the forest.

The majority of the built-up area is located at the center of the city indicated red and sprawl towards its periphery mostly due to the people's interest settling near and around the east-west highway; mostly people reside from the remote part of the city. The water body was found to be located at the center and the settlement due to the flowing river nearby and the increasing interest of local people in fish farming. The bare area with grey color denotes the sand at the ridge of the riverbank spread over the north to the west to the center of the city, degraded land, and dry stream sprawl in the southern part along the forest and the agriculture. The grass patches were found to be sparse across the forest and agricultural land. Map 3.1 presenting the LULC map 2020 with six classes of the city prepared after using the supervised classification method.

The area of the LULC was calculated from the classified map. Table 3.1 depicts that the forest coverage was found to be 127.8 square kilometers in 2020 that occupy 48.8 % which is considered to be the highest coverage among six classes. Similarly, the agricultural land occupies 47 Sq Km which is 18 % of the total coverage. According to the municipal source, the agricultural land is depleting rapidly. This study also reflects that the cultivated area is found to be dramatically reduced in comparison to the percentage coverage in 2010; 48% of the arable land was deduced to 18% in 2020. The major reason would be the influx of migrants from other districts and the rural part of the city itself as well and started making buildings so that the agriculture could be change into the built-up area. The residential areas are emerging haphazardly in the sub-metropolitan city. According to the city profile, the built-up area in the city was 6.15% in 2010 (Metropolitan, 2017). The area has been increased by 50% i.e. 13 % in 2020 (Table 3.1). Besides the migrants' interest to build a

house, increasing built-up area could be a reason for private and individual land brokers. They buy agricultural land and turn it into residential plots with higher resale value. The people have been following the same trend to gain profit over the years. Similarly, the east-west highway, the link road joining the main roads as well as parallel roads development is rapid in the city; that would be the reason for building houses along the roadsides and landless squatters that leads to rising the built-up area in the city.

Table 3. 1. LULC coverage in supervised classification

LULC Classes	**Area Sq Km**	**Percentage**
Agriculture	47.0	18.0
Bare Area	14.2	5.4
Builtup Area	34.0	13.0
Forest	127.8	48.8
Grass	24.8	9.5
Waterbody	13.9	5.3

The grassland covers an area of 24.8 sq KM which occupy 9.5 % of the city in 2020 whereas it was approximately covered 3% in 2010. The bushy and grassy area has increased by three times more in this study would be due to an increase in fallow land and the community-based forest program implemented in the city. The bushes came across the field due to illegal fire especially April/May and haphazard logging (Kissinger & Herold, 2017).

The city has a 14.2 square KM bare area which is a 5.4% of the total coverage – the second-lowest land cover of the city. It was declined by 2% as compared to the area of 2010, the reason would be an increment of households and utilized the area by the landless squatters; this land was converted into either built-up or agricultural land. The seasonal onset of rainfall makes the river flow high during summer and gets dry or low flow during the dry season as a result the dry exposed sediments are deposited along the riverside.

The water covers 13.9 Sq KM which includes 5.3 % of the total land. The coverage includes ririversstreams, and ponds in the city; it has increased in comparison to the area coverage by 0.97% in 2010. In addition to the running water, the ponds are constructed for the fishery

would lead to an increased waterbody in the city. The Bagmati River flows from the north and takes a path to the west in the middle of the city and the Karra stream runs from east to west and conjunct with the river at the center.

3.2. Confusion Matrix in Supervised Classification

The image classification process always demands the accuracy of thematic maps before being front to the users (Foody, 2013). The assessment output may vary from application to application but need to rely on the resulted quantitative output to know the map reliability (Cagalton, 2002). According to Thomlinson et al., (1999), the minimum overall accuracy should be 85% and each class accuracy should be 70%. If the classified accuracy of the data meets that requirement, the data considered relatively accurate to the ground. Similarly, Anderson et al., (1976), states that an acceptable accuracy limit for satellite land cover classifications is 85 percent. Cagalton, (2002) stressed the same thing. Considering that accuracy limit, the reclassification was done for LULC of the sub-metropolitan city to meet the minimum requirement.

Table 3. 2. Confusion matrix in supervised classification

ClassValue	Agriculture	Bare Area	Builtup Area	Forest	Grassland	Waterbody	Total	User's Accuracy
Agriculture	76	0	6	1	3	0	86	0.88
Bare Area	4	25	5	0	0	0	34	0.74
Builtup Area	3	7	37	3	1	0	51	0.73
Forest	0	0	1	101	1	0	103	0.98
Grassland	7	0	5	1	55	0	69	0.80
Waterbody	0	0	2	3	0	12	17	0.71
Total	90	32	56	109	60	12	360	
Producer's Accuracy	0.84	0.78	0.66	0.93	0.92	1.00		
Overall Accuracy								**0.85**
Kappa								**0.81**

Table 3. 2 shows that the summary outputs of a quantitative accuracy assessment of the classified map taking the reference pixel at the horizontal and classified pixels at the vertical site of the scene.

Similarly, in Table 2.6, out of 360 pixels, a total of 306 are correctly classified which gives 85% overall accuracy; that means the classified image has a 15 % error in the overall image. The matrix shows that 101 out of 103 forest pixels are correctly classified which gives 93 % producer accuracy and the remaining 7% pixels are omitted from the classified coverage of the forest; the majority of omitted pixels lie on the built-up area might due to the farm forest; and waterbody due to the tree shadows that affect on the low reflectance. In agriculture**,** 76 out of 86 pixels are correctly classified and the rest of those lies on the built-up area might due to kitchen garden and orchard, on the grassland might be the reason farm crop near the busy area, and on the bare area due to the degraded and not used for any purpose. In a built-up area, out of 51, 37 pixels are 73% correctly classified. Similarly in the bare area and water body have 25 and 12 correctly classified pixels respectively.

The user's accuracy (UA) for the forest is 98% which is relatively found highest among all LULC classes from the point of view of the map user, the 98% forest class is accurate or it is reliable to that extent for further use. Though the producer's accuracy (PA) for a forest is 93%, the reliability is 5% more correct than this. The PA is 84% for agriculture and UA is 88%. The agriculture accuracy shows that the identified agriculture area was found less in the image than the actual coverage of it is high on the ground. Similarly, for the built-up area, the UA is 73% whereas the PA is 66%. On the contrary. Though 92% of the reference grassland has been correctly identified as "grassland", only 80% of the area identified as grassland. Likewise, 78% of the reference bare area was correctly identified, only 74% of that area identified as actual bare area. Similarly, 100% of the water body was identified as waterbody, but the actual bare area was found to be 71%.

The kappa is one of the commonly used statistics to test the degree of agreement by chance (Viera & Garrett, 2005). The values range from 0 to 1 where 0 interprets no agreement between the classified and reference images and 1 gives the classified images and the ground truth images are identical (Cohen, 1960). So, the higher the kappa coefficient, the more accurate the classification is. The level of the agreement depends on the value of Kappa that gives the percentage reliability of the data. The value 0 to 0.20 gives the 0-4% reliability that interprets no agreement, 0.21 to 0.39 gives 4-15% reliability with the minimal agreement, 0.40 to 0.59 gives 15-35% reliability that interprets the weak level of agreement, 0.60 to 0.79 gives 35-63% reliability with the moderate agreement, 0.80 to 0.90 gives 64-81% reliability interprets the strong level of agreement and bove 0.90 gives 82-100% that interprets the almost perfect level of agreement (Mchugh, 2012).

To test the degree of reliability of each map, the Kappa statistics were generated along with the confusion matrix table in ArcGIS. Table 3.2 shows that the kappa statistics 0.81 which gives the 64-81% reliability interprets the strong level of agreement between classified and original map.

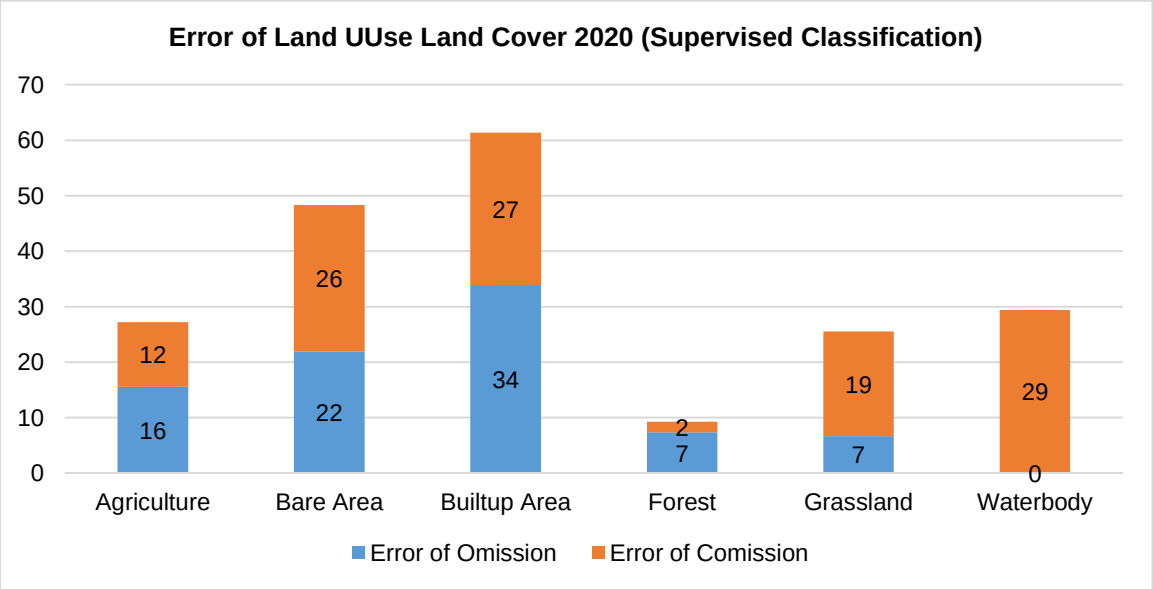

Figure 3. 1. Omission and commission error of supervised classification

Figure 3.1 depicts the percentage error that occurred in classified maps prepared using the supervised classification method. The forest has the least error of commission which is 2% whereas the built-up area has the highest that is 27 followed by the 26 of bare area. The error of omission has not occurred in water bodies followed by least in the forest as well as grassland with 7% whereas it is highest in the built-up area by 34 % followed by the bare area by 22%.

3.3. LULC 2020 in Segment Mean Shift Method

The segment mean shift classification with the Sentinel 2B imagery has LULC 2020 output, the area coverage by each class, and the reliability of the map based on the statistics of the confusion matrix of the Hetauda Sub-metropolitan city. As similar to the supervised classification method, there are six classes in total such as forest, grassland, built-up, agriculture, barren land, and waterbody, which have been classified from the scene.

Map 3.2 shows that the metropolitan city is mostly covered by the forest in the northwest and the southeast region which is denoted by the leafy green color on the map. The forest patches are visible at the center of the city and surrounded by agricultural land that is denoted with yellow color. The forest area has more spacious and becomes dense due to the region of natural forest managed by the forest department. Similarly, the forest protection program has been implementing in a national forest as well as community forest for years hence the degraded forest land has converted to bushy land and the bushy land converted to the forest.

The majority of the built-up area is located at the center indicated red and sprawl towards the periphery mostly due to the people's interest settling at the periphery of the east-west highway from the remote part of the city. The water body was found concentrated at the center and near the settlement due to the flowing river nearby and the increasing interest

of local people in fish farming. The water patches found where the regular flow of water in stream and river. The bare area with grey color denotes the sand at the ridge of the riverbank spread over the north to the west passes at the center of the city, degraded land, and dry stream sprawl in the southern part along the forest and the agriculture. The grass patches were found to be sparse across the forest and agricultural land.

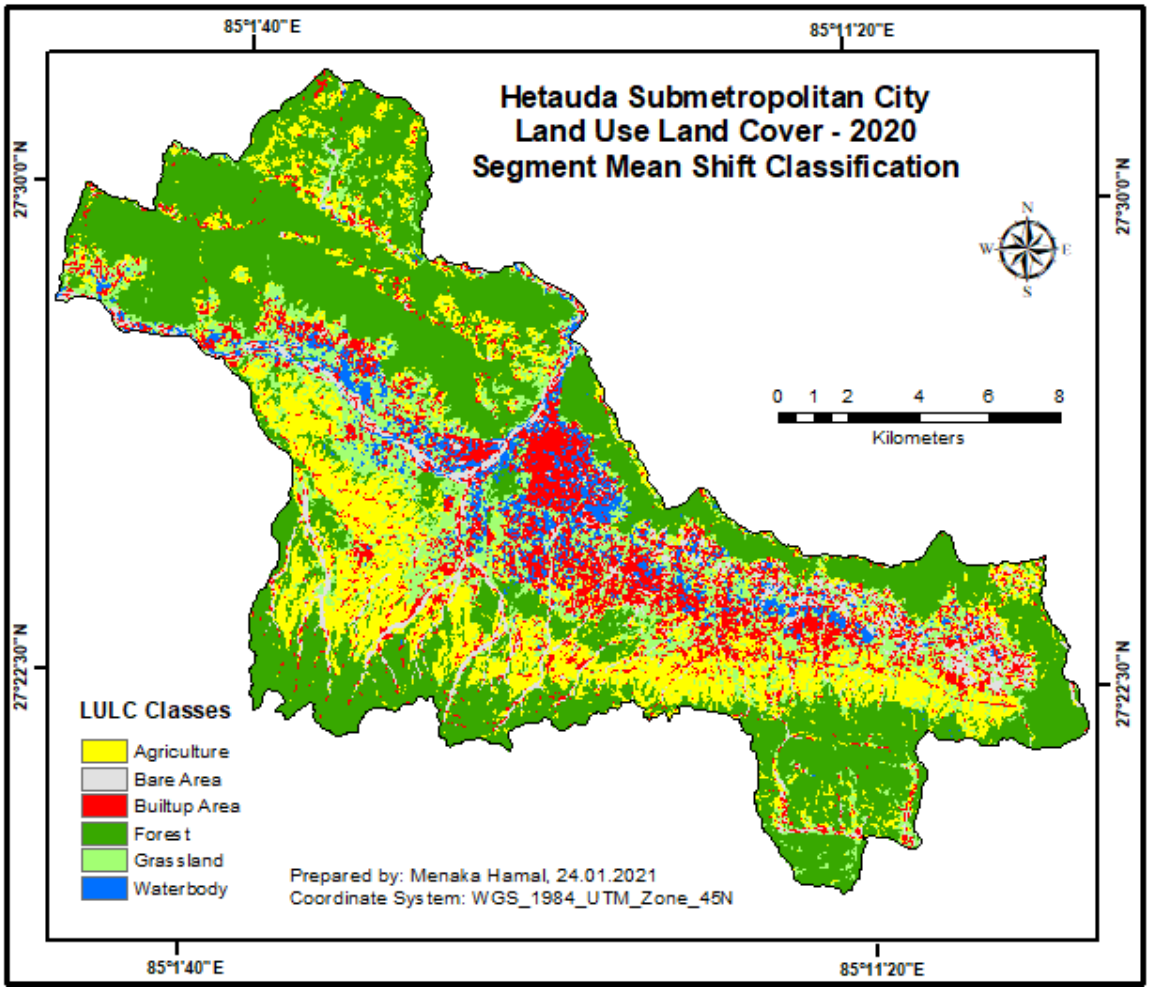

Map 3. 2. Land Use Land Cover 2020 in segment mean shift method

Map 3.4 presenting the LULC map 2020 with six classes of the city prepared after using the segment mean shift classification. This classified map has smoother and visually appalling LULC classes than the map of the supervised classification method.

Table 3.3 shows that the area covered by the forest is 121.05 square kilometers which

aris6.3 % of the total area of the city. Similarly, the agriculture coverage has been 48 sq KM (18.3 %) followed by 34.48 sq Km (13.2%) grassland. The built-up area, grassland, bare area, and waterbody coverage were 32.7 sq KM (12.5%), 13.75 sq KM (5.3%), and 11.69 sq KM (4.5%) respectively out of the total area of the city.

Table 3. 3. LULC coverage in segment mean shift method

LULC Class	Area Sq KM	Percentage
Agriculture	48.0	18.3
Bare Area	13.8	5.3
Builtup Area	32.7	12.5
Forest	121.1	46.3
Grassland	34.5	13.2
Waterbody	11.7	4.5

The forest coverage was 41.46 % in 2010 but this study found that it increased by approximately 5% due to government intervention in the community as well as a national forest, abandon land from migrated people from rural to urban part of the city. The forest area is not only increasing in this city but also throughout Nepal in 2010 (RSS, 2016).

This study also reflects that the cultivated area is found to be dramatically reduced in comparison to the percentage coverage in 2010; 48% of the arable land was deduced to 18% in 2020. The major reason would be the influx of migrants from other districts and the rural part of the city itself as well and started making buildings so that the agriculture could be change into the built-up area.

The residential areas are emerging haphazardly in the sub-metropolitan city. According to the city profile, the built-up area in the city was 6.15% in 2010. This study shows that the built-up has been increased by 50% i.e. 12.5 % in 2020 (Table 3.3). Besides the migrants' interest to build a house, increasing built-up area could be a reason for private and individual land brokers. They buy agricultural land and turn it into residential plots with higher resale value. The people have been following the same trend to gain profit over the years. Similarly, the east-west highway, the link road joining the main roads as well as

parallel roads development is rapid in the city; that would be the reason for building houses along the roadsides and landless squatters that leads to rising the built-up area in the city.

The grassland covers an area of 13.2% of the city in 2020 whereas it was approximately covered 3% in 2010. The bushy and grassy area has increased by 10% more in this study would be due to an increase in fallow land and the community-based forest program implemented in the city.

The city has a 5.3% bare area which is the second-lowest land cover of the city. It was declined by 2% as compared to the area of 2010, the reason would be an increment of households and utilized the area by the landless squatters; this land was converted into either built-up or agricultural land.

The water covers 4.5% which includes the river, stream, and ponds in the city; it has increased in comparison to the area coverage by 0.97% in 2010. In addition to the running water, the ponds are constructed for the fishery would lead to an increased water body in the city. The Bagmati River flows from the north and takes a path to the west in the middle of the city and the Karra stream runs from east to west and conjunct with the river at the center.

3.4. Confusion Matrix in Segment Mean Shift Method

Table 3.4 shows that the summary of a quantitative accuracy assessment of the classified map taking the reference pixel at the horizontal cell and classified pixels at the vertical cell of the scene. Out of 360 pixels, a total of 325 are correctly classified which gives 90% overall accuracy; that means the classified image has a 10 % error in the overall image.

Table 3.4 matrix shows that 101 out of 103 forest pixels are correctly classified which gives 94 % producer accuracy and the remaining 6% pixels are omitted from the classified coverage of the forest; the majority of omitted pixels lie on the built-up area might due to

the farm forest; and the grassland due to the bushy that effects on the reflectance of the pixels. In agriculture, 79 out of 86 pixels are correctly classified that gives the 92% of the accuracy and the 8% of misclassified pixels lies on the built-up area might due to the kitchen garden and orchard, on the bare land might be the reason for the exposed soil that has the similar spectral character with the bare area pixels and due to the degraded land that is not used for any purpose. In a built-up area, out of 51, 46 pixels are 90% correctly classified. Similarly in the bare area have 56 out of 69 pixels that gives the 81% of correctness and 12 out of 17 pixels correctly classified of water body with reflect 71% accuracy of it.

Table 3. 4. Confusion matrix in segment mean shift method

Class Value	**Agriculture**	**Bare Area**	**Builtup Area**	**Forest**	**Grassland**	**Waterbody**	**Total**	**User's Accuracy**
Agriculture	79	0	1	2	4	0	86	0.92
Bare Area	4	56	8	0	0	1	69	0.81
Builtup Area	3	1	46	1	0	0	51	0.90
Forest	2	0	0	101	0	0	103	0.98
Grassland	1	0	0	2	31	0	34	0.91
Waterbody	1	0	3	1	0	12	17	0.71
Total	90	57	58	107	35	13	360	0
Producer's Accuracy	0.88	0.98	0.79	0.94	0.89	0.92		
Overall Accuracy								**0.90**
Kappa								**0.88**

Table 3.4 shows that the user's accuracy (UA) for the forest is 98% which is relatively found highest among all LULC classes from the point of view of the map user (Lillesand et al., 2015), the 98% forest class is accurate or it is reliable to that extent for further use. Though the producer's accuracy (PA) for a forest is 94%, the reliability is 5% more accurate than this. The PA is 88% for agriculture and UA is 92%. The agriculture accuracy shows that the identified agriculture area was found less in the image than the actual coverage of it is high on the ground. Similarly, for the built-up area, the UA is 90% whereas the PA is 79%. The grassland PA 89% and the UA 91%. Though 98% of the bare area has been correctly

identified as “as bare area”, only 81% of the area identified as bare land. Likewise, 92% of the reference water body was correctly identified, only 71% of that area identified as actual water body (Table 3.4).

The matrix shows that the segment mean shift classified map is more accurate than the classified map in supervised classification.

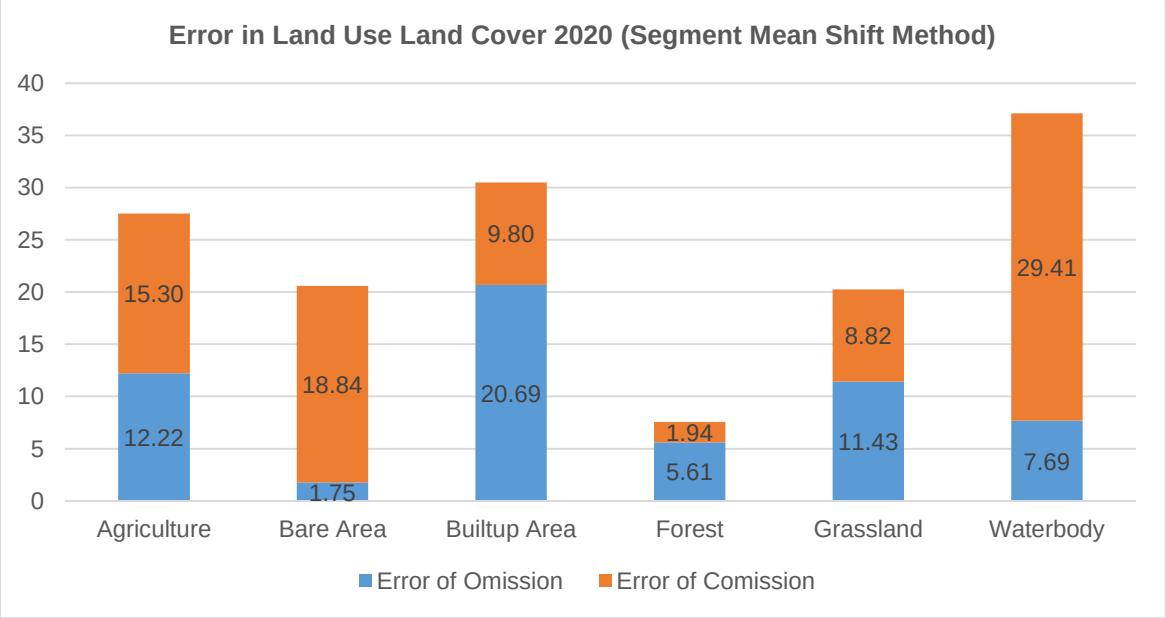

Figure 3. 2. Omission and commission error of segment mean shift method

The overall accuracy of supervised classification was found to be 85 % whereas this method has 90%. Similarly, the Kappa statistics has 81% that is 5 % more accurate than that.

Figure 3.2 depicts the percentage error that occurred in classified maps prepared using the segment mean shift method. The forest has the least error of commission at 1.94 % followed by the grassland at 8.82% and the built-up area by 9.8% whereas the waterbody has the highest at 29.41% followed by the grassland at 8.82% and the built-up area by 9.8%. The error of omission is least in the bare area that is 1.75% followed by 5.61% forest

and 7.69% waterbody whereas it is highest in the built-up area that is 20.69% followed by 12.22% agriculture and 11.43% grassland.

To test the degree of reliability of each map, the Kappa statistics got generated along with the confusion matrix table in ArcGIS. Table 3.4 shows that the kappa statistics is 0.88 which gives the 64-81% reliability interprets the strong level of agreement between classified and original map (Mchugh, 2012). The kappa statistic shows that the classified map using segment mean shift classification was found to be more accurate by 7% more than the simple supervised classification.

3.5. LULC 2020 in OBIA

The LULC map has been obtained using the OBIA method in eCognition. The object-based image segmentation and the classification procedure were followed in the process. The reliability of the classified map was found out based on the statistics of the confusion matrix. As similar to the supervised classification method, there are six classes in total such as forest, grassland, built-up, agriculture, barren land, and waterbody in the classified scene.

Map 3.3 shows that the metropolitan city, as segment mean shift and supervised classification, is mostly covered by the forest in the northwest and the southeast region which is denoted by the leafy green color in the map. The forest patches are visible at the center of the city and surrounded by agricultural land that is denoted with yellow color. The forest area has more spacious and becomes dense due to the region of natural forest managed by the forest department. Similarly, the forest protection program has been implementing in a national forest as well as community forest for years hence the degraded land has converted to bushy land and this converted to the forest.

The majority of the built-up area is located at the center indicated red and sprawl towards the periphery mostly due to the people's interest settling at the periphery of the east-west highway from the remote part of the city. The water body was found near the settlements

and agriculture area due to the flowing river nearby and the increasing interest of local people in fish farming. The bare area with grey color denotes the sand at the ridge of the riverbank spread over the north to the west passes at the center of the city, degraded land, and dry stream sprawl in the southern part along the forest and the agriculture. The grass patches were found to be sparse across the forest and agricultural land.

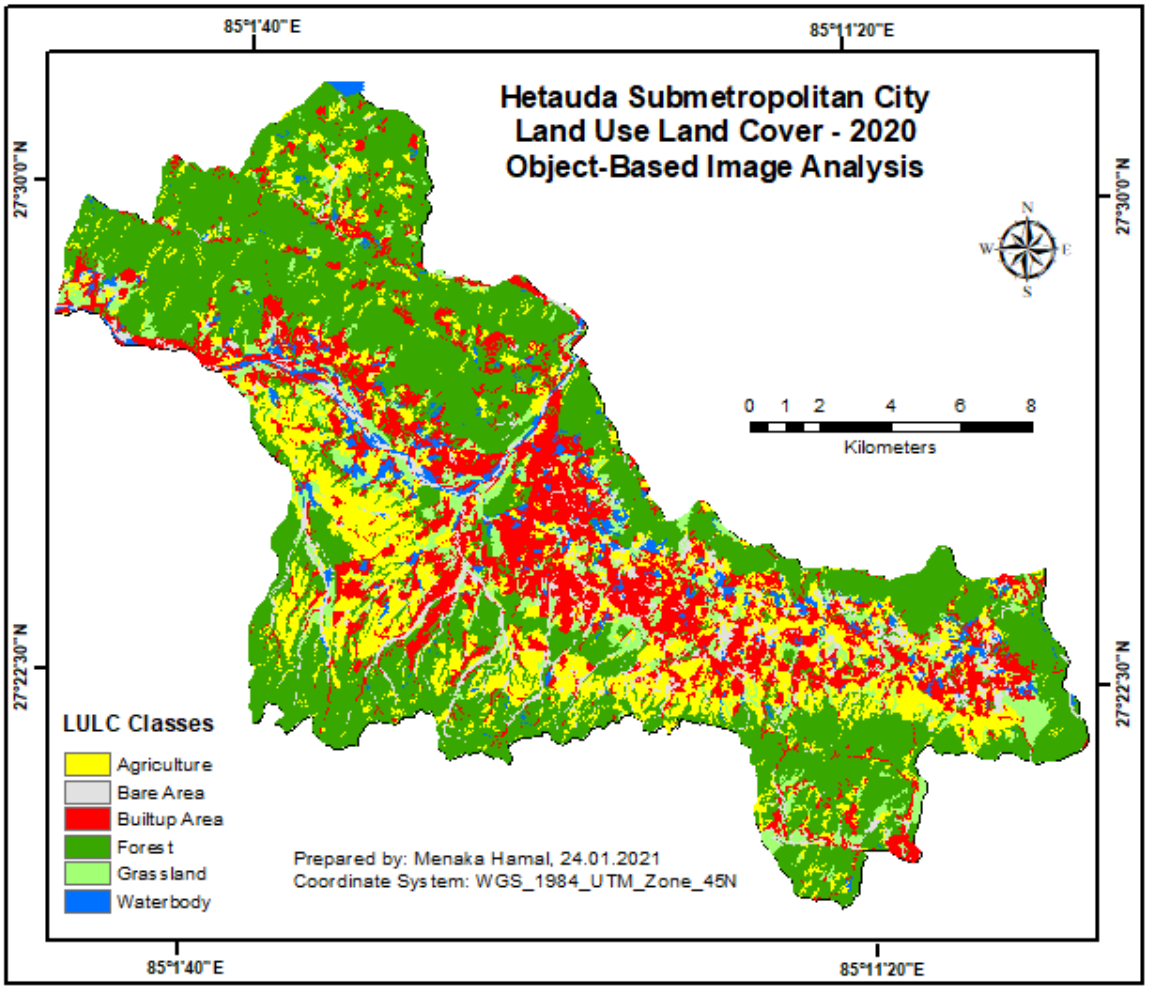

Map 3. 3. Land Use Land Cover 2020 in OBIA

Map 3.3 presenting the LULC map 2020 with six classes of the city prepared after using the OBIA method. This classified map has more smoot and visually appalling LULC classes than the map of the supervised classification method and looks similar to the map of segment mean shift.

Table 3.6 shows that the area covered by the forest is 127.1 square kilometers which is 48.4% of the total area of the city. Similarly, the agriculture coverage has been 43.7 sq KM (16.7 %) followed by 50.3 sq Km (19.2%) built-up area. The grassland, bare area, and waterbody coverage were 18.7 sq KM (7.1%), 13.8 sq KM (5.3%), and 8.7 sq KM (3.3%) respectively out of the total area of the city.

Table 3. 5. LULC coverage in OBIA

LULC Class	Area Sq Km	Percentage
Agriculture	43.7	16.7
Bare Area	13.8	5.3
Builtup Area	50.3	19.2
Forest	127.1	48.4
Grass	18.7	7.1
Waterbody	8.7	3.3

The forest coverage was 41.46 % in 2010 but this study found that it increased by approximately 2% due to government intervention in the community as well as a national forest, abandon land from migrated people from rural to urban part of the city. The forest area is not only increasing in this city but also throughout Nepal in 2010 (RSS, 2016).

The cultivated area is found to be dramatically reduced in comparison to the percentage coverage in 2010; 48% of the arable land was deduced to 16.7% in 2020. The major reason would be the influx of migrants from other districts and the rural part of the city itself as well and started making buildings so that the agriculture could be change into the built-up area.

The residential areas are emerging haphazardly in the sub-metropolitan city. According to the city profile, the built-up area in the city was 6.15% in 2010. This study shows that the built-up has been increased by triplex that is 19.2% in 2020 (Table 3.5). The reason could be the influx of migrants' interest to build a house, increasing built-up area could be a reason for private and individual land brokers. They buy agricultural land and turn it into residential plots with higher resale value. The people have been following the same trend to gain profit over the years. Similarly, the east-west highway, the link road joining the main

roads as well as parallel roads development is rapid in the city; that would be the reason for building houses along the roadsides and landless squatters that leads to rising the built-up area in the city.

The grassland covers an area of 7.1% of the city in 2020 whereas it was approximately covered 3% in 2010. The bushy and grassy area has increased by 50% would be due to an increase in fallow land and the community-based forest program implemented in the city.

The city has a 5.3% bare area which is the second-lowest land cover of the city. It was declined by 2% as compared to the area of 2010, the reason would be an increment of households and utilized the area by the landless squatters; this land was converted into either built-up or agricultural land.

The water covers 3.3% which includes the river, stream, and ponds in the city; it has increased in comparison to the area coverage by 0.97% in 2010. In addition to the running water, the ponds are constructed for the fishery would lead to an increased water body in the city. The Bagmati River flows from the north and takes a path to the west in the middle of the city and the Karra stream runs from east to west and conjunct with the river at the center.

3.6. Confusion Matrix in OBIA

Table 3.6 depicts the summary of a quantitative accuracy assessment of the classified image taking the reference pixel at the horizontal cell and classified pixels at the vertical cell of the scene. Out of 360 pixels, a total of 325 are correctly classified which gives 90% overall accuracy; that means the classified image has a 10 % error in the overall image.

The matrix shows that 102 out of 103 forest pixels are correctly classified which gives 99 % producer accuracy and only one pixel omitted from the classified coverage of the forest. In agriculture, 73 out of 86 pixels are correctly classified that gives the 85% of the pixels

are correctly classified and the 15% of misclassified pixels lies on the built-up area might due to the kitchen garden and orchard, on the grassland might be the reason for the similar spectral character with the crop. In a built-up area, out of 51, 44 pixels are 86% pixels are correctly classified. Similarly, in the bare area have 58 out of 69 pixels that gives the 84% of correctness and 13 out of 17 pixels correctly classified of water body with reflect 76% accuracy of it.

Table 3. 6. Confusion matrix in OBIA

Class Value	Agriculture	Bare Area	Builtup Area	Forest	Grassland	Waterbody	Total	User's Accuracy
Agriculture	73	1	0	11	1	0	86	0.85
Bare Area	1	29	4	0	0	0	69	0.85
Builtup Area	3	3	44	1	0	0	51	0.86
Forest	1	0	0	102	0	0	103	0.99
Grassland	3	0	2	6	58	0	34	0.84
Waterbody	0	0	3	0	1	13	17	0.76
Total	81	33	53	120	60	13	360	
Producer's Accuracy	0.90	0.88	0.83	0.85	0.97	1		
Overall Accuracy								**0.89**
Kappa								**0.86**

The user's accuracy (UA) for the forest is 99% which is relatively found highest among all LULC classes from the point of view of the map user (Lillesand et al., 2015), the 99% forest class is accurate or it is reliable to that extent for further use. Though the producer's accuracy (PA) for a forest is 85%, the reliability is 4% more accurate than this. The PA is 90% for agriculture and UA is 85%. The agriculture accuracy shows that the identified agriculture area was more in the image than the actual coverage of it on the ground. Similarly, for the built-up area, the UA is 86% whereas the PA is 83%; the actual coverage of it on the ground found to be hight by 3%. The grassland identified on the image is 89% whereas the actual coverage is 91%. Though 88% of the bare area has been correctly identified as bare area, only 85% of it is actual. Likewise, 100% of the reference water body was correctly identified on the image, but only 76% of that area identified as actual water body (Table 3.6).

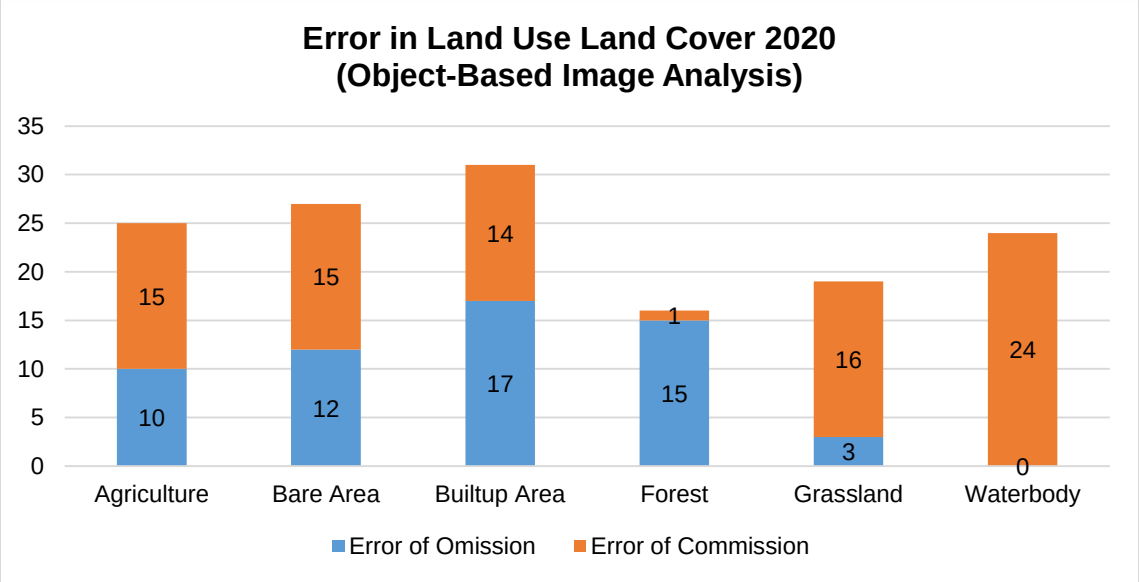

Figure 3. 3. Omission and commission error of OBIA

Figure 3.3 depicts the percentage error that occurred in classified maps prepared using the OBIA method. The forest has the least error of commission at 1.94 % followed by the grassland at 8.82% and the built-up area by 9.8% whereas the waterbody has the highest at 29.41% followed by the grassland at 8.82% and the built-up area by 9.8%. The error of omission is least in the bare area that is 1.75% followed by 5.61% forest and 7.69% waterbody whereas it is highest in the built-up area that is 20.69% followed by 12.22% agriculture and 11.43% grassland.

Sentinel 2B data were atmospherically and radiometrically corrected. The MLC and NN classifiers with the representative samples were used for image classification. The accuracy assessment was done using a stratified point sampling method.

3.7. Comparison of LULC reliability

The overall accuracy and kappa statistics were found to be highest in the segment mean shift method followed by OBIA whereas those were lowest in simple supervised classification (Figure 3.4).

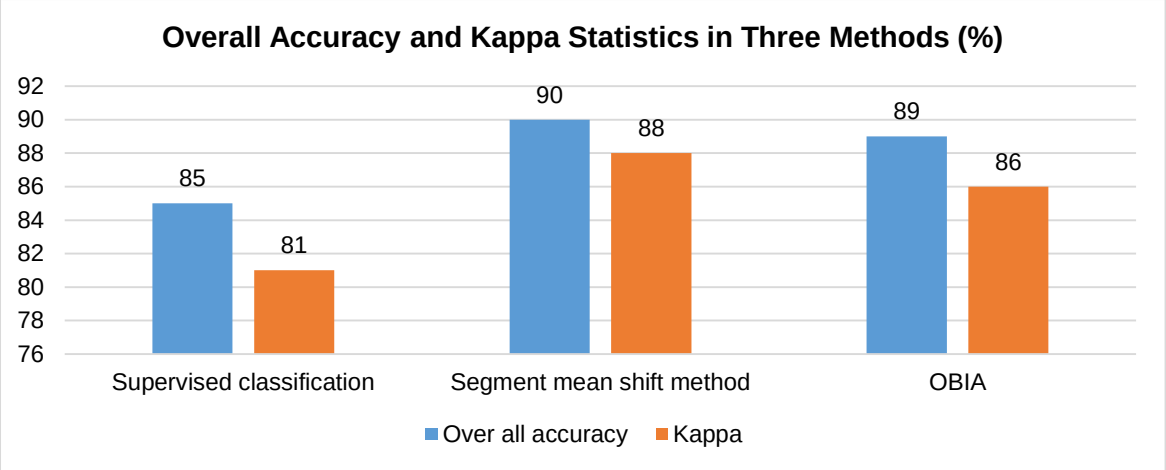

Figure 3. 4. Comparison of the reliability of three methods

The user's accuracy of each class gives how much of the class on the map present on the ground (Lillsand et al., 2015). Table 3.7 shows that the forest has the highest accuracy among other classes whereas the waterbody has the lowest. The highest forest accuracy was found in the three methods but OBIA has the highest among them. Therefore OBIA becomes the best fit method for the forest classification in the city. Agriculture was found to be the second-highest reliable with the segment mean shift method. Overall, the segment mean shift method and the OBIA has high accuracy than a simple supervised classification.

Table 3. 7. The thematic reliability of the three methods

User's Accuracy of Each Thematic Class (%)						
Methods	**Agriculture**	**Bare Area**	**Builtup Area**	**Grassland**	**Forest**	**Waterbody**
Supervised Classification	88	74	73	80	98	71
Segment Mean Shift	92	81	90	91	98	71
OBIA	85	85	86	84	99	76

The selection of appropriate training data set from the imagery was quite challenging in each classification method. The iteration in collecting training samples and their correction was made in the process of using three methods. In the supervised classification method in ERDAS Imagine, the raster was not vectorized. The sample data were directly collected

from the enhanced imagery based on the local knowledge and visual interpretation. The polygons were drawn from the unsegmented raster. The classification solely depended on the spectral information of each pixel; every pixel counted as a sample. Similarly, sufficient representative samples that fit for the MLC were drawn in the segment mean shift method in ArcGIS. The image was segmented using a segment mean shift segmentation algorithm in ArcGIS Desktop 10.6. The segments were not vectorized. Therefore, the sample collection process was time-consuming as compared to the OBIA; the sample collection was drawn by the reorganization of segments as coverage. However, the classification in OBIA in eCognition used both spatial and spectral information. The image was segmented using image segmentation algorithms – the multiresolution segmentation. The segments were vectorized; each segment was delineated by a polygon and distinguished the color as assigned in each class in the class hierarchy. Comparatively, taking samples in this method was more efficient than others. The samples were drawn till the data normally distributed over the scene, meet the normally distributed histogram and mean and variance that suitable for the ML classifier in supervised classification and segment mean shift, and nearest neighbor classifier in object-based image analysis.

The classified maps were more smooth and visually appealing with the methods that have a segmentation approach applied. The map with supervised classification looks as if there were some salt and pepper effects due to the sparse built-up area across the map. Though the built-up area looks more, but less accurate in supervised classification as compared to the segment mean shift classification and OBIA.

It can be summarized that the overall accuracy conveys the most appropriate method for the LULC classification with the Sentinel 2B imagery for the Hetauda Sub-metropolitan city was found to be the segment mean shift classification method, though it was time-consuming. The level of accuracy for OBIA was found to be approximate to the segment mean shift method. The object-based image analysis approaches are suitable for the LULC classification of the city.

Chapter-4: Conclusion

The LULC classification was done through the simple supervised classification, segment mean shift method, and OBIA and accessed the accuracy of the classified maps for the Hetauda Sub-metropolitan City of Nepal. The open-source Sentinel 2B imagery was acquired from European Space Agency for the time of 31 March 2020. The data set was level-C orthorectified with 10-meter spatial resolution. The two imageries UTM 45N projection were downloaded and mosaicked to make a single raster. The combined raster was atmospherically corrected to reduce the atmospheric noise using the nonlinear filter and the radiometrically corrected to increase the contrast of the overall image through the histogram equalization.

The enhanced imagery was used in the extraction of data within the administrative boundary of the city to get the six information classes – forest, agriculture, built-up area, bare area, grassland, and waterbody. In supervised classification, the training samples were taken by the visual interpretation based on the knowledge of the area and train samples to the MLC. In segment mean shift method, the enhanced image was segmented with the segment mean shift algorithm, collected samples, and train those in MLC. Similarly in OBIA, the imagery was segmented with a multiresolution segmentation algorithm that makes each segment into a polygon. The samples were selected from the vectorized raster based on assigned classes in the class hierarchy and train nearest neighbor classifier.

The appropriate value iteration for segmentation had a key role to get the appropriate size of the superpixels. spectral value - 18, spatial value - 15, and the segment size - 20 were found to be appropriate after iterations so that the image segments were built as our required size. Similarly, in object-based image analysis, the appropriate homogeneity criteria used in image segmentation had a key role to meet the required object size in the image before running a multiresolution segmentation algorithm in eCognition. Scale Factor

– 40, shape – 0.3, and compactness – 0.7 were found to be the best fit for the segmentation.

The city mostly covered by the forest in the northwest and the southeast region and some patches are visible at the center. The 125.3 sq KM is covered by the forest that becomes 47.8% of the total city area. Similarly, the average area covered by agriculture, built-up, bare land, grass, and waterbody by 46.2 sq KM (17.7%), 39 sq KM (14.9), 13.9 sq KM (5.3%), 26 sq KM (9.9%), 11.4 sq KM (4.4%) respectively. Forest, water, bare area, grassland, and the built-up area have increased than its area of 2010 whereas the agriculture has decreased drastically in the city.

The overall accuracy of the classified image of segment mean shift classification has 90%, OBIA has 89%, and supervised classification has 85%. Similarly, kappa statistics show a strong level of agreement - 0.88, 0.86, 0.81 for segment mean shift, OBIA, and supervised classification respectively. Regarding the average individual class accuracy, the forest was found to be 98% reliable whereas the waterbody was found to be the least one. Considering the appropriateness and the accuracy, the segment mean shift method would be more appropriate for the LULC classification of the Hetauda Sub-metropolitan city of Nepal.

References

Ait-Aoudia, S., Mahiou, R., Djebli, H., & Guerrout, E. H. (2012). *Satellite and aerial image mosaicing - A comparative insight*. *Proceedings of the International Conference on Information Visualisation*, (July), 652–657. https://doi.org/10.1109/IV.2012.113

Ai, J., Zhang, C., Chen, L., & Li, D. (2020). *Mapping annual land use and land cover changes in the Yangtze Estuary Region using an object-based classification framework and landsat time series data*. *Sustainability (Switzerland)*, *12*(2). https://doi.org/10.3390/su12020659

Al-Fares, W. (2013). *Historical Land Use/Land Cover Classification Using Remote Sensing : A Case Study of the Euphrates River Basin in Syria*. https://doi.org/10.1007/978-3-319-00624-6

Anand, A. (2018). *Image Classification*. (May), 41–58. Retrieved from https://www.researchgate.net/publication/324943335_Unit_13_Image_classification. Access on February 26 2021

Anand, A. (2017). *Unit 14 Accuracy Assessment*. (January 2017), 59–77. Retrieved from https://www.researchgate.net/publication/324943246_UNIT_14_ACCURACY_ASSESSMENT. Access on January 06 2021

Basayigit, L. (2015). *COMPARISON OF PIXEL-BASED AND OBJECT-BASED CLASSIFICATION*. Land Reclamation, Earth Observation & Surveying, Environmental Engineering, March 2018.

Buja, K., & Menza, C. (2013). *Sampling Design Tool for ArcGIS - Instruction Manual*. 1–16. Retrieved from http://www.arcgis.com/home/item.html?id=ecbe1fc44f35465f9dea42ef9b63e785 Access on January 06 2021

Clarke, M. R. B., Duda, R. O., & Hart, P. E. (1974). *Pattern Classification and Scene Analysis. Journal of the Royal Statistical Society. Series A (General)*, *137*(3), 442. https://doi.org/10.2307/2344977

Cohen, J. (1960). *A COFFICIENT OF AGREEMENT FOR NORMAL SCALES*. *XX*(1), 37–46. https://doi.org/10.1177/001316446002000104

Congalton, R. G. (2001). *Accuracy assessment and validation of remotely sensed and other spatial information. International Journal of Wildland Fire*, *10*(3–4), 321–328. https://doi.org/10.1071/wf01031

Copernicus, (2020). *Sentinel 2 Space Craft Overview*. Retrieved from https://spaceflight101.com/copernicus/sentinel-2/ Access on January 06 2020

Darwish, A., Leukert, K., & Reinhardt, W. (2003). I*mage Segmentation for the Purpose of Object-Based Classification. International Geoscience and Remote Sensing Symposium (IGARSS)*, *3*, 2039–2041.

DOA. (2018). *Inter-Provincial Dependency for Agricultural Development*. Ministry of Agriculture, Land Management and Cooperative.

Duda, T., & Canty, M. (2002). *Unsupervised classification of satellite imagery: Choosing a good algorithm*. *International Journal of Remote Sensing*, *23*(11), 2193–2212. https://doi.org/10.1080/01431160110078467

eCognition,. (2020). *Basic Rule Set Editing*. Retrieved from https://docs.ecognition.com/v9.5.0/eCognition_documentation/User%20Guide%20Developer/4%20Basic%20Rule%20Set%20Editing.htm Access on February 19, 2021

eCognition,. (2021). *About Classification*. Retrieved from https://docs.ecognition.com/v9.5.0/eCognition_documentation/User%20Guide%20Architect/8%20About%20Classification.htm Access on March 03 2021.

ERDAS (2016). *Introduction to Imagine Software and Image Data ERDAS Imagine 2016*. Retrieved from http://knightlab.org/rscc/labs/Lab01_Imagine_Intro-2016.pdf. Access on March 13 2021

ESA, (2020). *Copernicus Open Access Hub*. Retrieved from https://scihub.copernicus.eu/dhus/#/home Access November 06 2020

ESA, (2021). *Sentinel-2 Products Specification Document*. European Space Agency. Retrieved fromhttps://sentinel.esa.int/documents/247904/685211/Sentinel-2+Products+Specification+Document+%28PSD%29/0f7bedeb-9fbb-4b60-91aa-809162de456c Access on February 19 2021

ESRI, 2020. *Understanding Segmentation and Classification*. Retrieved from https://desktop.arcgis.com/en/arcmap/10.3/tools/spatial-analyst-toolbox/understanding-segmentation-and-classification.htm Access on January 08 2021

ESRI (2020a). *A Quick Tour of Spatial Analyst*. Retrieved from https://desktop.arcgis.com/en/arcmap/latest/extensions/spatial-analyst/a-quick-tour-of-spatial-analyst.htm Access on March 18 2020

ESRI (2020b). *Understanding of Segmentation and Classification*. Retrieved from https://pro.arcgis.com/en/pro-app/tool-reference/spatial-analyst/understanding-segmentation-and-classification.htm Access on March 18 2020

ESRI (2020c). *Segment Mean Shift*. Retrieved from https://pro.arcgis.com/en/pro-app/tool-reference/spatial-analyst/segment-mean-shift.htm Access on March 18 2020

FAO, (2021). *Land Cover Classification System (LCCS).* Food and Agriculture Organization. Retrieved from http://www.fao.org/land-water/land/land-governance/land-resources-planning-toolbox/category/details/en/c/1036361/#:~:text=The%20Land%20Cover%20Classification%20System,and%20mapping%20of%20land%20cover.&text=LCCS%20is%20a%20real%20a,covers%20all%20their%20possible%20combinations Access on February 21 2021

ESRI,(2021).Mosaic Operators. Retrieved from https://desktop.arcgis.com/en/arcmap/10.3/manage-data/raster-and-images/mosaic-operators.htm Access on March 13 2021

Foody, G. (2010). *Assessing the Accuracy of Remotely Sensed Data: Principles and Practices.* In *The Photogrammetric Record* (Vol. 25). https://doi.org/10.1111/j.1477-9730.2010.00574_2.x

Foody, G. M. (2013). *Thematic Map Comparison. Photogrammetric Engineering & Remote Sensing*, *70*(5), 627–633. https://doi.org/10.14358/pers.70.5.627

Food and Agriculture Organization of the United Nations [FAO]. (2016). *Map accuracy assessment and area estimation : a practical guide*. *National Forest Monitoring Assessment Working Paper*, *E*(46), 69. Retrieved from http://www.fao.org/3/a-i5601e.pdf

GISGeography., (2021). *Nearest Neighbor Classification Guide in eCognition*. Retrieved from https://gisgeography.com/nearest-neighbor-classification-guide-ecognition/ Access on March 03 2021

GIS Geography (2020). *Raster Resampling for Discrete and Continuous Data*. Retrieved from https://gisgeography.com/raster-resampling/ Access on April 22 2020.

Hadjimitsis, D.G. and Themistocleous, K. (2008). *The importance of considering atmospheric correction in the pre-processing of satellite remote sensing data intended for the management and detection of cultural sites: a Case Study of the Cyprus Area*. (October 2016). Retrieved from https://www.researchgate.net/publication/257067491https://doi.org/10.1109/igarss.2003.1294332

Haldar, S. K. (2018). Photogeology, Remote Sensing, and Geographic Information System in Mineral Exploration. *Mineral Exploration*, 47–68. https://doi.org/10.1016/b978-0-12-814022-2.00003-4

GoN, (2017). *City Profile of Hetauda Sub-Metropolitan City 2017.* Government of Nepal. Office of the Hetauda Sub-Metropolitan City, Makwanur.

Hossain, M. D., & Chen, D. (2019). Segmentation for Object-Based Image Analysis (OBIA): A review of algorithms and challenges from remote sensing perspective. *ISPRS Journal of Photogrammetry and Remote Sensing*, *150*(November 2018), 115–134. https://doi.org/10.1016/j.isprsjprs.2019.02.009

I.M.Enderle, D., & WeihJr, R. C. (2005). *Integrating Supervised and Unsupervised Classification Methods to Develop a More Accurate Land Cover Classification*. *Journal of the Arkansas Academy of Science*, *59*, 65–73.

Intergraph. (2018). *Top 10 Reasons to Use ERDAS IMAGINE*. 8–9. Retrieved from https://www.geosystems.fr/images/PDF/INGR-ERDAS-IMAGINE-TOP10.pdf

Kissinger, G. M. Herold, V. D. S. (2017). *Drivers of Deforestation and Forest Degradation in Bhutan.* In *A synthesis report for REDD+ Policymakers*. Retrieved from http://www.era-mx.org/biblio/Drivers of deforestation and forest degradation.pdf

Knorn, J., Rabe, A., Radeloff, V. C., Kuemmerle, T., Kozak, J., & Hostert, P. (2009). *Land cover mapping of large areas using chain classification of neighboring Landsat satellite images. Remote Sensing of Environment*, *113*(5), 957–964. https://doi.org/10.1016/j.rse.2009.01.010

Kurlin, V., & Harvey, D. (2018). *Superpixels optimized by color and shape*. *Lecture Notes in Computer Science (Including Subseries Lecture Notes in Artificial Intelligence and Lecture Notes in Bioinformatics)*, *10746 LNCS*, 297–311. https://doi.org/10.1007/978-3-319-78199-0_20

Lin, L., & Mengyuan, S. (2014). *Comparison on fusion algorithms of Zy-3 panchromatic and multi-spectral images*.

Lu, D., & Weng, Q. (2007). *A survey of image classification methods and techniques for improving classification performance*. *International Journal of Remote Sensing*, *28*(5), 823–870. https://doi.org/10.1080/01431160600746456

Mchugh, M. L. (2012). *Lessons in biostatistics Interpreter reliability : the kappa statistic*. 276– 282. https://doi.org/10.11613/BM.2012.031

MGL, (2013). *Accuracy Assessment of an Image Classification in ArcMap*. Map & GIS Library. < https://www.youtube.com/watch?v=FaZGAUS_Nlo&t=699s>. Accessed on July 29 2020

Milan, S., Vaclav, H., Roger, B,. (2020). *Image pre-processing.* Retrieved from https://link.springer.com/chapter/10.1007/978-1-4899-3216-7_4 Access on February 16 2021

MOFAGA, (2020). *Local Level Detail*. Ministry of Federal Affairs and General Administration. Retrieved from http://103.69.124.141/gis/ Access on April 4 2020.

Mustak, S. (2013). *Correction of Atmospheric Haze in Resourcesat-1 Liss-4 Mx Data for Urban Analysis: an Improved Dark Object Subtraction Approach*. *ISPRS - International Archives of the Photogrammetry, Remote Sensing and Spatial Information Sciences*, *XL-1/W3* (October), 283–287. https://doi.org/10.5194/isprsarchives-xl-1-w3-283-2013

Paudel, B., Zhang, Y. li, Li, S. cheng, Liu, L. shan, Wu, X., & Khanal, N. R. (2016). *Review of studies on land use and land cover change in Nepal*. *Journal of Mountain Science*, *13*(4), 643–660. https://doi.org/10.1007/s11629-015-3604-9

Ruppert, G., Hussain, M., & Heimo, M. (2018). *Accuracy Assessment of Satellite Image Classification Depending on Training Sample Introduction*. (February). https://doi.org/10.17713/ajs.v28i4.522

RSS (2016). *Forest cover has increased in Nepal of late*. Rastrya Samachar Samiti. Retrieved from https://thehimalayantimes.com/nepal/forest-cover-increased-nepal late. Access on 04 February 2021

Schowengerdt, R. A. (2007). Chapter 9: Them*atic Classification. Remote Sensing,* 387–456. Retrieved from http://linkinghub.elsevier.com/retrieve/pii/B978012369407250012 7%0Ahttp://www.sciencedirect.com/science/article/pii/B9780123694072500127%5Cnhttp://linkinghub.elsevier.com/retrieve/pii/B9780123694072500127

Serpico, S. B., Dellepiane, S., Moser, G., Angiati, E., Boni, G., Rudari, R., & Candela, L. (2012). *Extracting information from remote sensing data for applications to flood monitoring and damage evaluation*. Proceedings of the 2012 Tyrrhenian Workshop on Advances in Radar and Remote Sensing: From Earth Observation to Homeland

Security, TyWRRS 2012, (September 2014), 275–282. https://doi.org/10.1109/TyWRRS.2012.6381142

Sonka, M., Hlavac, V., & Boyle, R. (2014). *Image processing, Analysis, and Machine Vision-Cengage Learning* (p. 930). p. 930.

Stutz, D., Hermans, A., & Leibe, B. (2018). *Superpixels: An evaluation of the state-of-the-art*. *Computer Vision and Image Understanding*, *166*, 1–27. https://doi.org/10.1016/j.cviu.2017.03.007

SUHET. (2015). *Sentinel-2 User Handbook*. Sentinel User Handbook and Exploitation Tools. Europian Space Agency and European Commission.

Talukdar, S., Singha, P., Mahato, S., Shahfahad, Pal, S., Liou, Y. A., & Rahman, A. (2020). *Land-use land-cover classification by machine learning classifiers for satellite observations-A review*. *Remote Sensing*, *12*(7). https://doi.org/10.3390/rs12071135

Thomlinson, J. R., Bolstad, P. V., & Cohen, W. B. (1999). *Coordinating methodologies for scaling landcover classifications from site-specific to global: Steps toward validating global map products. Remote Sensing of Environment*, *70*(1), 16–28. https://doi.org/10.1016/S0034-4257(99)00055-3

Towards, (2020). *Transform Grayscale Images to RGB Using Python's Matplotlib*. Retrieved from https://towardsdatascience.com/transform-grayscale-images-to- rgb-using-pythons-matplotlib-6a0625d992dd Access on February 19 2021

Trimble, (2021). *The Power of eCognition*. Retrieved from https://docs.ecognition.com/v9.5.0/eCognition_documentation/Modules/1%20eCognition%20at%20a%20glance/01%20Introduction%20to%20the%20Power%20of%20eCognition.htm. Access on April 03, 2021

UoT, (2021).*15 - Data quality: quality assessment*. University of Twente, Netherland. Retrieved from https://ltb.itc.utwente.nl/498/learningoutcome/show/59281 Access on 19 February 2021

Vaiopoulos, D. Vassilopoulos, A., Evelpidou, N. Vassilas, N. Perantonis. S. Charou, E. S. V. (1999). *Land cover thematic map production by photointerpretation and quantitative analysis of satellite imagery*. (February 2020). Retrieved from https://www.researchgate.net/publication/339166228%0ALand

Veljanovski, T., Kanjir, U., & Oštir, K. (2011). *Object-based image analysis of remote sensing data*. *Geodetski Vestnik*, *55*(04), 641–664. https://doi.org/10.15292/geodetski-vestnik.2011.04.641-664

Viera, A. J., & Garrett, J. M. (2005). *Understanding Interobserver Agreement: The Kappa Statistic*. *Family Medicine*, *37*(5), 360–363. Retrieved from http://www1.cs.columbia.edu/~julia/courses/CS6998/Interrater_agreement.Kappa_statistic.pdf

Annexures

Annex 1: Training Sample Histograms in Supervised Classification

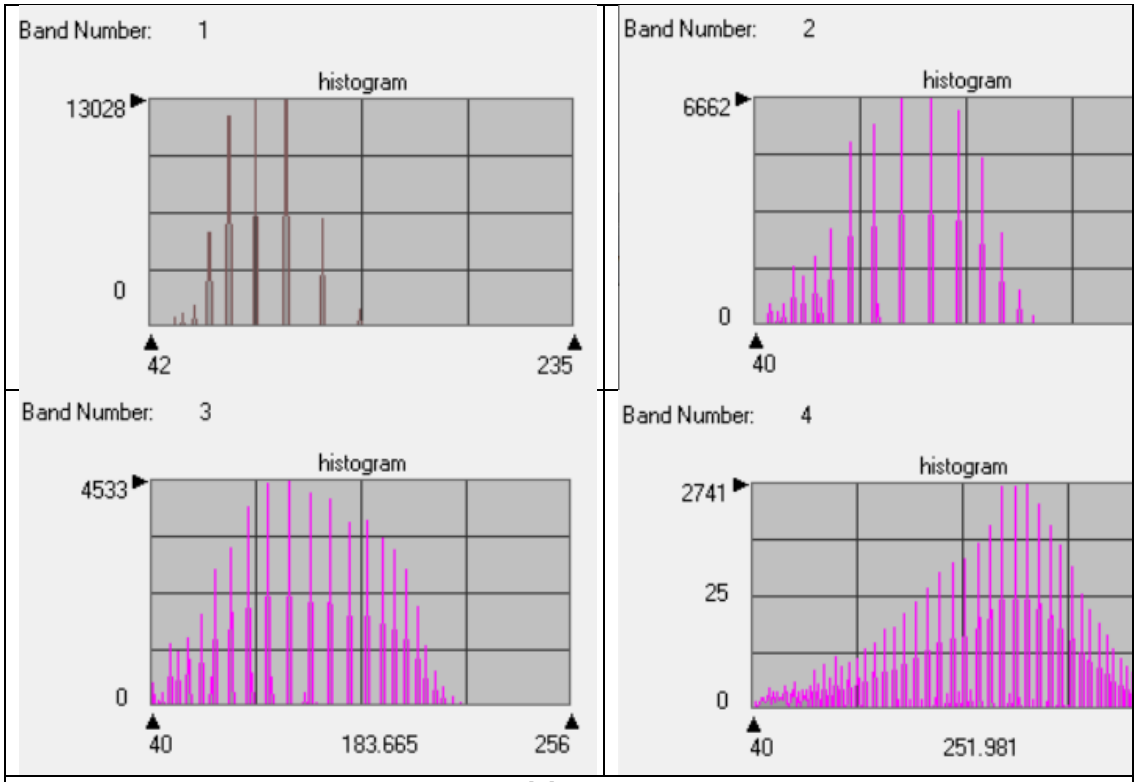

(1) Forest

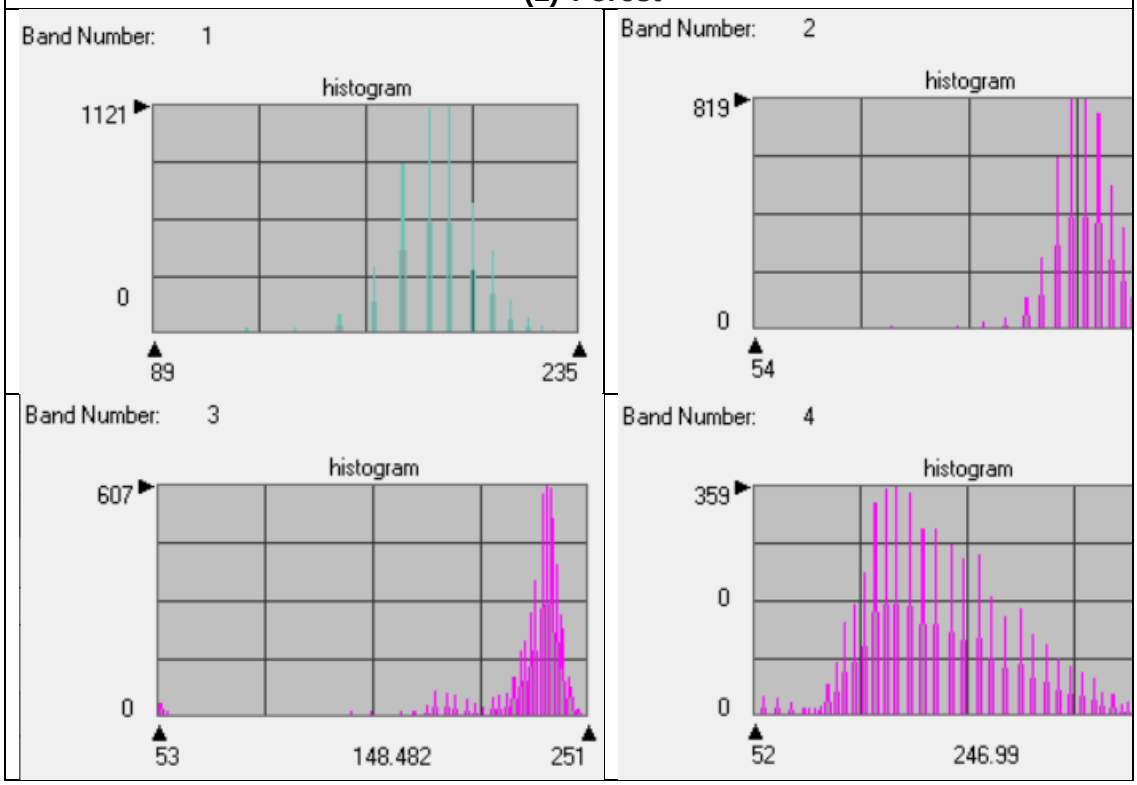

(2) Agriculture

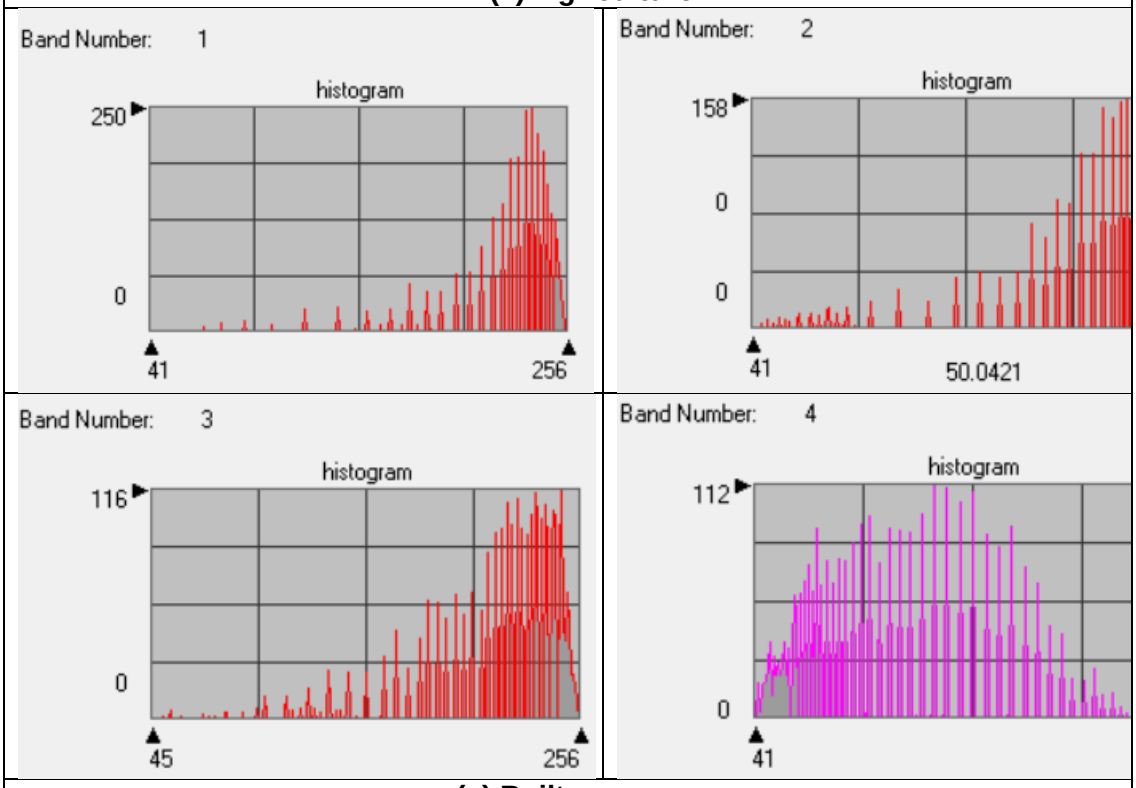

(c) Built-up area

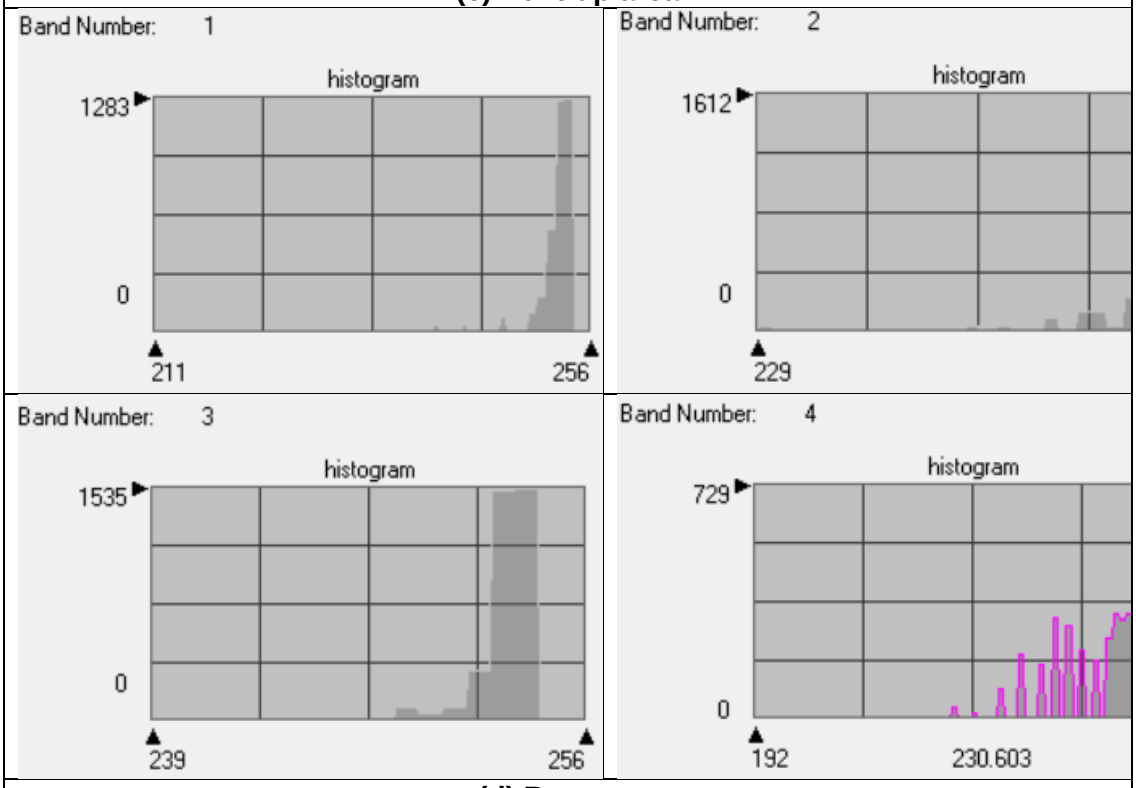

(d) Bare area

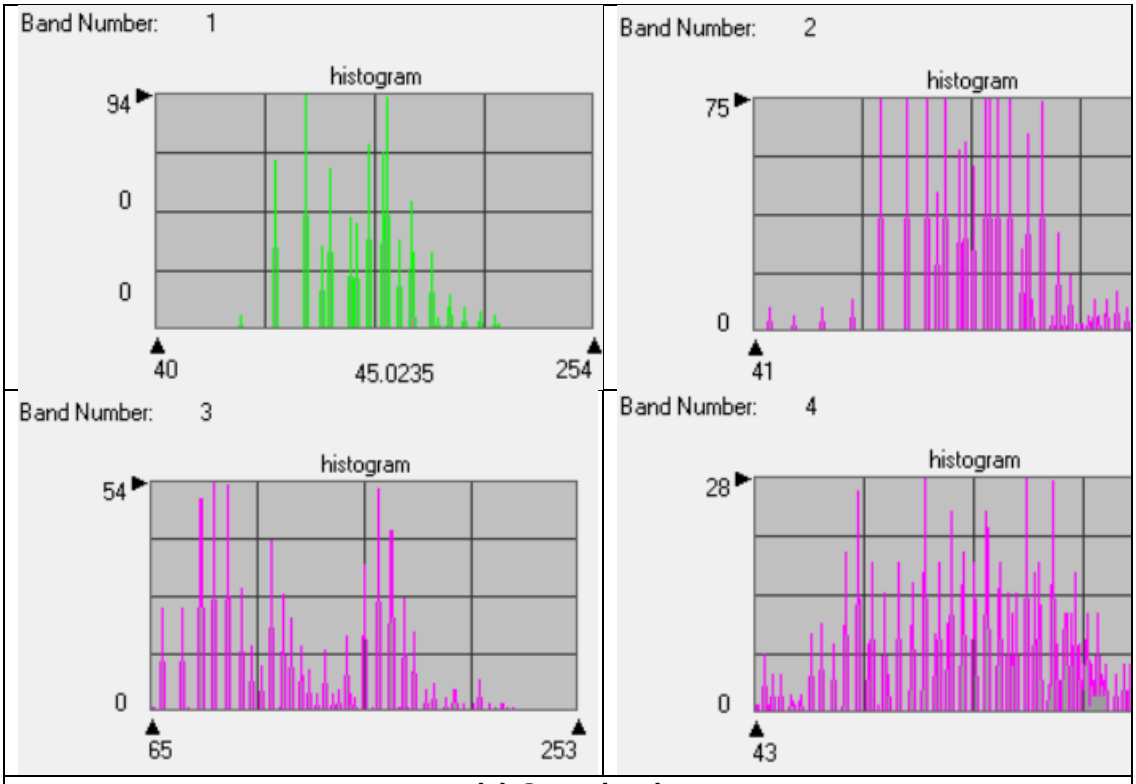

(e) Grassland

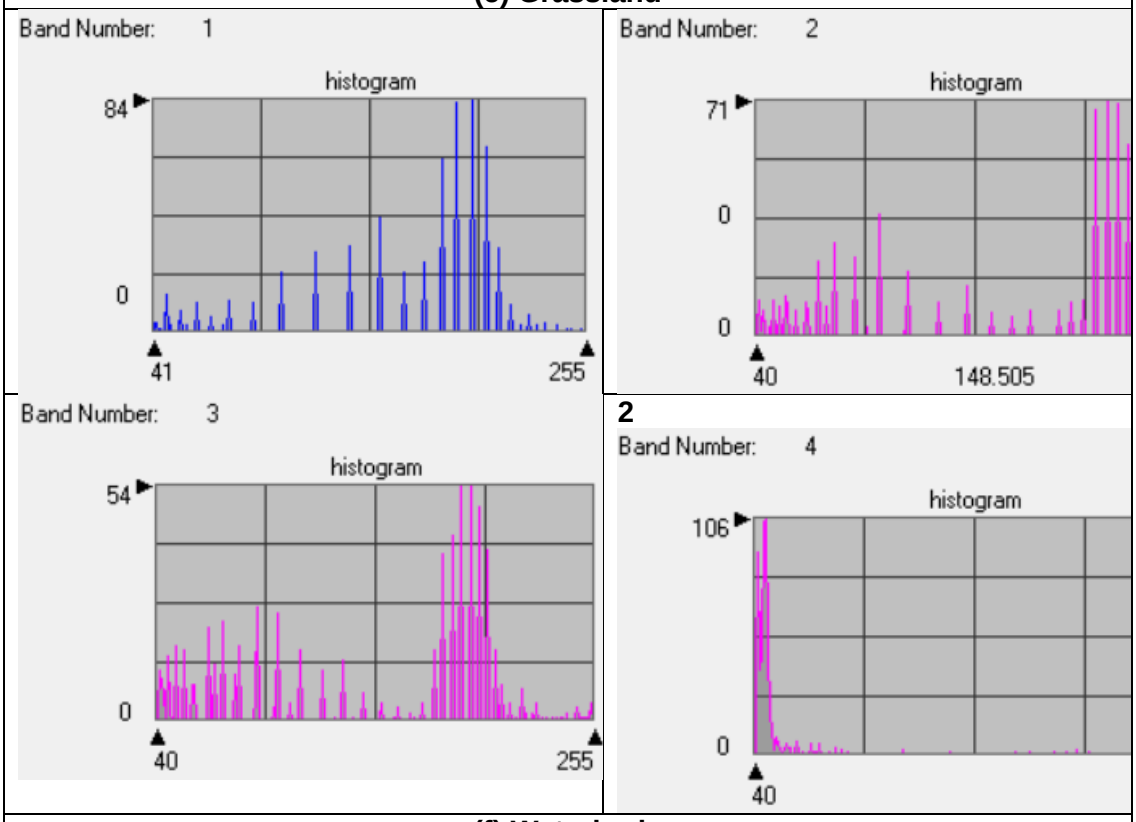

(f) Waterbody

Annex 2: Training Samples Statistics in Supervised Classification

Univariate

Layer	Minimum	Maximum	Mean	Std. Dev.
1	42.000	234.000	89.169	17.999
2	40.000	255.000	114.372	33.257
3	40.000	255.000	119.376	38.523
4	40.000	255.000	156.145	52.052

Covariance

Layer	1	2	3	4
1	323.975	496.502	542.355	301.783
2	496.502	1106.045	1125.345	965.540
3	542.355	1125.345	1484.051	802.257
4	301.783	965.540	802.257	2709.375

(a) Forest

Univariate

Layer	Minimum	Maximum	Mean	Std. Dev.
1	89.000	234.000	188.355	14.747
2	54.000	244.000	203.460	15.798
3	53.000	250.000	227.584	15.278
4	52.000	248.000	141.761	33.133

Covariance

Layer	1	2	3	4
1	217.469	208.341	113.500	268.485
2	208.341	249.581	153.090	289.740
3	113.500	153.090	233.421	15.388
4	268.485	289.740	15.388	1097.773

(b) Agriculture

Univariate

Layer	Minimum	Maximum	Mean	Std. Dev.
1	41.000	255.000	224.959	32.136
2	41.000	255.000	215.925	38.852
3	45.000	255.000	218.469	32.184
4	41.000	255.000	110.257	46.872

Covariance

Layer	1	2	3	4
1	1032.745	748.879	571.813	115.205
2	748.879	1509.480	862.572	466.913
3	571.813	862.572	1035.838	304.726
4	115.205	466.913	304.726	2196.961

(C) Built-up

Univariate

Layer	Minimum	Maximum	Mean	Sto
1	211.000	255.000	254.364	
2	229.000	255.000	254.773	
3	239.000	255.000	254.681	
4	192.000	255.000	250.706	

Covariance

Layer	1	2	3	
1	4.865	1.425	0.733	
2	1.425	0.824	0.576	
3	0.733	0.576	0.650	
4	2.724	2.535	3.696	

(d) Bare area

Univariate

Layer	Minimum	Maximum	Mean	Std. Dev.
1	40.000	253.000	165.031	24.739
2	41.000	252.000	172.663	26.224
3	65.000	252.000	171.985	25.140
4	43.000	254.000	173.119	44.665

Covariance

Layer	1	2	3	4
1	612.024	575.566	480.720	512.101
2	575.566	687.716	530.480	711.353
3	480.720	530.480	632.032	376.896
4	512.101	711.353	376.896	1994.931

(e) Grassland

Univariate

Layer	Minimum	Maximum	Mean	St
1	40.000	254.000	152.076	
2	40.000	254.000	119.313	
3	40.000	255.000	114.161	
4	40.000	255.000	65.649	

Covariance

Layer	1	2	3	
1	2772.126	2712.829	2290.747	
2	2712.829	4083.945	3589.576	
3	2290.747	3589.576	4093.608	
4	1217.442	2125.108	2196.821	

(f) Waterbody

Annex 3: Training Sample Histograms in Segment Mean Shift

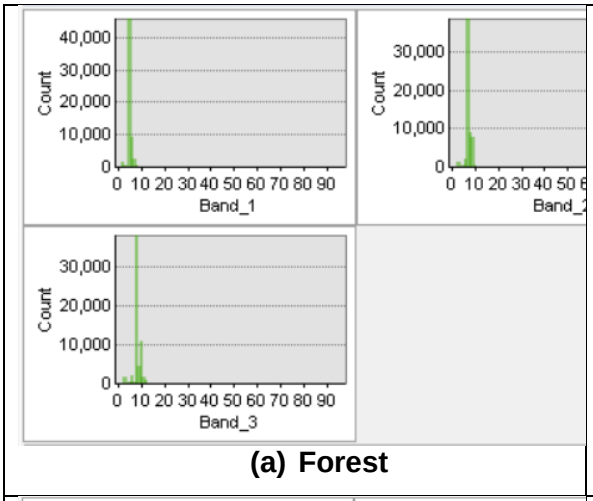

(a) Forest

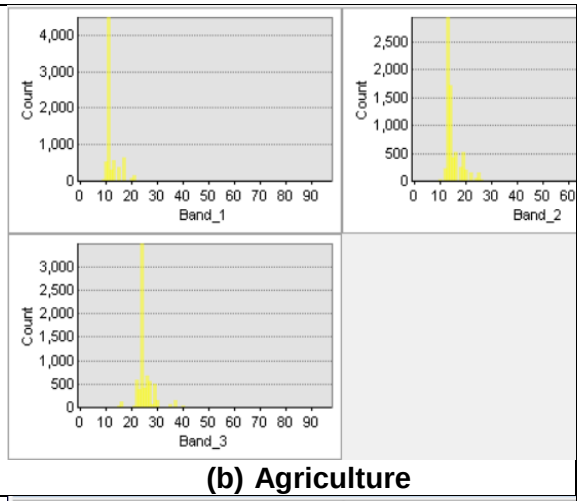

(b) Agriculture

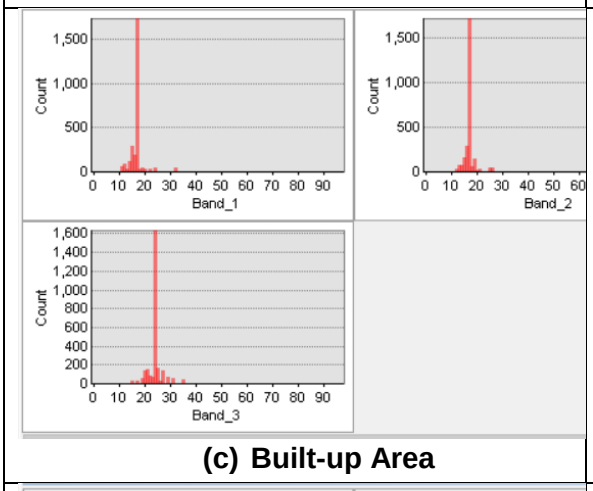

(c) Built-up Area

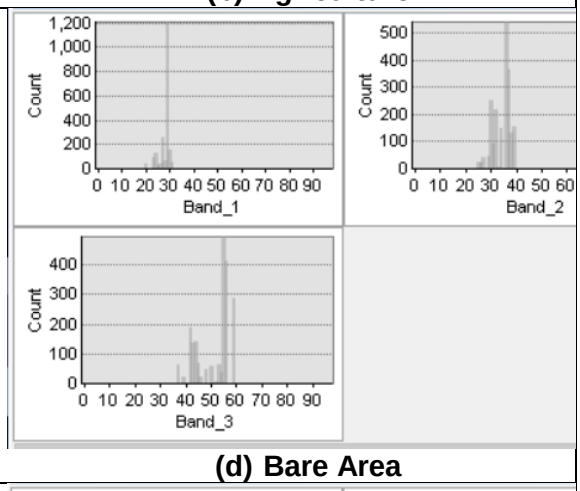

(d) Bare Area

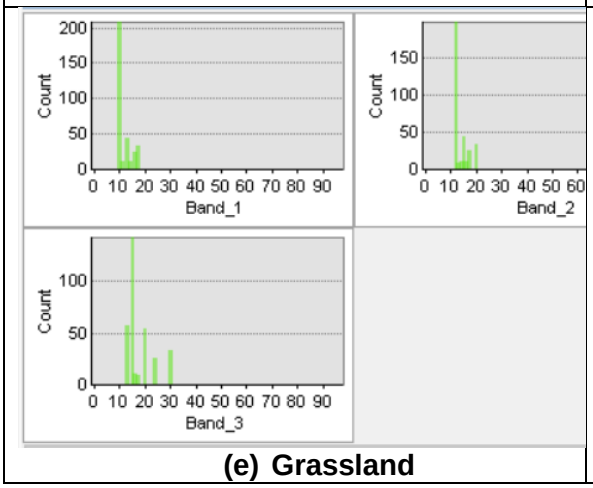

(e) Grassland

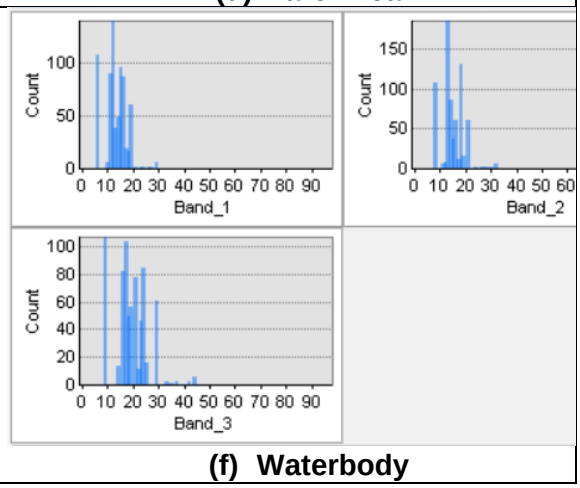

(f) Waterbody

Annex 4: Training Sample Statistics in Segment Mean Shift

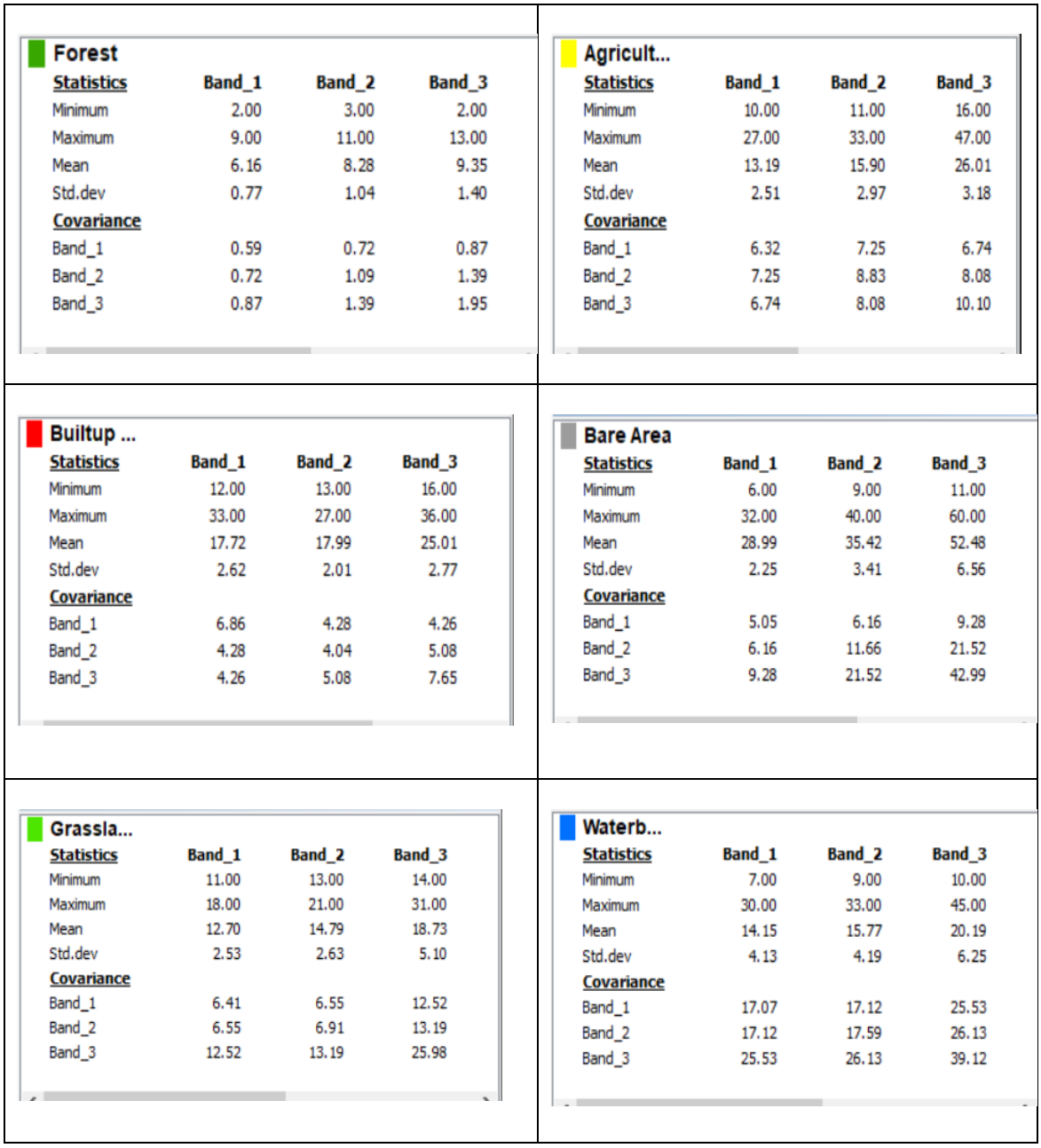

Forest

Statistics	Band_1	Band_2	Band_3
Minimum	2.00	3.00	2.00
Maximum	9.00	11.00	13.00
Mean	6.16	8.28	9.35
Std.dev	0.77	1.04	1.40
Covariance			
Band_1	0.59	0.72	0.87
Band_2	0.72	1.09	1.39
Band_3	0.87	1.39	1.95

Agricult...

Statistics	Band_1	Band_2	Band_3
Minimum	10.00	11.00	16.00
Maximum	27.00	33.00	47.00
Mean	13.19	15.90	26.01
Std.dev	2.51	2.97	3.18
Covariance			
Band_1	6.32	7.25	6.74
Band_2	7.25	8.83	8.08
Band_3	6.74	8.08	10.10

Builtup ...

Statistics	Band_1	Band_2	Band_3
Minimum	12.00	13.00	16.00
Maximum	33.00	27.00	36.00
Mean	17.72	17.99	25.01
Std.dev	2.62	2.01	2.77
Covariance			
Band_1	6.86	4.28	4.26
Band_2	4.28	4.04	5.08
Band_3	4.26	5.08	7.65

Bare Area

Statistics	Band_1	Band_2	Band_3
Minimum	6.00	9.00	11.00
Maximum	32.00	40.00	60.00
Mean	28.99	35.42	52.48
Std.dev	2.25	3.41	6.56
Covariance			
Band_1	5.05	6.16	9.28
Band_2	6.16	11.66	21.52
Band_3	9.28	21.52	42.99

Grassla...

Statistics	Band_1	Band_2	Band_3
Minimum	11.00	13.00	14.00
Maximum	18.00	21.00	31.00
Mean	12.70	14.79	18.73
Std.dev	2.53	2.63	5.10
Covariance			
Band_1	6.41	6.55	12.52
Band_2	6.55	6.91	13.19
Band_3	12.52	13.19	25.98

Waterb...

Statistics	Band_1	Band_2	Band_3
Minimum	7.00	9.00	10.00
Maximum	30.00	33.00	45.00
Mean	14.15	15.77	20.19
Std.dev	4.13	4.19	6.25
Covariance			
Band_1	17.07	17.12	25.53
Band_2	17.12	17.59	26.13
Band_3	25.53	26.13	39.12

Annex 5: Training Sample Histograms and Statistics in OBIA

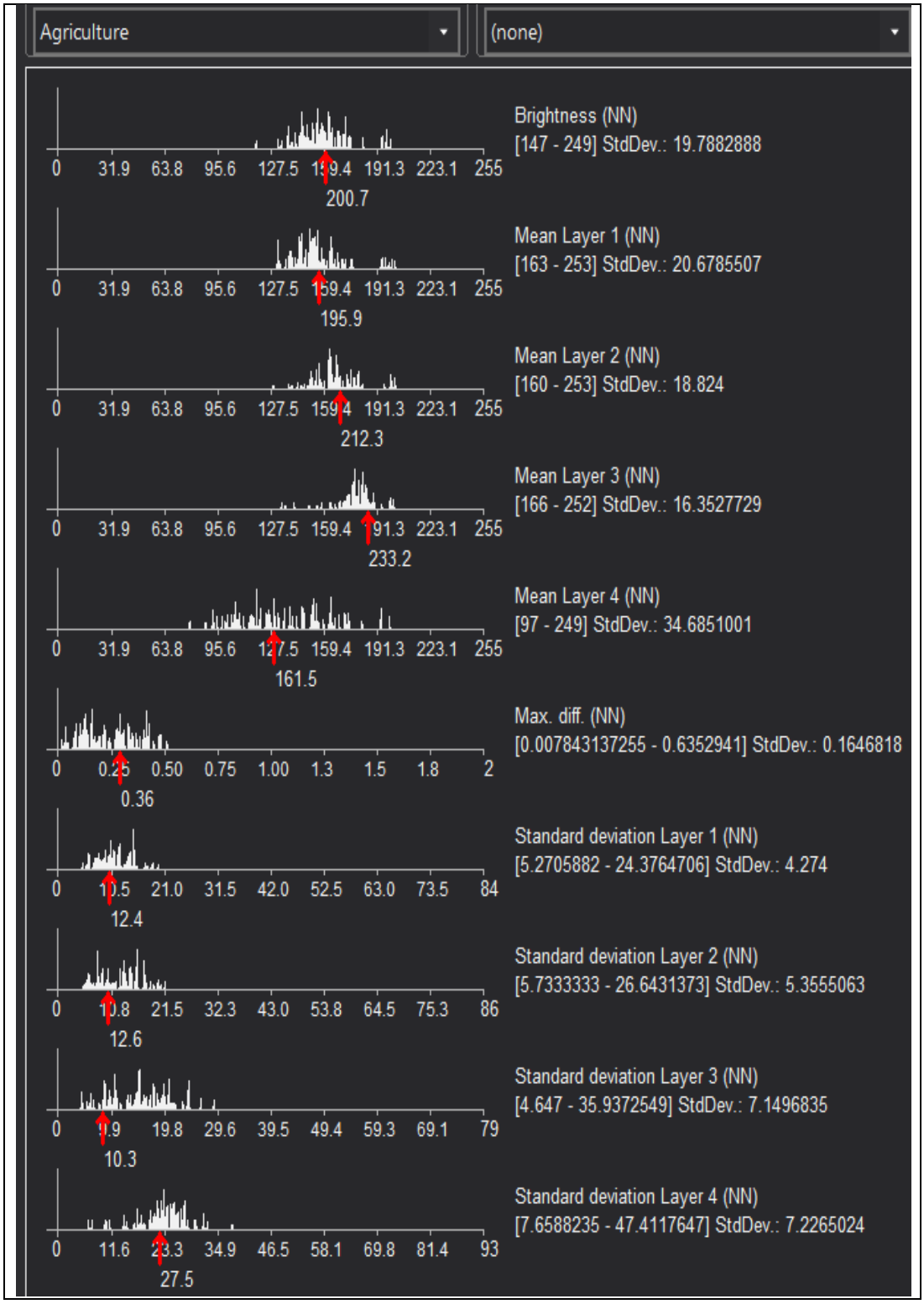

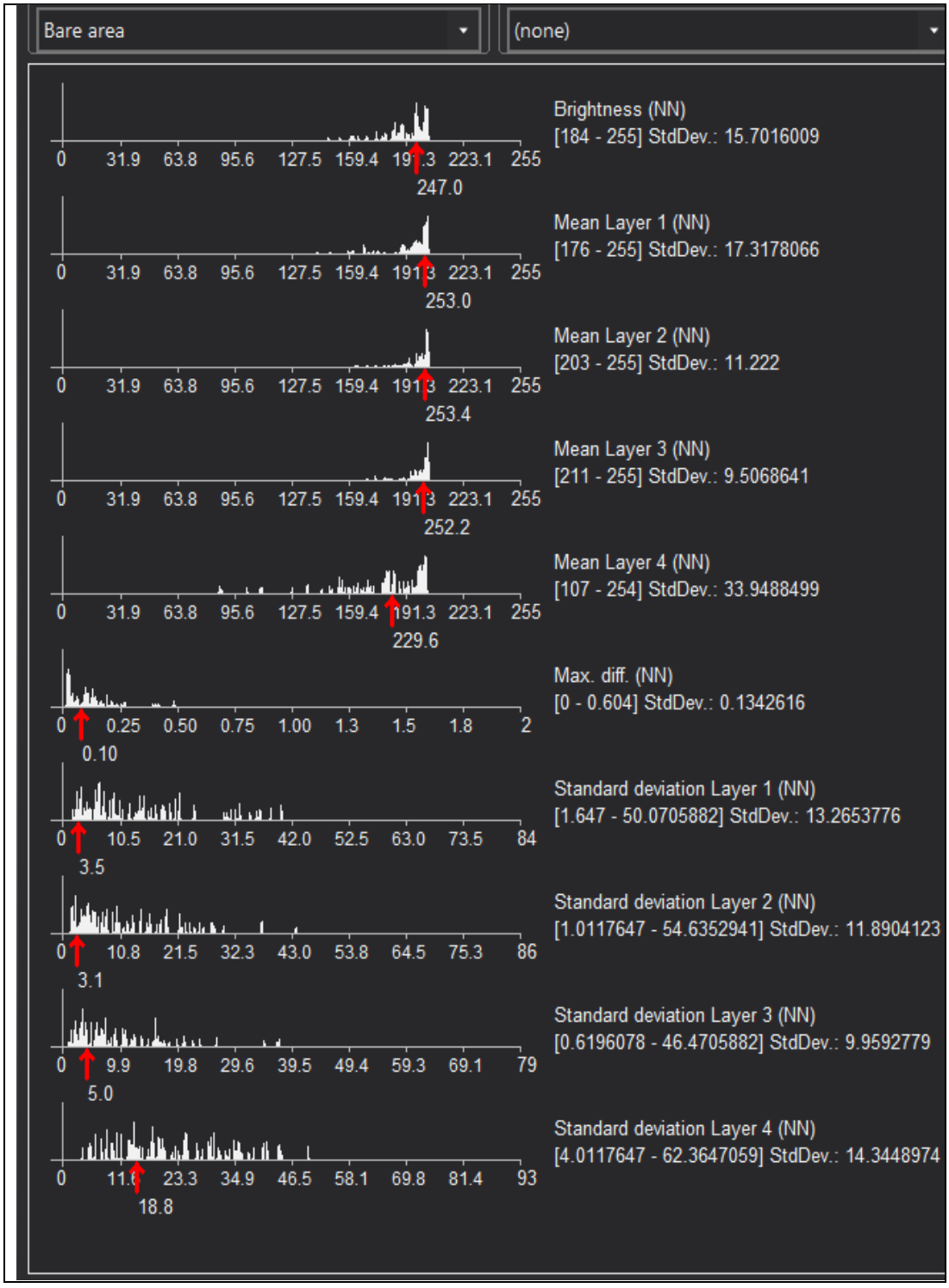
Bare area
(none)
Brightness (NN)
[184 - 255] StdDev.: 15.7016009
0 31.9 63.8 95.6 127.5 159.4 191.3 223.1 255
247.0
Mean Layer 1 (NN)
[176 - 255] StdDev.: 17.3178066
0 31.9 63.8 95.6 127.5 159.4 191.3 223.1 255
253.0
Mean Layer 2 (NN)
[203 - 255] StdDev.: 11.222
0 31.9 63.8 95.6 127.5 159.4 191.3 223.1 255
253.4
Mean Layer 3 (NN)
[211 - 255] StdDev.: 9.5068641
0 31.9 63.8 95.6 127.5 159.4 191.3 223.1 255
252.2
Mean Layer 4 (NN)
[107 - 254] StdDev.: 33.9488499
0 31.9 63.8 95.6 127.5 159.4 191.3 223.1 255
229.6
Max. diff. (NN)
[0 - 0.604] StdDev.: 0.1342616
0 0.25 0.50 0.75 1.00 1.3 1.5 1.8 2
0.10
Standard deviation Layer 1 (NN)
[1.647 - 50.0705882] StdDev.: 13.2653776
0 10.5 21.0 31.5 42.0 52.5 63.0 73.5 84
3.5
Standard deviation Layer 2 (NN)
[1.0117647 - 54.6352941] StdDev.: 11.8904123
0 10.8 21.5 32.3 43.0 53.8 64.5 75.3 86
3.1
Standard deviation Layer 3 (NN)
[0.6196078 - 46.4705882] StdDev.: 9.9592779
0 9.9 19.8 29.6 39.5 49.4 59.3 69.1 79
5.0
Standard deviation Layer 4 (NN)
[4.0117647 - 62.3647059] StdDev.: 14.3448974
0 11.6 23.3 34.9 46.5 58.1 69.8 81.4 93
18.8

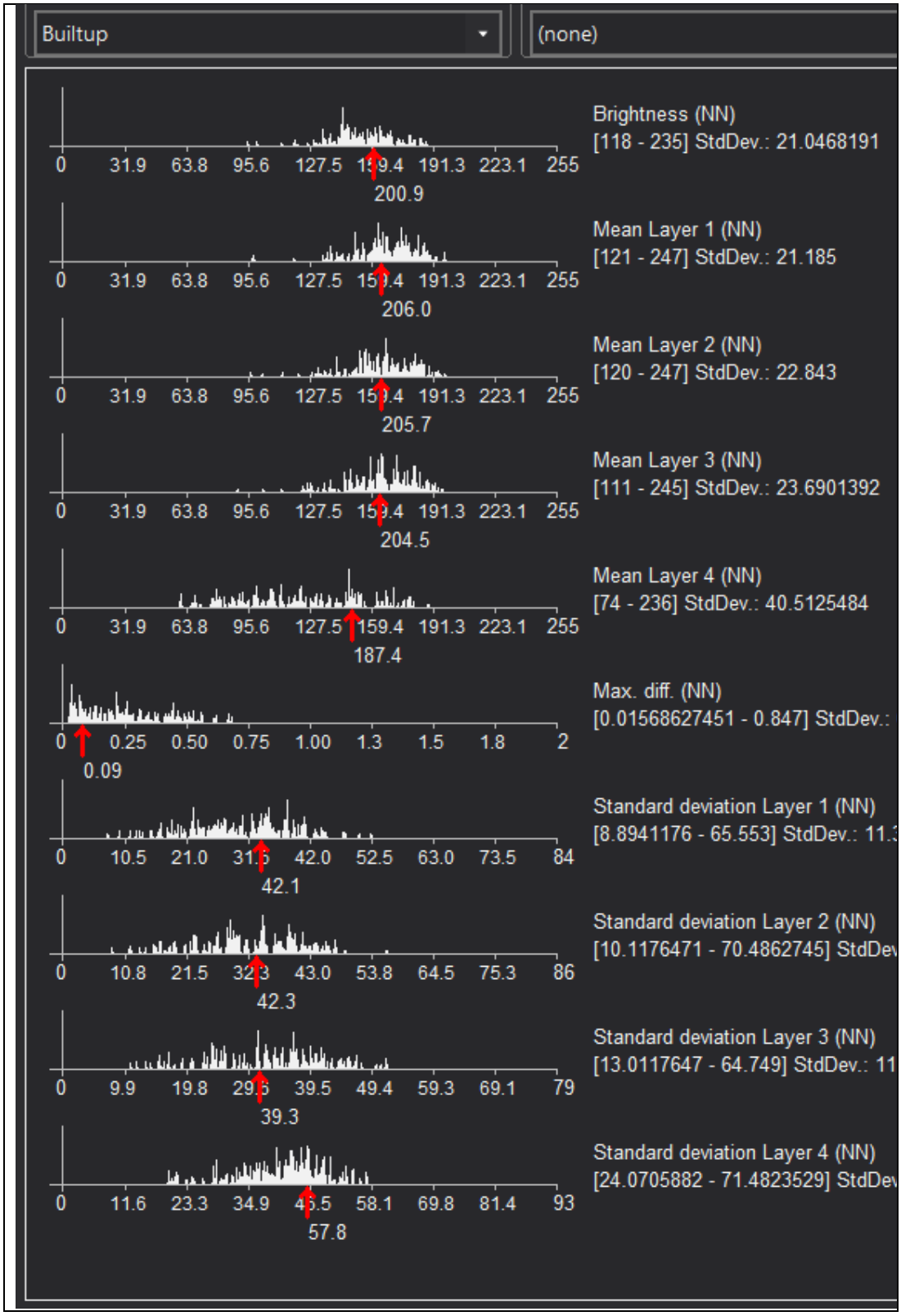
Builtup
(none)
Brightness (NN)
[118 - 235] StdDev.: 21.0468191
0 31.9 63.8 95.6 127.5 159.4 191.3 223.1 255
200.9
Mean Layer 1 (NN)
[121 - 247] StdDev.: 21.185
0 31.9 63.8 95.6 127.5 159.4 191.3 223.1 255
206.0
Mean Layer 2 (NN)
[120 - 247] StdDev.: 22.843
0 31.9 63.8 95.6 127.5 159.4 191.3 223.1 255
205.7
Mean Layer 3 (NN)
[111 - 245] StdDev.: 23.6901392
0 31.9 63.8 95.6 127.5 159.4 191.3 223.1 255
204.5
Mean Layer 4 (NN)
[74 - 236] StdDev.: 40.5125484
0 31.9 63.8 95.6 127.5 159.4 191.3 223.1 255
187.4
Max. diff. (NN)
[0.01568627451 - 0.847] StdDev.:
0 0.25 0.50 0.75 1.00 1.3 1.5 1.8 2
0.09
Standard deviation Layer 1 (NN)
[8.8941176 - 65.553] StdDev.: 11.
0 10.5 21.0 31.5 42.0 52.5 63.0 73.5 84
42.1
Standard deviation Layer 2 (NN)
[10.1176471 - 70.4862745] StdDev
0 10.8 21.5 32.3 43.0 53.8 64.5 75.3 86
42.3
Standard deviation Layer 3 (NN)
[13.0117647 - 64.749] StdDev.: 11
0 9.9 19.8 29.6 39.5 49.4 59.3 69.1 79
39.3
Standard deviation Layer 4 (NN)
[24.0705882 - 71.4823529] StdDev
0 11.6 23.3 34.9 46.5 58.1 69.8 81.4 93
57.8

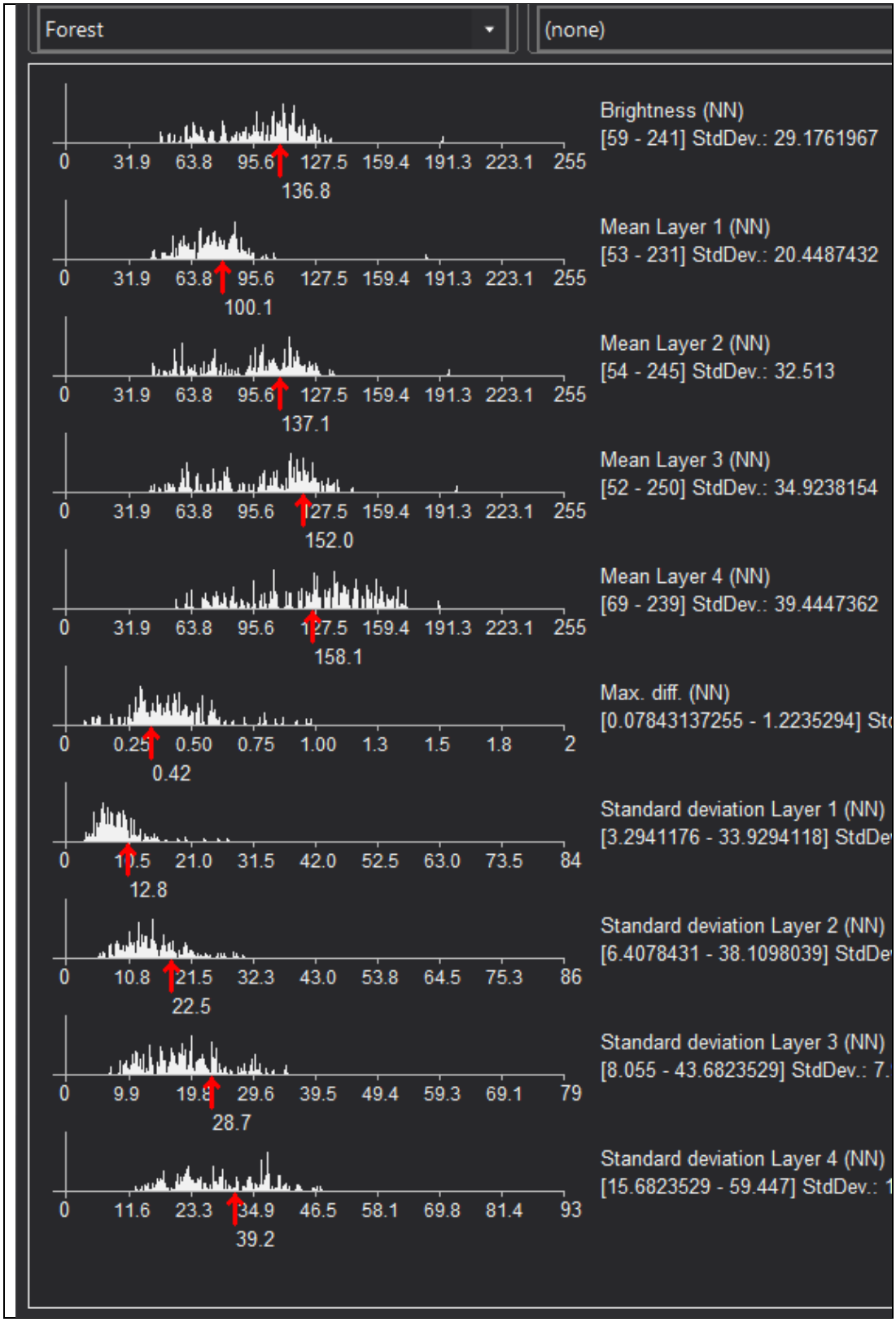
Forest
(none)
Brightness (NN)
[59 - 241] StdDev.: 29.1761967
0 31.9 63.8 95.6 127.5 159.4 191.3 223.1 255
136.8
Mean Layer 1 (NN)
[53 - 231] StdDev.: 20.4487432
0 31.9 63.8 95.6 127.5 159.4 191.3 223.1 255
100.1
Mean Layer 2 (NN)
[54 - 245] StdDev.: 32.513
0 31.9 63.8 95.6 127.5 159.4 191.3 223.1 255
137.1
Mean Layer 3 (NN)
[52 - 250] StdDev.: 34.9238154
0 31.9 63.8 95.6 127.5 159.4 191.3 223.1 255
152.0
Mean Layer 4 (NN)
[69 - 239] StdDev.: 39.4447362
0 31.9 63.8 95.6 127.5 159.4 191.3 223.1 255
158.1
Max. diff. (NN)
[0.07843137255 - 1.2235294] St
0 0.25 0.50 0.75 1.00 1.3 1.5 1.8 2
0.42
Standard deviation Layer 1 (NN)
[3.2941176 - 33.9294118] StdDe
0 10.5 21.0 31.5 42.0 52.5 63.0 73.5 84
12.8
Standard deviation Layer 2 (NN)
[6.4078431 - 38.1098039] StdDe
0 10.8 21.5 32.3 43.0 53.8 64.5 75.3 86
22.5
Standard deviation Layer 3 (NN)
[8.055 - 43.6823529] StdDev.: 7.
0 9.9 19.8 29.6 39.5 49.4 59.3 69.1 79
28.7
Standard deviation Layer 4 (NN)
[15.6823529 - 59.447] StdDev.: 1
0 11.6 23.3 34.9 46.5 58.1 69.8 81.4 93
39.2

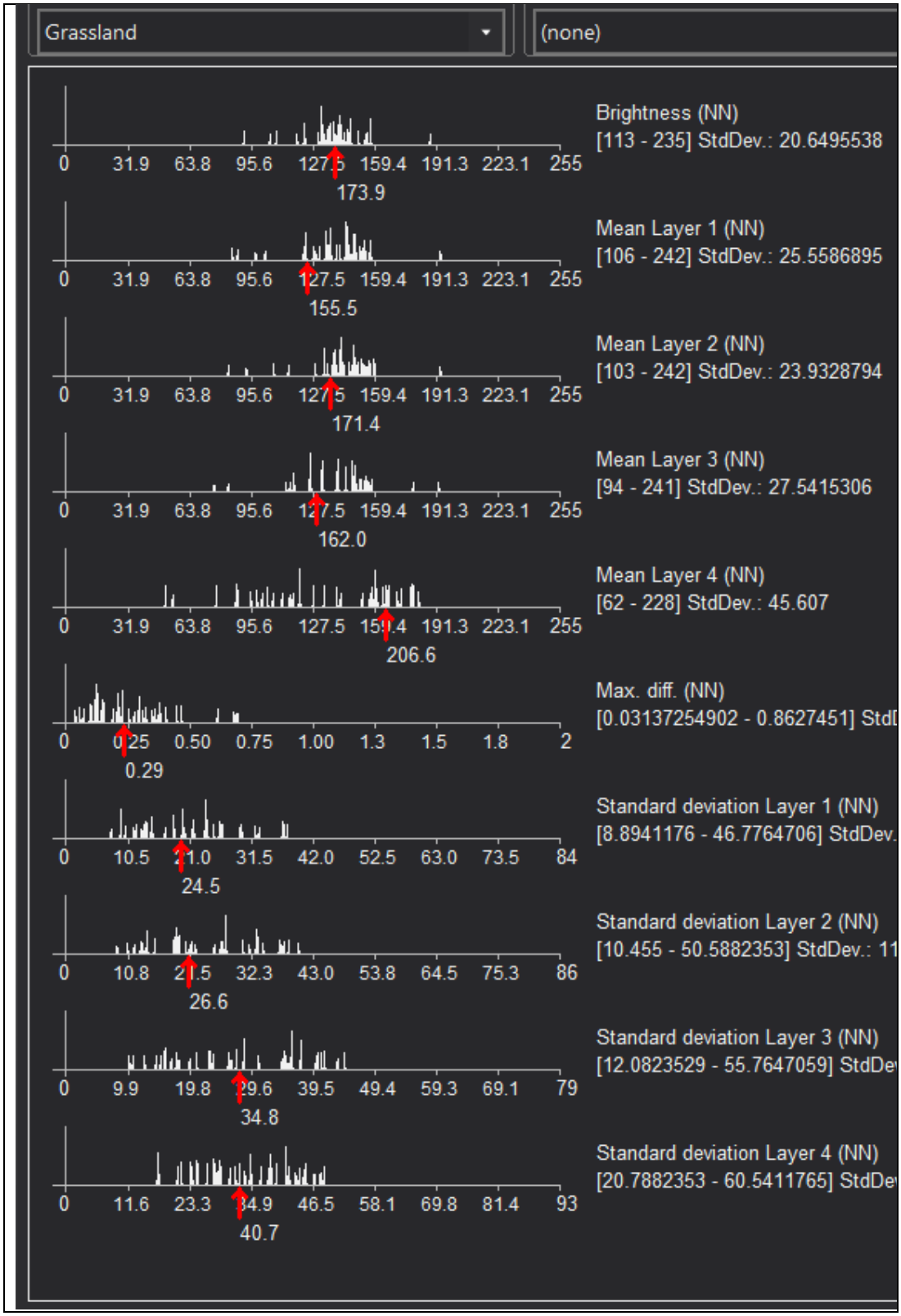
Grassland
(none)
Brightness (NN)
[113 - 235] StdDev.: 20.6495538
0 31.9 63.8 95.6 127.5 159.4 191.3 223.1 255
173.9
Mean Layer 1 (NN)
[106 - 242] StdDev.: 25.5586895
0 31.9 63.8 95.6 127.5 159.4 191.3 223.1 255
155.5
Mean Layer 2 (NN)
[103 - 242] StdDev.: 23.9328794
0 31.9 63.8 95.6 127.5 159.4 191.3 223.1 255
171.4
Mean Layer 3 (NN)
[94 - 241] StdDev.: 27.5415306
0 31.9 63.8 95.6 127.5 159.4 191.3 223.1 255
162.0
Mean Layer 4 (NN)
[62 - 228] StdDev.: 45.607
0 31.9 63.8 95.6 127.5 159.4 191.3 223.1 255
206.6
Max. diff. (NN)
[0.03137254902 - 0.8627451] StdD
0 0.25 0.50 0.75 1.00 1.3 1.5 1.8 2
0.29
Standard deviation Layer 1 (NN)
[8.8941176 - 46.7764706] StdDev.
0 10.5 21.0 31.5 42.0 52.5 63.0 73.5 84
24.5
Standard deviation Layer 2 (NN)
[10.455 - 50.5882353] StdDev.: 11
0 10.8 21.5 32.3 43.0 53.8 64.5 75.3 86
26.6
Standard deviation Layer 3 (NN)
[12.0823529 - 55.7647059] StdDe
0 9.9 19.8 29.6 39.5 49.4 59.3 69.1 79
34.8
Standard deviation Layer 4 (NN)
[20.7882353 - 60.5411765] StdDe
0 11.6 23.3 34.9 46.5 58.1 69.8 81.4 93
40.7

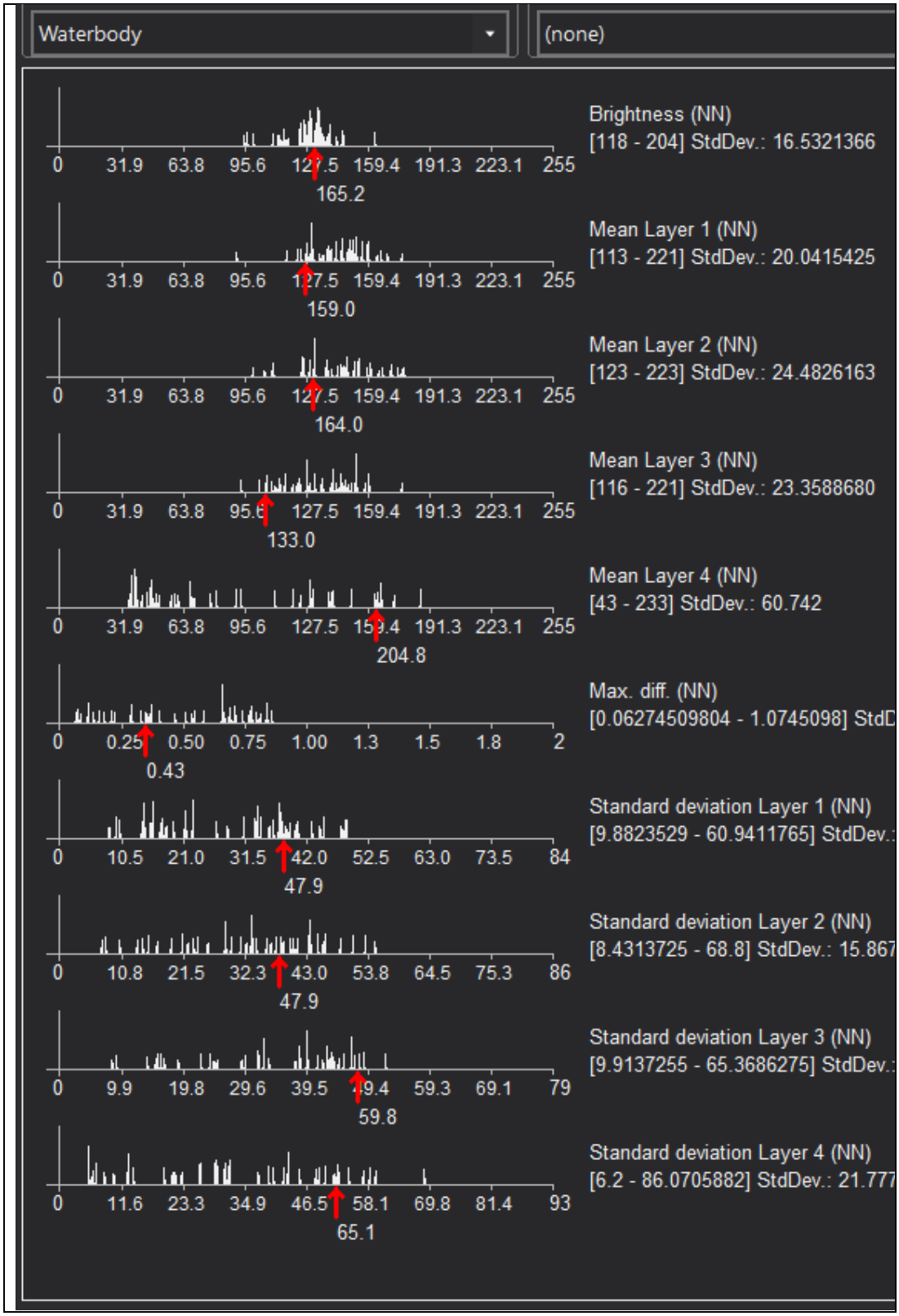
Waterbody
(none)
Brightness (NN)
[118 - 204] StdDev.: 16.5321366
0 31.9 63.8 95.6 127.5 159.4 191.3 223.1 255
165.2
Mean Layer 1 (NN)
[113 - 221] StdDev.: 20.0415425
0 31.9 63.8 95.6 127.5 159.4 191.3 223.1 255
159.0
Mean Layer 2 (NN)
[123 - 223] StdDev.: 24.4826163
0 31.9 63.8 95.6 127.5 159.4 191.3 223.1 255
164.0
Mean Layer 3 (NN)
[116 - 221] StdDev.: 23.3588680
0 31.9 63.8 95.6 127.5 159.4 191.3 223.1 255
133.0
Mean Layer 4 (NN)
[43 - 233] StdDev.: 60.742
0 31.9 63.8 95.6 127.5 159.4 191.3 223.1 255
204.8
Max. diff. (NN)
[0.06274509804 - 1.0745098] StdD
0 0.25 0.50 0.75 1.00 1.3 1.5 1.8 2
0.43
Standard deviation Layer 1 (NN)
[9.8823529 - 60.9411765] StdDev.:
0 10.5 21.0 31.5 42.0 52.5 63.0 73.5 84
47.9
Standard deviation Layer 2 (NN)
[8.4313725 - 68.8] StdDev.: 15.867
0 10.8 21.5 32.3 43.0 53.8 64.5 75.3 86
47.9
Standard deviation Layer 3 (NN)
[9.9137255 - 65.3686275] StdDev.:
0 9.9 19.8 29.6 39.5 49.4 59.3 69.1 79
59.8
Standard deviation Layer 4 (NN)
[6.2 - 86.0705882] StdDev.: 21.777
0 11.6 23.3 34.9 46.5 58.1 69.8 81.4 93
65.1